Aus der Klinik für Hämatologie, Hämostaseologie, Onkologie und
Stammzelltransplantation der Medizinischen Hochschule Hannover

The E3 Ligase Itch is a Novel Positive Regulator of Mesenchymal Stem Cells

Dissertation

zur Erlangung des Doktorgrades der Medizin

in der Medizinischen Hochschule Hannover

vorgelegt von Christoph Schünemann

aus Braunschweig

Hannover 2019

Angenommen vom Senat der Medizinischen Hochschule Hannover am 08.05.2020

Gedruckt mit Genehmigung der Medizinischen Hochschule Hannover

Präsident:	Prof. Dr. med. Michael P. Manns
Betreuer der Arbeit:	Prof. Dr. med. Michael Heuser
1. Referent:	PD Dr. rer. nat. Michael Morgan
2. Referent:	PD Dr. rer. nat. Dirk Heckl

Tag der mündlichen Prüfung: 08.05.2020

Prüfungsausschuss:

Vorsitz:	Prof. Dr. med. Thomas Werfel
1. Prüfer:	Prof. Dr. med. Georg Scheumann
2. Prüfer:	Prof. Dr. med. Torsten Witte

Für meine Familie

CONTENTS

LIST OF FIGURES

LIST OF TABLES

1. INTRODUCTION

1.1 Mesenchymal Stem Cells.

Stem cells possess a unique combination of two features that defines their identity. Firstly, stem cells develop into differentiated functional cell types. Secondly, they possess self-renewing capacity as they can generate at least one stem cell upon cell division (Orford and Scadden, 2008). Embryonic stem cells (ES cells) are pluripotent and differentiate into all cell types of the body. Multipotent stem cells can generate a restricted subset of specialized progeny (Jaenisch and Young, 2008). Adult stem cells replenish cells within specialized tissues or organs postnatally. They maintain tissue integrity during steady state as well as in response to stress. This task requires a coordinated control of self-renewing divisions and lineage commitment (Jaenisch and Young, 2008; Orford and Scadden, 2008).

In the 1960s McCulloch and Till postulated the existence of adult stem cells within the hematopoietic system. For the first time they provided experimental evidence for self-renewal and lineage differentiation through quantitative bone marrow transplantation experiments (McCulloch and Till, 1960). Subsequently, heterotopic bone marrow transplantation experiments revealed the presence of bone forming progenitors within the bone marrow (Friedenstein et al., 1966; Tavassoli and Crosby, 1968). Progenitor cells with osteogenic differentiation potential were separated from their hematopoietic counterpart by their ability to adhere to the culture dish. These spindle-shaped cells exhibited clonal growths and could form bone upon ectopic transplantation in vivo (Owen and Friedenstein, 1988). The discovery of these cells in human bone marrow samples led to the designation “colony forming unit fibroblasts” (CFU-F) (Castro-Malaspina et al., 1980). Further studies on CFU-Fs revealed an in vitro differentiation capacity into multiple specialized cell types including adipocytes, chondrocytes or myocytes. These findings led to the term “mesenchymal stem cell” for the in vitro expanded CFU-Fs (Caplan, 1991). The concept of “mesenchymal stem cells” was broadened by the proposal of a “mesengenic process” (Caplan, 1994). This concept implemented a common progenitor cell that would perpetuate a variety of mesenchymal tissues, including fat, bone, cartilage, muscle or tendon, throughout postnatal life (Caplan, 1994).

The nomenclature “mesenchymal stem cell” was controversial because evidence for the existence of such a stem cell in vivo was lacking. Neither serial transplantation experiments nor in vivo fate demonstrations had been performed at that time. In the following decade, further controversies about “mesenchymal stem cells” arose, e. g. when these cells were differentiated into neurons (Woodbury et al., 2000) or successfully isolated from many different organs (da Silva Meirelles et al., 2006). It became evident that considerable heterogeneity existed among the in vitro cultured CFU-F clones and subsequently in the understanding of “mesenchymal stem cells” between different investigators (Bianco et al., 2008). To improve comparability and translational research in the field, the International Society for Cellular Therapy (ISCT) provided a definition for in vitro cultured human “multipotent mesenchymal stromal cells” (Horwitz et al., 2005). The terminology was proposed to demarcate the in vitro cultured CFU-Fs from mesenchymal stem cells with experimentally proven stem cell identity in vivo. For convenience, the abbreviation “MSC” was kept for multipotent mesenchymal stromal cells, though. The definition comprised adipogenic, osteogenic and chondrogenic differentiation potential as well as a distinct immunophenotype including CD73, CD90 and CD105 expression (Horwitz et al., 2005; Dominici et al., 2006).

Advances in microscopy, immunofluorescent labeling techniques and engineering genetic mouse models paved the way for the experimental demonstration of mesenchymal stem cell (MSC) self-renewal and multipotency in vivo. Accordingly, the existence of mesenchymal stem cells in the strict sense could be proven at the end of the 2000s: In various studies, MSCs were detected in perivascular regions of the bone marrow, where they exhibited an essential component of the hematopoietic stem cell (HSC) niche (Morikawa et al., 2009; Méndez-Ferrer et al., 2010). Prospectively identified MSCs highly enriched for CFU-Fs, could be serially transplanted and differentiated into at least two cell types of skeletal tissue in vivo with the help of ingenious techniques (Morikawa et al., 2009; Méndez-Ferrer et al., 2010).

To the present day, our knowledge regarding murine MSC ontogeny, localization and differentiation has further emerged through meticulous in vivo studies, single cell analyses and transplantation experiments (Chen et al., 2018). Nevertheless, controversies regarding the MSC concept remain (Bianco, 2014). A consistent

definition for the identification of murine MSCs is lacking. Various surface marker combinations and transgene-based reporter strains have been proven to identify murine mesenchymal stem cell subsets *(Table 1)* (Mohamed and Franceschi, 2017). Considerable overlap among the cells that are identified by these different MSC signatures is assumed, but experimental data to proof this hypothesis is incomplete and conflicting results exist (Chen et al., 2018). More recently, the concept of skeletal stem cells (SSC) has been introduced (Bianco and Robey, 2015). SSCs are multipotent progenitors of skeletal tissues that can differentiate into osteoblasts and chondrocytes as well as into bone marrow adipocytes and stromal cells. This concept emphasizes the skeletal derivation and the skeletal progeny of the progenitor cell subset. Furthermore, the new terminology with an abbreviation clearly distinct from “MSC” underlines the fundamental difference to the multipotent mesenchymal stromal cell concept (Bianco and Robey, 2015). To date, the terms mesenchymal stem cell and skeletal stem cell are widely used interchangeably in mouse studies (Mohamed and Franceschi, 2017; Chen et al., 2018). *Table 1* lists currently used signatures for the prospective identification of MSCs / SSCs in mouse models (modified from Mohamed and Franceschi, 2017).

Table 1. Putative murine MSC markers (modified from Mohamed and Franceschi, 2017).

Marker	Identified cells (progeny or MSC subset)	Reference
PDGFRα+ Sca-1+	Ocn-expressing osteoblasts, reticular cells, endothelial cells and perilipin+ adipocytes (in adipose tissue)	Morikawa et al., 2009
PDGFRα+ CD51+	Nes-GFP- and Nes-expressing cells	Pinho et al., 2013
CD51+ CD200+	Osteoblasts, chondrocytes, stromal cells	Chan et al., 2015
Nes-GFP	Perivascular stromal cells endothelial cells, Osx-expressing cells, osteoblasts, osteocytes	Méndez-Ferrer et al., 2010
Mx1-Cre	Osx-expressing cells and Ocn-expressing osteoblasts	Park et al., 2012
Prx1-Cre	Osteolineages in osteogenic fronts, periosteum, dura and osteocytes	Greenbaum et al., 2013
OSX-CreER	Osteoblasts, stromal cells and Nes-GFP+ cells	Mizoguchi et al., 2014
Col2-CreER	Chondrocytes, perichondrial cells in the growth plate, Col1(2.3)-GFP+ osteoblasts, osteocytes and CXCL12+ stromal cells	Ono et al., 2014
Sox9-CreER/Acan-Cre-ER	Sox9-expressing chondrocytes, perichondrial cells, and Col1(2.3)-GFP+ osteoblasts (also Ocn-positive)	Ono et al., 2014
LepR-Cre	Col1(2.3)-GFP+ osteoblasts, perilipin+ adipocytes, and aggrecan+ chondrocytes (fracture only)	Zhou et al., 2014
Grem1-CreER	Chondrocytes, Col1(2.3)-GFP+ osteoblasts and reticular marrow stromal cells	Worthley et al., 2015
Gli1-CreER	Osteolineages in osteogenic fronts, periosteum, dura and osteocytes	Zhao et al., 2015
Axin2-CreER	Osx-expressing osteoblasts and osteocytes	Maruyama et al., 2016
Hoxa11-GFP	Sox9-expressing chondrocytes and Osx-expressing osteoblasts	Rux et al., 2016

1.2 The Ubiquitin Proteasome System.

The Ubiquitin Proteasome System serves as an intracellular pathway of protein degradation: Firstly, the attachment of a ubiquitin chain tags a distinct intracellular protein for destruction. Secondarily, this protein is degraded through the downstream 26S proteasome and ubiquitin is released (Ciechanover, 2015).

Ubiquitin is a highly conserved 76 amino acid polypeptide. Ubiquitination is the process of ubiquitin attachment to a substrate, which is catalyzed by the ubiquitin enzymes E1 - E3. This process is tightly regulated, highly specific and energy consuming (Ciechanover, 2015). The multistep process begins with an E1 (ubiquitin activating enzyme) that binds ubiquitin in an ATP-dependent manner. Subsequently, the E2 (ubiquitin conjugating enzyme) catalyzes the transfer of the activated ubiquitin to the E2 itself. The E3 (ubiquitin ligase) binds the substrate and mediates the ubiquitin transfer to this target protein. E3 ligases with different conjugation mechanisms exist (Glickman and Ciechanover, 2002). HECT (homologous to the E6-AP COOH terminus) type E3 ligases catalyze the ubiquitin transfer to themselves in an intermediate step. Then, ubiquitin is transferred to the substrate (Weissman, 2001). RING (really new interesting gene) finger type E3 ligases directly catalyze the transfer of ubiquitin from E2 to the target protein (Weissman, 2001). Typically, ubiquitin will be covalently bound to internal lysine residues of the target protein. Several courses of ubiquitination can generate an ubiquitin chain attached to the lysine residue of a substrate. In this case, ubiquitin is conjugated to Lys-48 of the previously conjugated ubiquitin. This ubiquitin chain can be recognized by the 26S proteasome (Glickman and Ciechanover, 2002). The proteasome degrades the substrate protein and an attached deubiquitinating enzyme (DUB) cleaves ubiquitin for recycling. DUBs also exist independently from the proteasome complex and regulate the process of ubiquitination through counteracting the E3 ligase function (Clague et al., 2015).

Finding a pathway for selective and specific proteolysis within a cell was the driver that led to the discovery of the Ubiquitin Proteasome System. This target specificity is mediated by E3 ubiquitin ligases (Ciechanover, 2015). E3 ligases bind their substrates through the identification of specific amino acid sequences or structural motifs. Further adaptor proteins may be involved in this process (Glickman and

Ciechanover, 2002). More than 600 different E3 ligases exist in mammalian genomes (Clague et al., 2015). E3 ligases typically interact with different substrates and many substrates can be identified by different E3 ligases. Most E3 ligases can bind different E2 enzymes sequentially (Glickman and Ciechanover, 2002). Approximately 40 E2 and only two E1 enzymes exist in mammals (Clague et al., 2015).

Regulation of protein stability through the Ubiquitin Proteasome pathway is involved in virtually all cellular processes including the degradation of misfolded and denatured proteins. Moreover, ubiquitinating and deubiquitinating enzymes exert regulatory roles in a wide range of cellular processes in a proteasome-independent mode (Glickman and Ciechanover, 2002). Different patterns of ubiquitination exist and these result in different ubiquitin moieties. Monoubiquitination has been shown to regulate cellular localization of proteins (Weissman, 2001). Polyubiquitination through Lys-63 of ubiquitin has been involved in a variety of cellular processes such as DNA repair and membrane trafficking (Glickman and Ciechanover, 2002). Several other ubiquitination patterns such as ubiquitination via further lysine residues, branched ubiquitin chains or N-terminal ubiquitination have been described (Clague et al., 2015). Some of these posttranslational modifications act in a proteasome-dependent and others in various proteasome-independent ways (Weissman, 2001). Moreover, polyubiquitin fusion proteins can be generated and exist within cells (Glickman and Ciechanover, 2002). The proteasome complex itself may not always degrade proteins to polypeptides without any function. Instead, protein processing to alter cellular activity, as for example by truncation, is a regulatory mechanism. Additionally, the proteasome complex may regulate cellular processes in a proteolysis-independent manner, e. g. as a scaffold or through adaptor functions (Glickman and Ciechanover, 2002). The proteasomal and multiple alternative pathways render a variety of mechanisms through which E3 ligases and deubiquitinases regulate cellular processes. Mutations in different genes that encode E3 ligases as well as deregulation of the ubiquitination process have been associated with a variety of disorders such as neurodegenerative and malignant diseases (Ciechanover, 2015). Because of the diversity of E3s and DUBs, many substrate relationships and regulatory mechanisms remain incompletely understood (Weissman, 2001). Deciphering these networks is expected to refine our current

understanding on a diverse range of biological processes and to identify a variety of novel drug targets (Weissman, 2001; Glickman and Ciechanover, 2002).

1.3 The E3 Ubiquitin Ligase Itch.

Itch belongs to the group of HECT-domain containing E3 ubiquitin ligases (Perry et al., 1998). The C-terminal HECT domain covalently binds ubiquitin prior to the transfer of ubiquitin to the substrate (Weissman, 2001). The protein further contains an N-terminal C2 domain and four WW domains *(Figure 1)* (Perry et al., 1998). The C2 domain mediates membrane associations through phospholipid binding. The WW domains mediate specific protein interactions through the recognition of proline-rich motifs and proline-containing phosphoserine/phosphothreonine motifs (Aki et al., 2015). Itch has several known phosphorylation sites at different serine/threonine and tyrosine residues. Phosphorylation can regulate the E3 ligase activity as well as Itch autoubiquitination (Aki et al., 2015). Autoubiquitination as a regulatory mechanism leads to Itch activation but promotes proteasomal degradation of Itch protein (Noyes et al., 2016).

The Itch gene locus that encodes the E3 ligase was discovered in 1998 through the study of a radiation-induced mutant mouse (Perry et al., 1998). This non-agouti 18H mouse had been generated and characterized to study the genetics of mouse coat color. The phenotype that comprised severe autoinflammation involving the skin suggested that another gene in addition to the agouti locus was mutated (Hustad et al., 1995). Subsequently, it was demonstrated that an inversion on chromosome 2 disrupted a new gene resulting in a null allele (Perry et al., 1998). The structural analysis revealed that this gene encoded a HECT domain containing E3 ligase *(Figure 1)* (Perry et al., 1998). Itch or “Itchy, E3 ubiquitin protein ligase” and especially its human homologue, is also known as AIP4 (atrophin-interacting-protein 4) (Aki et al., 2015). The mouse gene is located on chromosome 2. The encoded protein of 864 amino acids has a relative molecular weight of 113 kDa. The protein is widely expressed among a variety of different cell types and tissues (Perry et al., 1998).

Itch-deficient mice on C57BL/6 background develop systemic autoinflammation at three to four months. This disease involves the skin, the lungs and the intestinal tract. They exhibit splenomegaly and lymphoid hyperplasia in lymph nodes and thymus. Most of the mice die at four to six months (Hustad et al., 1995). Several studies aimed to identify the role of Itch within the immune system. To date, Itch has been established as an important regulator of T cells. The E3 ligase is involved in the control of different T cell subsets as well as in the regulation of different T cell functions (Aki et al., 2015). The first landmark study to elucidate the autoimmune phenotype of the Itch knockout mouse identified Itch as a negative regulator of T helper cell 2 (Th2) polarization (Fang et al., 2002). Itch prevented the expression of Th2 cytokines interleukin 4 (IL-4) and interleukin 5 (IL-5) through negative regulation of the transcription factor JunB via ubiquitination and proteasomal degradation. Itch-deficient mice exhibited increased IL-4 and IL-5 levels and a Th2 bias (Fang et al., 2002). Besides adoptive immunity and particularly T cells, the role of Itch has been studied in innate immunity as well as in hematopoiesis. Though widely expressed, the function of Itch in non-hematopoietic cells remains incompletely understood (Aki et al., 2015).

The first identified substrate of the E3 ligase Itch was Notch receptor. Itch was shown to interact with Notch and to ubiquitinate NICD (Notch intracellular domain) at the N-terminus (Qiu et al., 2000). To date, multiple Itch interaction partners and substrates have been identified. Itch is involved in the regulation of various signaling pathways *(Table 2)* (Aki et al., 2015).

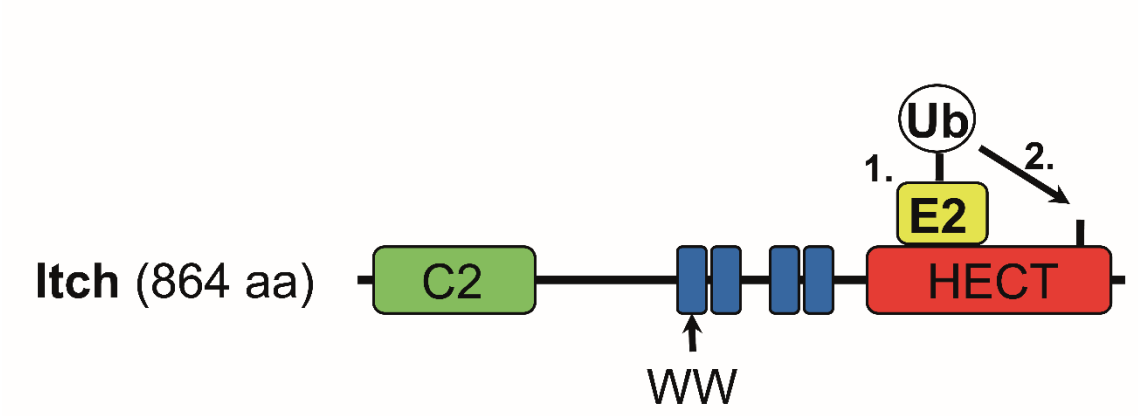

Figure 1. Schematic structure of Itch protein (modified from Aki et al., 2015). Green: N-terminal C2 domain, amino acid (aa) 17 - 140. Blue: 4 central WW domains at aa 290, 322, 402, 442. Red: C-terminal HECT domain, aa 509 – 862. The N-terminal HECT domain lobe contains the E2 enzyme binding region. The E2-Ubiquitin (Ub) complex is bound (1.). The C-terminal HECT domain lobe contains the active site cysteine residue (C832) that binds the activated Ubiquitin (2.).

Table 2. Selected Itch interaction proteins (modified from Aki et al., 2015).

Substrates			**Other binding partners**
Transmembrane	***Signaling molecules***	***Transcription factors***	
CXCR4	c-FLIP	Foxo1	ATM
Erb4	c-IAP	Gli1	Cbl-b
Notch	Dvl	JunB	CYLD
TRPV4	LATS1	P45NF-E2	Fyn
	MKK4	p63	JNK1
	MAVS	p73	NDFIP2
	Smad2	TIEG1	Numb
	TAK1		TAXBP1
			USP9X

1.4 E3 Ubiquitin Ligases Regulate Stem Cell Functions.

Stem cells require a tightly controlled intracellular signaling network to regulate fate decisions. Imbalances in self-renewal and commitment towards specialized cell types will compromise tissue integrity. Disturbances in the regulatory program that controls self-renewal have been associated with carcinogenesis (Orford and Scadden, 2008). Post-translational modifications play an essential role in the control of stem cell functions (Werner et al., 2017).

Regulation through ubiquitination has been proven in embryonic as well as in adult stem cells (Strikoudis et al., 2014). Multiple mechanisms by which ubiquitination affects stem cell fate decisions have emerged (Werner et al., 2017). Stem cells need to adjust their program to local and systemic demands. Information will be provided through secreted molecules or cell-to-cell contact within specialized stem cell niches (Orford and Scadden, 2008). Localization and stability of receptor complexes can be regulated through ubiquitination for appropriate integration of extracellular signals (Werner et al., 2017). Downstream effector proteins can be altered in their activation state, binding partner affinity or stability via ubiquitin tags. Ubiquitin ligases further target transcription factors as well as cell cycle regulators. The latter process has been proven crucial for stem cell quiescence and thus maintenance of the systemic stem cell pool (Werner et al., 2017). Moreover, epigenetic mechanisms play a role in stem cell fate decisions and are particularly investigated in cell reprogramming, induced pluripotent stem cells (iPS cells) and carcinogenesis (Strikoudis et al., 2014). Ubiquitination of histones can lead to transcriptional activation as well as transcriptional repression. It may also result in subsequent chromatin modifications (Strikoudis et al., 2014).

1.4.1 The E3 Ubiquitin Ligase Itch in Stem Cells.

To date, the E3 ubiquitin ligase Itch has been primarily studied within the immune system and especially in the regulation of T cells (Aki et al., 2015). Itch protein is expressed in a wide range of different tissues and cells types, though. More recently, its role in the control of stem and progenitor cell populations has been discovered (Aki et al., 2015).

Liao et al. studied the function of Itch in embryonic stem cells (ES cells) through a loss-of-function approach (Liao et al., 2013). Down-regulation of Itch via sh-RNA resulted in decreased self-renewal in a murine ES cell line. The authors further demonstrated that Itch expression levels increased upon induction of somatic cell reprogramming. Knock-down of Itch diminished the yield of iPS clones following transduction with four reprogramming transcription factors (Oct4, Sox2, Klf4, cMyc). The positive regulation of ES cell self-renewal and induced somatic reprogramming was attributed to the interaction of Itch with the transcription factor Oct4 (Liao et al., 2013). Oct4 is considered a core regulatory component of ES cell self-renewal (Jaenisch and Young, 2008). Oct4 ubiquitination through Itch in ES cells led to increased transcriptional activity (Liao et al., 2013).

In contrast to the positive effect of Itch on ES cells, Rathinam et al. identified Itch as a negative regulator of hematopoietic stem cell self-renewal (Rathinam et al., 2011). The Itch knockout mouse showed increased frequencies of hematopoietic stem and progenitor cells, including long term HSCs. Itch-deficient HSCs hyperproliferated and exhibited an augmented repopulation activity in serial and competitive transplantation assays. The loss of Itch led to increased Notch1 signaling. Itch ubiquitinated Notch1 in HSCs and downregulation of Notch signaling in the absence of Itch partially rescued the HSC phenotype in vitro and in vivo (Rathinam et al., 2011).

Several studies have investigated the role of Itch in skin regeneration and wound healing (Rossi et al., 2006; Giamboi-Miraglia et al., 2015). Rossi et al. found that p63 ubiquitination through Itch in keratinocytes resulted in p63 degradation (Rossi et al., 2006). Itch levels increased whereas dNp63 levels concomitantly decreased during human and mouse keratinocyte differentiation. P63 has been established as a key regulator in the development and regeneration of different epithelial tissues and dNp63 is vital for basal layer formation (Rossi et al., 2006). It was further demonstrated that Itch-deficient keratinocytes hyperproliferated in vivo and that Itch knockout mice exhibited a thickened basal layer at developmental stages and as newborns (Giamboi-Miraglia et al., 2015). This hyperplasia was not present in adult mice. Itch-deficient skin further exhibited superior wound healing capacities. The absence of Itch resulted in increased p63, cJun and JunB protein levels as well as increased Notch signaling in keratinocytes (Giamboi-Miraglia et al., 2015).

Together, these results suggested that Itch negatively regulated stem cells within the skin basal layer.

1.4.2 Mesenchymal Stem Cell Regulation Through E3 Ubiquitin Ligases.

The molecular circuits that control hematopoietic stem cell functions have been most intensively investigated as compared with other tissues. A variety of E3 ligases are currently known to regulate HSC quiescence, self-renewal and differentiation (Strikoudis et al., 2014). Genetic mouse models sharpened our understanding of these regulatory mechanisms and established the basis for clinical applications (Orford and Scadden, 2008). Though HSCs serve as a paradigm for adult stem cell biology, the function of particular E3 ligases need to be investigated and interpreted independently in other stem cells (Strikoudis et al., 2014).

A detailed understanding of the molecular network that guides MSC functions is just beginning to emerge. In contrast to HSCs, few E3 ligases have been identified to regulate MSC self-renewal and differentiation through direct in vivo identification of the stem cell subset:

The von Hippel Lindau protein (VHL) is an E3 ubiquitin ligase and a critical negative regulator of hypoxia inducible factors (HIF) (Mangiavini et al., 2015). The Vhl-Hif axis has been investigated at multiple steps of skeletogenesis during development as well as in postnatal osteoblast and chondrocyte differentiation. Postnatally, Vhl seemed to positively regulate early chondroblast commitment and to restrict osteoblast differentiation in a Hif-dependent manner (Mangiavini et al., 2014; Weng et al., 2014). Interestingly, Prx1-Cre-driven conditional deletion of Vhl led to fibrosis and mesenchymal soft tissue tumors (Mangiavini et al., 2015). These findings were not described when Vhl was deleted at a later stage of osteoblast or chondrocyte commitment (Weng et al., 2014; Mangiavini et al., 2015). A detailed molecular signature of the vimentin and S100 positive, hyperproliferating, fibroblastic cells has not been described. The soft tissue tumor development was dependent on the Hif-1α-inducible matrix protein Ctgf (connective tissue growth factor) (Mangiavini et al., 2015).

The E3 ligase Cbl was studied in early osteoblast commitment using the CblY737F knock-in mouse (Scanlon et al., 2017). Through a point mutation, the Cbl-Pi3k

interaction is abrogated. In a fracture model, CblY737F mice exhibited periosteal thickening with relative accumulation of Osx-RFP positive progenitors. This resulted in enhanced osteogenic differentiation and ossification of the fracture (Scanlon et al., 2017).

1.5 Aim and Objectives of the Study.

Mesenchymal stem cells are highly investigated in preclinical and clinical studies for a variety of applications (Bianco et al., 2013; Galipeau and Sensébé, 2018). One important strategy is MSC transplantation that holds a promise in regenerative medicine as well as an immunomodulatory concept. Furthermore, tissue engineering for regenerative purposes and ex vivo modeling of a hematopoiesis-supporting environment with cultured MSCs remain major prospective goals.

MSCs and their progeny are involved in various mechanisms of human diseases. For this purpose, they exhibit a potential target for many therapeutic approaches, e. g. the manipulation of osteoblast commitment to improve fracture healing or to treat osteoporosis. Another example is the role of MSCs within the hematopoietic stem cell niche, which is expected to render new drug targets to treat hematologic malignancies (Bianco et al., 2013).

Until now however, MSC-based technologies have hardly reached the clinic, yet (Bianco et al., 2013; Galipeau and Sensébé, 2018). Incomplete understanding of MSC biology hampers novel translational strategies (Bianco, 2014). Compared to HSCs, the molecular mechanisms that control MSC functions in vivo remain poorly understood. The identification of MSC regulators in genetic mouse models provides the astonishing opportunity to connect a single gene with the functionality of a total organism. In contrast to clinical trials, consequent studies of MSCs in genetic mouse models in vivo have just begun to emerge. The controversies about the MSC concept contributed to this fact very likely.

Knowledge on the molecular mechanisms that control the preservation of the stem cell pool within the skeleton will open new avenues for translational MSC research. Likewise, a thorough understanding of the signals that guide in vivo differentiation

of MSCs into specialized cell types will refine any translational approach to manipulate repair processes or the hematopoietic niche.

The aim of this study was to identify novel regulatory mechanisms of mesenchymal stem cells through posttranslational modification. I hypothesized that the E3 ligase Itch regulates mesenchymal stem cell homeostasis and / or function based on the following facts:

1. ITCH has been previously identified as a regulator of stem cells (Rossi et al., 2006; Rathinam et al., 2011; Liao et al., 2013; Giamboi-Miraglia et al., 2015).
2. Human ITCH deficiency is a rare syndrome that causes a syndromic disease including autoinflammation and dysmorphic features of the skeleton (Lohr et al., 2010). The latter suggests a role for ITCH beyond the hematopoietic system but within the mesenchymal / skeletal tissue.
3. The E3 ligase has been demonstrated to regulate signaling pathways such as Notch, Wnt and Hedgehog (Aki et al., 2015). These evolutionary conserved pathways play pivotal roles in the regulation of stem cells (Orford and Scadden, 2008).

To investigate the research hypothesis, I employed a loss of function approach through the Itch knockout mouse model. **The first goal was to characterize the MSC pool in Itch-deficient mice.** Methodologically, the MSC subset was identified by the immunophenotype CD45− TER119− PDGFRα+ Sca-1+ (PαS). These PαS MSCs showed highest enrichment in CFU-Fs, differentiated into osteoblasts and adipocytes upon systemic transplantation as well as they participated in the HSC niche (Morikawa et al., 2009; Zhou et al., 2014).

The second goal was the investigation of the cellular phenotype of Itch-deficient MSCs to elucidate a potential alteration of MSC number or function in the mouse. In vitro studies on cultured MSCs served as a model system to generate hypotheses on the cellular phenotype in vivo. Of note, the isolation and culture of murine MSCs is considerably impaired by low yield, growth capacity and purity of stem cells (Phinney et al., 1999). In contrast to human MSCs, different methodological refinements are required for successful murine MSC cultures. Hence, the basis for these in vitro experiments was the establishment of Itch knockout MSC cultures.

Thirdly, the functional consequences of the loss of Itch within the skeletal tissue were studied. Any affection of a progenitor cell compartment may potentially affect the descending cell types and tissues. Importantly, the global knockout of Itch in the mouse model needed to be considered. Skeletal phenotypes could not exclusively be attributed to a potential alteration of MSCs.

Finally, I aimed to identify the molecular functions of Itch in MSCs. For this purpose, an educated guess based on the literature as well as on the previous experimental findings was made to identify potential Itch targets in MSCs. Because Itch executes its functions on the protein level through posttranslational modifications, expression level of potential substrates was primarily analyzed by Western Blot.

2. MATERIAL AND METHODS

Reagents and equipment with corresponding manufacturer and country are listed in appendix (*Table 8*).

2.1 Mice.

The B6.C3H(101)-In(2a;Itch)18H mouse strain (hereafter referred to as 'Itch$^{-/-}$') has been previously described (Hustad et al., 1995). This mouse resulted from induced mutagenesis experiments on the agouti locus. This strain carries the inversion In(2a;Itch) (synonyms: nonagouti 18 Harwell *or* a^{18H} mutation) on C57BL/6 (B6) background and the phenotype has previously been described (Hustad et al., 1995). It was postulated that an inversion on chromosome 2 affected another gene besides the agouti locus. Subsequent studies on that mouse led to the discovery of Itch and demonstrated a disruption of the gene that results in a null allele (Perry et al., 1998).

Mice were kept in the Institutional Animal Care Facility at Columbia University School of Medicine under specific pathogen-free conditions. All protocols were approved by the Institutional Animal Care and Use Committee of Columbia University Medical Center.

Heterozygous breeding pairs (Itch$^{+/-}$ X Itch$^{+/-}$) and homozygous breeding pairs (Itch$^{+/+}$ X Itch$^{-/-}$) were set up to obtain Itch$^{-/-}$ mice. Gender-matched littermates with either Itch$^{+/+}$ or Itch$^{+/-}$ genotype were used as controls (Ctrl). Itch$^{+/-}$ mice show no altered phenotype. DNA for genotyping was isolated from ear clips. Polymerase chain reaction (PCR) was performed with a common reverse primer (5′-TCTATGCTCTGTTGTCTCCCATGC-3′) and specific forward wild-type (5′-ATCGTCTACTCACCCCACATAAGG-3′) and forward knock-out (5′-AAGAAGCAGCAGAGACAACGAGTG-3′) primers. Products of 194 bp (wild-type - common primers) and 294 bp (knock-out - common primers) were obtained and analyzed on an agarose gel. Mice were sacrificed for experiments at 6-8 weeks of age unless otherwise stated.

2.2 Cell Preparation.

2.2.1 Bone Cell Isolation.

Long bones (femora and tibiae) were harvested, cleaned from soft tissue with forceps and put in phosphate buffered saline (PBS) with 2 % fetal calf serum (FCS) on ice as previously described (Rathinam et al., 2011). Bones from 1 - 4 mice per genotype were pooled per experiment. MSCs were isolation from bone pieces based on Morikawa et al. (Morikawa et al., 2009). Bone ends were cut off and bone marrow was flushed out using a 27-gauge needle, yielding pale bones. Bones were crushed with scissors and a pestle into fragments of 1 mm maximum. All fragments were transferred into PBS and digested with collagenase P (2.5 mg/ml) and incubated at 37 °C for 45 minutes. Cell suspension was vortexed every 15 minutes. After incubation, the bone suspension was diluted with PBS, vortexed rigorously and supernatants were collected for three times. Collected cell suspension was filtered through a 70 µm cell strainer and centrifuged at 260 g for 5 minutes. Total bone cell pellet was resuspended in ACK (ammonium-chloride-potassium) red cell lysis buffer and incubated at room temperature for 2 minutes. The reaction was stopped through dilution with PBS. Total bone cells were centrifuged and resuspended in desired medium and volume. Cells were counted in a Neubauer chamber, only trypan blue-negative cells were included.

2.2.2 Bone Marrow Cell Isolation.

Bone marrow was isolated as previously described (Rathinam et al., 2011). Long bones (femora and tibiae) were harvested, cleaned from soft tissue with forceps and put on ice in PBS with 2 % FCS. Bone ends were cut off, bone marrow was flushed out using a 27-gauge needle and collected. Bone marrow was centrifuged (260 g, 5 minutes), resuspended in ACK red cell lysis buffer and incubated at room temperature for 2 minutes. Cell suspension was diluted with PBS and filtered through a 70 µm cell strainer. Bone marrow cells were centrifuged and resuspended in desired medium and volume. Cells were counted in a Neubauer chamber, only trypan blue-negative cells were included.

2.3 Cell Culture.

2.3.1 MSC Culture.

Bone cells were isolated and resuspended in MSC culture medium. Unless otherwise stated, MSCs were cultured in commercially available complete Mesencult Medium (Basal Medium + 10 % Stimulatory Supplement (medium-containing)) as previously described (Hussain et al., 2012). Complete Mesencult Medium was supplemented with 2 mM L-Glutamine and 1 % Penicillin-Streptomycin. Cells were kept at 5 % CO_2 and 37 °C in humidified incubators.

MSC adherent cultures were performed as previously described (Morikawa et al., 2009). Bone cells were seeded in 6 well-plates (2 ml per well) at 1 – 2 x 10^5 cells per cm^2. 24 hours after plating, non-adherent cells were removed with the first medium change. The second medium change was performed after 5 - 7 days. In subsequent passages (P) medium was changed every 3 - 4 days. MSCs were passaged at 70 – 90 % confluency. For this purpose, medium was removed, cells were washed with PBS and incubated with 0.25 % trypsin-EDTA (ethylenediaminetetraacetic acid) for 3 minutes. Reaction was stopped by the addition of culture medium and cells were collected.

Hematopoietic cells were removed from bone cell cultures at passage P2 - P3 through immunodepletion as previously described (Xu et al., 2010). For this purpose, collected bone cells were centrifuged (260 g, 5 minutes) and resuspended in MACS buffer (PBS with 2 % FCS and 2mM EDTA). Cells were incubated with biotin-conjugated anti-mouse CD45 (1:5) and anti-mouse TER119 (1:10) antibodies on ice for 15 minutes. Cells were washed, resuspended in MACS buffer and incubated with streptavidin Micro Beads (200 µl in 500 µl total volume). Cells were washed, resuspended in MACS buffer and separated on MACS midi columns. CD45 and TER119 negative cells were collected, centrifuged and resuspended in culture medium and reseeded. Purified MSCs were seeded at 2000 cells per cm^2. In vitro assays were performed on MSCs at P3 - P10.

2.3.2 CFU-F Assay.

CFU-F assays were performed based on Morikawa et al. (Morikawa et al., 2009). Cells were seeded at 1 x 10^5 per cm^2 in 6 well-plates in MSC culture medium. Non-

adherent cells were removed after 24 hours with the first medium change. Second medium change was conducted after 5 - 7 days and then medium was changed every 3 - 4 days. On day 14, culture plates were set on a grid and colonies were counted on light microscopy by meandering thoroughly over the grid. Colonies with > 30 cells with typical spindle-shaped MSC morphology were counted.

2.3.3 MSC Differentiation Experiments.

Bone cell suspension *(p. 17)* was analyzed by flow cytometry to assess MSC frequency. Cell suspensions of Itch$^{-/-}$ and control mice were diluted to contain equal numbers of MSCs per ml (e. g. 500 MSCs per ml). Total bone cells with equal absolute numbers of MSCs were seeded in MSC culture medium. 24 hours later, non-adherent cells were removed and medium was changed to respective differentiation medium.

Osteogenic assay procedure:

Total bone cells containing 500 PαS MSCs were seeded in a 10 cm dish. After 24 hours, medium was changed to commercially available osteogenic differentiation medium with dexamethasone, ascorbate and b-glycerophosphate. Cells were cultured according to the manufacturer's recommendations. Medium was changed every 3 - 4 days for 3 weeks.

After three weeks, osteogenic cultures were stained with alizarin red according to the manufacturer's recommendations. Cultures were washed with PBS, fixed with 10 % formalin and washed with distilled water. Alizarin red salt was dissolved in distilled water (2 g / 100 ml) and filtered. Cultures were incubated with alizarin red staining solution for 45 minutes at room temperature. Culture plates were washed with distilled water, filled with PBS and kept sealed. Digital images were acquired with AxioCam MRm Rev 3. Quantification of alizarin red was made using ImageJ software (Schneider et al., 2012). Alizarin red positive areas were identified via color threshold using undifferentiated controls.

CFU-Osteoblast (CFU-Ob) assay:

Total bone cells containing 500 PαS MSCs were seeded in a 10 cm dish. After 24 hours, medium was changed to commercially available osteogenic differentiation

medium. Cells were cultured according to the manufacturer's recommendations. Medium was changed every 3 - 4 days for 10 days. For quantification of colonies culture plates were set on a grid. Colonies were counted on light microscopy by meandering thoroughly over the grid. Colonies with > 30 cells were counted.

Adipogenic assay procedure:

Total bone cells containing 500 PαS MSCs were seeded in one well on a 6 well-plate (9 cm^2). After 24 hours, medium was changed to commercially available adipogenic induction medium with human-insulin, dexamethasone, indomethacin and IBMX (3-isobuty-l-methyl-xanthine). Cells were cultured according to the manufacturer's recommendations. After 3 days of culture, medium was changed to the commercially available adipogenic maintenance medium (human-insulin containing). 3 cycles of induction and maintenance culture were performed. Cells were cultured for another 3 days in fresh adipogenic maintenance medium after the last cycle.

Adipogenic cultures were stained with Oil Red O according to the manufacturer's recommendations. Cultures were washed with PBS, fixed with 10 % formalin and washed with distilled water. Cultures were incubated with 60 % isopropanol at room temperature for 5 minutes. Oil Red O powder was dissolved in 99 % isopropanol (300 mg per 100 ml). 3 parts of the solution were mixed with 2 parts of distilled water and subsequently filtered. 60 % isopropanol was discarded and cultures were incubated with staining solution for 5 minutes. Plates were thoroughly rinsed with water, filled with distilled water and kept sealed. Digital images were acquired with AxioCam MRm Rev 3. Quantification of Oil Red O was made using ImageJ software (Schneider et al., 2012). Oil Red O positive areas were identified via color threshold using undifferentiated controls.

2.4 Flow Cytometry.

2.4.1 Surface Marker Analyses.

Flow cytometry was performed as previously described (Rathinam et al., 2011) on total bone cells ex vivo as well as on cultured MSCs. Total bone cells were filtered

at least three times through a 70 µm nylon mesh during cell isolation and sample preparation prior to acquisition. Cultured cells were trypsinized for sample preparation.

Cells were resuspended in 100 µl PBS with 2 % FCS for staining. The antibody panels and concentrations were established and optimized for a reliable identification of the desired target populations. Antibodies and concentrations that were used in the study are listed in *Table 3*.

Table 3. List of monoclonal antibodies used for flow cytometry.

Antibody	Clone	Concentration, bone cells ex vivo	Concentration, cultured cells	Manufacturer
FITC anti-mouse CD90.2	30-H12	2:100	1:100	Becton, Dickinson and Company (BD), Franklin Lakes, USA
PE anti-mouse Sca-1	D7	1:200	1:200	BD
APC anti-mouse PDGFRα	APA5	1:100	1:100	BioLegend, San Diego, USA
APCCy7 anti-mouse CD45.2	104	5:100	1:100	BD
APCCy7 anti-mouse TER119	TER119	2.5:100	1:100	BD

Cells were analyzed by flow cytometry with LSRII using FACSDIVA software for acquisition. Compensation and gating strategies were established using respective isotype controls. Data were analyzed with FlowJo software.

2.4.2 Viability Assessment Through Propidium Iodide.

Propidium iodide staining was performed as previously described (Kriegel et al., 2009). MSCs were investigated at 50 – 70 % confluency. For medium starvation, MSC culture medium was removed, cells were washed with PBS and Dulbecco's Modified Eagle Medium (DMEM) with 2% bovine serum albumin (BSA) and 1% Penicillin-Streptomycin was added.

Prior to analysis, medium was removed, cells were washed with PBS and incubated with trypsin-EDTA (0.25%) for 3 minutes. Reaction was stopped by the addition of culture medium. All subsequent steps were performed on ice. Cells were collected

and centrifuged (260 g, 5 minutes). Cells were resuspended in 100 µl PBS with 2 % FCS and 0.1 µg of propidium iodide. Samples were analyzed with FACScan or LSRII and acquisition was conducted using CellQuest or FACSDIVA software. Data were analyzed with FlowJo software.

2.4.3 CFSE Labeling Studies.

Carboxyfluorescein succinimidyl ester (CFSE) permeates cell membranes and covalently binds to intracellular molecules. The intracellular fluorescent dye is divided between both daughter cells upon cell division. CFSE dilution was monitored to assess cell proliferation. CFSE labeling was performed with CFSE Cell Proliferation Kit as previously described (Rathinam et al., 2011). MSCs were pre-warmed at 37 °C after collection through trypsinization in DMEM without supplements. CFSE was prepared in Dimethyl sulfoxide (DMSO) and diluted to 5 µM in the final staining solution with DMEM (no supplements). Cells were incubated in 3 ml staining solution for 10 minutes at 37 °C. Serum containing medium was added. Cells were centrifuged (260 g, 5 minutes) and washed once in serum-containing medium. Finally, MSCs were resuspended in MSC culture medium and seeded at 2000 cells per cm^2. An aliquot of cells was immediately analyzed by flow cytometry to determine initial labeling efficiency (d0). Cells were collected by trypsinization and analyzed on day 2, 4 and 6 again. Samples were analyzed with FACScan or LSRII and acquisition was conducted using CellQuest or FACSDIVA software. Data were analyzed with FlowJo software.

2.5 Osteoblast Numbers in H&E Stained Bone Sections.

Bone sections were taken as previously described (Wu et al., 2009). Femora of mice were harvested and thoroughly cleaned from soft tissue with forceps. Bones were fixed in 4% paraformaldehyde.

The following steps were performed by the Central facility for musculoskeletal disorders at Yale Medical School: Decalcification, preparation of sections and staining with hematoxylin and eosin.

H&E (hematoxylin and eosin) stained sections were received. Digital images were acquired with AxioCam MRm Rev 3. Region of interest was defined within the secondary spongiosa of the distal femur proximal to the growth plate. Bone perimeter (B.Pm) and osteoblasts (N.Ob) were quantified as previously described (Parfitt et al., 1987; Jilka et al., 1999) with ImageJ software (Schneider et al., 2012).

2.6 Micro-CT Analyses of Bones.

Micro-CT analysis was performed as previously described (Yao et al., 2017). Femora of mice were harvested and thoroughly cleaned from soft tissue with forceps. Bones were fixed in 70 % ethanol at 4 °C. Micro-CT analysis was performed at the Yale University School of Medicine Micro-CT Core Facility using a Scanco µCT-35 instrument. Technical set up and data acquisition was conducted by the Core Facility. Trabecular bone was analyzed within the endosteal borders of the distal femoral metaphysis (1 mm from the growth plate and extending 1 mm proximally) to include the secondary spongiosa. Cortical bone was analyzed distally from the diaphyseal mid-point between the growth plates. Preprocessed 2D and 3D data were received. Analyses were finalized in accordance with current recommendations (Bouxsein et al., 2010).

2.7 Western Blot and Immunoprecipitation.

2.7.1 Protein Extraction.

MSCs were collected by trypsinization, counted and washed once in PBS. Protein extraction was performed as previously described (Rathinam et al., 2011). Cell pellet was dried and cells were lysed in cell lysis solution. Cell lysis solution was prepared with commercially available Cell Lysis Buffer and Protease Inhibitor Cocktail complete (EDTA-free) according to the manufacturer's instructions. 1 x 10^6 cells were lysed in 100 µl of cell lysis solution and incubated on ice for 20 minutes. Solution was centrifuged at 14,000 g for 10 minutes at 4 °C. Supernatant containing proteins was collected. Protein lysates were stored at -80 °C.

2.7.2 Western Blot.

Western Blot was performed as previously described (Rathinam et al., 2011). Proteins were thawed and handled on ice. NuPAGE LDS sample buffer and 2-Mercaptoethanol were added and proteins denaturized at 75 °C for 10 minutes.

8 - 12 % SDS-PA (sodium dodecyl sulfate–polyacrylamide) gels were casted using distilled water, Tris buffer, 8 - 12% SDS (sodium dodecyl sulfate) solution, acrylamide, APS (ammonium persulfate) and TEMED (N,N,N',N'-tetramethylethylenediamine).

A protein standard was loaded in one well of each gel. Proteins were subjected to gel electrophoresis (SDS-PAGE) in electrophoresis chambers at 110 V. Proteins were transferred in tanks for wet electroblotting on a magnetic stirrer to PVDF (polyvinylidene difluoride) membranes for 90 minutes at 130 V at 4 °C.

Membranes were blocked in 5 % skim milk or in 5 % BSA for the detection of phosphorylated proteins for 2 hours at room temperature. Membranes were stained in PBS with 0.5 % BSA. Membranes were incubated with primary antibodies at 4 °C overnight. Membranes were incubated with secondary antibodies conjugated to HRP (horseradish peroxidase) for 1 hour at room temperature. Primary and secondary antibodies that were used in this study are listed in *Table 4* and *Table 5*. After primary and secondary antibody staining, membranes were washed 4 x 10 minutes in PBS with 0.05 % Tween 20. Membranes were incubated with SuperSignal West Pico Chemiluminescent Substrate Kit according to the manufacturer's recommendation for 1 - 2 minutes at room temperature for visualization on Image station 440.

Table 4. List of primary antibodies used for Western Blot.

Antibody	Clone	Species	Concentration	Manufacturer
Actin	I-19	goat	1:2000	Santa Cruz Biotechnology (Santa Cruz), Dallas, USA
Akt (pan)	C67E7	rabbit	1:1000	Cell Signaling Technology (Cell Signaling), Danvers, USA
Cleaved Notch1 (Val1744)	D3B8	rabbit	1:1000	Cell Signaling

Itch	Clone32	mouse	1:500	BD
MEK1/2	D1A5	rabbit	1:1000	Cell Signaling
Notch1	C44H11	rabbit	1:1000	Cell Signaling
p38α MAPK	7D6	rabbit	1:1000	Cell Signaling
p44/42 MAPK (ERK1/2)	137F5	rabbit	1:1000	Cell Signaling
phospho-Akt (Thr308)	244F9	rabbit	1:500	Cell Signaling
phospho-MEK1/2 (Ser221)	166F8	rabbit	1:500	Cell Signaling
phospho-NF-κB p65 (Ser536)	93H1	rabbit	1:500	Cell Signaling
phospho-p38 MAPK (Thr180/Tyr182)	12F8	rabbit	1:500	Cell Signaling
phospho-p44/42 MAPK (ERK1/2)(Thr202/Tyr204)	197G2	rabbit	1:500	Cell Signaling
phospho-PDK1 (Ser241)	C49H2	rabbit	1:500	Cell Signaling
phospho-PI3 Kinase p85/p55(Tyr458/Tyr199)	n.a.	rabbit	1:500	Cell Signaling
phospho-Src (Tyr527)	n.a.	rabbit	1:500	Cell Signaling

Table 5. List of secondary antibodies used for Western Blot.

Antibody	Concentration	Manufacturer
HRP-conjugated anti–mouse IgG	1:2000	Cell Signaling
HRP-conjugated anti–rabbit IgG	1:2000 to 1:4000	Cell Signaling
HRP-conjugated anti–goat IgG	1:6000	Santa Cruz

2.7.3 Co-Immunoprecipitation.

Co-Immunoprecipitation was performed as previously described (Rathinam et al., 2011) with the commercially available Pierce Co-Immunoprecipitation Kit. Anti-Cleaved Notch 1 and anti-Itch antibodies *(Table 4)* were immobilized with the provided resin. As negative controls rabbit IgG (for anti-Notch1) and mouse IgG (for anti-Itch) were immobilized. Protein samples were isolated from ICN1^{high}, Itch^{high} and GFP^{high} MSCs *(p.28)* and diluted with the provided IP Lysis / Wash buffer to 500 µl. Proteins were incubated on a mixer overnight at 4 °C with the resin-conjugated antibodies at a final dilution of 1:100. Flow-through of three washes were collected and analyzed as controls. Co-IP elute was prepared with the provided sample buffer in the kit. SDS-PAGE and Western Blot were performed as described above *(p.23)*.

2.8 Real-Time PCR.

RNA extraction, cDNA synthesis and Real-Time PCR were performed as previously described (Rathinam et al., 2011). RNA was isolated from in vitro cultured MSCs. Cells were trypsinized and lysed for RNA extraction using the commercially available RNeasy Mini Kit according to the provided instructions. RNA was stored at -80 °C. cDNA was synthesized with Invitrogen SuperScript II Reverse Transcriptase and Oligo(dT)12-18 Primer according to the manufacturer's instructions. Reactions were performed on a T100 Thermal Cycler. Real-Time PCR was performed with the SYBR green method and ROX reference dye using the commercially available Kapa SYBR Fast mastermix according to the manufacturer's instructions. Real-Time PCR primers were designed with PerlPrimer (Marshall, 2004). Intended specificity of all primer pairs was validated by melt curve analysis and agarose gel electrophoresis. Real-Time PCR primers are listed in *Table 6*. Samples were run in doublets on a CFX Connect Real-Time PCR Detection System machine. Data was acquired and analyzed with CFX manager. Hprt (Hypoxanthine-guanine phosphoribosyltransferase) was used as a housekeeping gene. Fold-change in gene expression in corresponding samples was calculated with the delta-delta CT method (Livak and Schmittgen, 2001).

Table 6. Real-Time PCR primer.

Gene	Forward (5'-3')	Reverse (5'-3')
Hes1	GCTACCGATCACTAAGTAGCCC	GAATGCCGGGAGCTATCTTTC
Hes5	GAGATGCTCAGTCCCAAGGAG	GCGAAGGCTTTGCTGTGTTTC
Hey1	GAGAATGGAAACTTGAGTTCGG	CCACAGTCATCTGCAAGATCTC
Heyl	GCCTTTCTGAATTGCGACGA	CATCAAAGAACCCTGTGCCA
Hprt	AGCTACTGTAATGATCAGTCAACG	AGAGGTCCTTTTCACCAGCA
Itch	AGACCAGAACCTCTACCTCCT	ATCAGTTCTCTTCTCCCATCCA
Notch1	GTACAGAAGGTTACACAGGGA	AGAGGTAGGAGTTGTCACGG
Notch2	GATTCTGATCCGCAACCGTG	GGTGTCTCTTCCTTATTGTCCTG
Notch3	AGCGACTTGATTTCCCATACC	GCCATGTTCTTCATTCCCAG
Notch4	CTCTTGCCACTCAATTTCCCT	TTGCAGAGTTGGGTATCCCTG

2.9 Itch Cloning.

The 2595 bp long Itch coding sequence was amplified from MSC cDNA (primer sense: 5'-ACGAGATCTATGTCTGACAGTGGACCACAG-3' and primer antisense: 5'-ACGGTCGACTTACTCTTGTCCAAATCCTTC-3') using Invitrogen Platinum Taq DNA Polymerase High Fidelity and a gradient annealing temperature. The PCR product was cut out of an agarose gel and extracted with QIAquick Gel Extraction Kit according to the manufacturer's instructions. The gel purified PCR product was cloned into pCR-XL-TOPO vector that is provided with Invitrogen TOPO XL PCR CloningKit according to the manufacturer's instructions. This kit utilized TA cloning technique that allowed direct transformation of the reaction product into the provided TOP10 E. coli. Transformation was performed according to the manufacturer's instructions for One shot TOP10 chemically competent E. coli. Transformed bacteria were incubated on LB agar plates containing 50 µg/mL kanamycin overnight at 37 °C. Single colonies were picked and incubated in LB medium with kanamycin at 37 °C overnight. Plasmid purification was performed with QIAprep Spin Miniprep Kit according to the manufacturer's instructions. Plasmids were first screened through restriction enzyme digestion for correct insertion. Inserts of plasmids with the correct restriction pattern were sequenced. A plasmid with the correct Itch sequence was chosen and digested with BglII and SalI restriction enzymes according to the manufacturer's instructions. The released insert was gel purified. pGFP-RV vector was digested with BglII and XhoI restriction enzymes and with phosphatase (Quick CIP, Quick Dephosphorylation Kit) according to the provided instructions. Insert and vector were ligated with T4 DNA Ligase according to the manufacturer's instructions. Ligation mix was transformed into TOP10 chemically competent E. coli and colonies were picked on LB agar plates with ampicillin 100 µg/ml as described above. Individual colonies were grown in liquid LB medium with ampicillin and plasmids were isolated with a mini preparation as described above. Correct insertion into pGFP-RV vector was validated through restriction enzyme digestion.

2.10 Virus Production and Transduction of Cells.

Sufficient amounts of the generated Itch-pGFP-RV, pGFP-RV backbone, pVSV-G and MSCV ICN1-IRES-GFP (Rathinam et al., 2006) were produced in bacterial cultures and purified with plasmid maxiprep kit according to the manufacturer's instructions. Production of retroviral particles and transduction has been described previously (Rathinam et al., 2011). Retroviruses were produced in Phoenix-GP cells. Phoenix-GP packaging cell lines express gag-pol. The co-transfection with desired envelope and retroviral vectors allows the production of replication-incompetent pseudotyped viral particles (Swift et al., 2001). Phoenix-GP cells were washed with PBS and cultured in Gibco Opti-MEM for transfection at 70 % confluency. Invitrogen Lipofectamine 2000 was used as described in the provided protocol for transfection. Cells were transfected on 10 cm plates in 10 ml medium with 50 µg of desired plasmid DNA, 25 µg VSV-G plasmid and 150 µl Lipofectamine. Following overnight incubation, medium was changed to DMEM with 20 % FCS. Virus containing supernatant was collected after 24, 48 and 72 hours, pooled, filtered through 0.22 µm and stored at -20 °C. In vitro cultured MSCs were transduced with virus mixed with fresh MSC culture medium (3:1) with 8 µg/ml polybrene overnight and further cultured in MSC culture medium. Flowcytometric analyses of GFP expression revealed that transduction efficiency was 5 - 15 %. Because of relatively low efficiency but stable GFP expression over several passages, transduced MSCs were expanded and sorted. GFP-high-expressing MSCs were sorted with a FACSAria II at the Flow Cytometry Core, Department of Microbiology & Immunology, Columbia University. GFP-high cells that were previously transduced with MSCV ICN1-IRES-GFP, Itch-pGFP-RV and pGFP-RV empty backbone vector were further cultured and are hereinafter referred to as ICN1^{high}, Itch^{high} and GFP^{high} MSCs, respectively.

2.11 Statistical Analyses.

Statistical analyses and visualization were done with the help of GraphPad Prism version 5 (GraphPad Software Inc., USA) unless otherwise stated. Two-sided, unpaired Student's t-test was used to test statistical significance of hypotheses.

Differences above $P \geq 0.05$ were considered not statistically significant. Statistical significance is denoted as *, $P < 0.05$; **, $P < 0.01$; ***, $P < 0.001$. P values less than 0.001 are shown as < 0.001.

2.12 Reagents and Equipment.

Reagents and equipment are listed in appendix *(Table 8)*.

3. RESULTS

3.1 Investigation of the Mesenchymal Stem Cell Pool in Itch-Deficient Mice.

3.1.1 Reduced Colony Forming Unit Fibroblasts (CFU-F) in the Absence of Itch.

First experiments to address the MSC pool in Itch$^{-/-}$ mice employed a colony forming unit (CFU-F) assay. The CFU-F assay relies on the plastic-adherence of MSCs in culture and historically led to the discovery of non-hematopoietic progenitor cells within the bone (Friedenstein et al., 1970).

To obtain a cell suspension of total bone cells, femora and tibiae were harvested. Then bone marrow was flushed out and solid bones were crushed into pieces. Fragments were collagenase digested and filtered through a cell strainer. For individual experiments, long bones of two mice were pooled per genotype. Cells were seeded at 1 x 10^5 per cm² and non-adherent cells were removed after 24 hours. Medium was changed every 3 - 4 days. Colonies were counted on day 14 *(Figure 2 photos A - C)*.

Four independent experiments revealed **significantly reduced colony numbers in Itch$^{-/-}$ bone cell cultures as compared with control cultures** (9.75 ± 2.02 vs. 2.50 ± 1.32 per 1 x 10^6 cells, P = 0.0238) *(Figure 2 plot D, app. Table 9)*. **These results suggested significantly reduced CFU-F in Itch$^{-/-}$ bone (bone-cell-derived CFU-F).** Of note, there was **no morphological difference between control and Itch$^{-/-}$ cultures in the large, highly translucent, spindle-shaped and colony forming cells** *(Figure 2 A & B)*.

It has been established, that MSCs depict a dynamic and stress-responsive stem and progenitor cell compartment (Park et al., 2012). The generic Itch$^{-/-}$ mouse exhibits an excessive hematopoietic stem and progenitor cell (HSPC) pool within the bone marrow (Rathinam et al., 2011). Any disturbance of the HSPC pool may mimic or cause a stress response. This potential stress response may attract MSC evasion preferentially to the marrow spaces.

To investigate Itch$^{-/-}$ MSCs within the bone marrow cavity, CFU-F assays were performed on bone marrow (bone-marrow-derived CFU-F). For this purpose, bone marrow cells were seeded at 1 x 10^5 per cm² and non-adherent cells were removed

after 24 hours. Culture medium was changed every 3 - 4 days. Colonies were counted on day 14.

Analysis of two independent experiments revealed a **trend towards lower numbers of bone-marrow-derived CFU-F in Itch$^{-/-}$ mice as compared with control mice** (10.50 ± 2.50 vs. 1.5 ± 0.50 per 1 x 10^6 cells, P = 0.0717) *(Figure 2 E, app. Table 10)*. This tendency of reduced bone-marrow-derived CFU-F in Itch$^{-/-}$ mice resembled the above-mentioned findings of bone-cell-derived CFU-F.

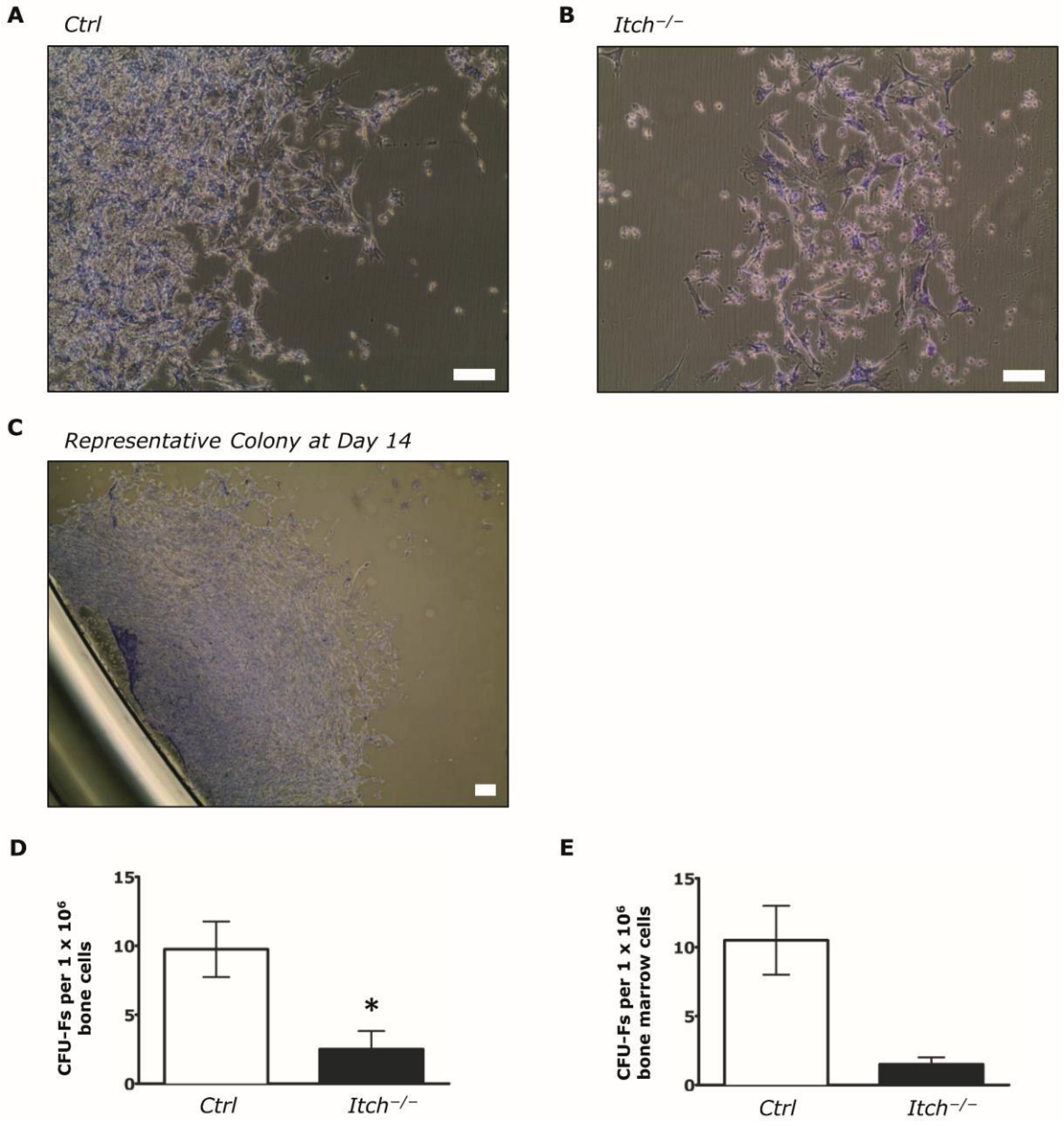

Figure 2. Reduction of CFU-Fs in Itch$^{-/-}$ mice. Cells were seeded at 1x10^5 cells per cm^2. Non-adherent cells were removed after 24 hours. Medium was changed every 3 - 4 days. Colonies were counted at day 14. (A & B) MSCs depict a typical spindle-shaped morphology. Bars indicate 100 µm. Giemsa staining (for illustration only). (A) Control MSCs and (B) Itch$^{-/-}$ MSCs. (C) Representative colony at day 14. Colonies with more than 30 cells were counted. Bar indicates 100 µm. Giemsa staining (for illustration only). (D & E) CFU-Fs at day 14 of culture per 1 x 10^6 cells. (D) Culture of total bone cells (N = 4). (E) Culture of bone marrow cells (N = 2). All data represent mean ± SEM. Two-tailed Student's t tests were used to assess statistical significance.

3.1.2 Reduced PαS MSCs in Itch-Deficient Mice.

Since the discovery of CFU-F within the bone marrow the concept of MSCs has substantially changed through the implementation of single cell analyses and in vivo techniques. To date, flow cytometry allows the prospective identification of MSCs. To identify MSCs in the presence and absence of Itch in vivo, the previously established immunophenotype CD45−TER119−PDGFRα+Sca-1+ (PαS MSCs) was utilized. PαS MSCs have been experimentally validated to exhibit highest CFU-F enrichment. Upon systemic transplantation they generate osteoblasts and adipocytes (Morikawa et al., 2009).

This flow cytometry experiment was performed on total bone cells. Two mice were pooled per genotype. Bone cell suspension was filtered through a cell strainer for at least three times during the processes of cell isolation, counting and sample preparation. The antibody panel and concentrations were established and optimized for reliable identification of the PαS population.

Figure 3 A depicts the applied gating strategy. The first gate (G1) comprises all potentially viable cells in forward scatter (FSC) and side scatter (SSC). Through the inclusion of the CD45 and TER119 negative fraction, all non-hematopoietic cells are identified (G2). PαS MSCs represent a distinct population of PDGFRα positive as well as Sca-1 highly positive cells (G3).

Mice of both genotypes exhibited **comparable percentages of non-hematopoietic cells (CD45−TER119−). Itch$^{-/-}$ mice exhibited decreased relative frequencies of CD45−TER119−PDGFRα+Sca-1+ MSCs** *(Figure 3 A)*. In five independent experiments **a 2 to 3-fold reduction of PαS MSC relative frequency could be documented in Itch$^{-/-}$ mice.**

Murine MSCs express the surface marker CD90 (Thy-1) in vivo (Morikawa, et al., 2009). **PαS subsets of Itch$^{-/-}$ and control mice expressed similarly high levels of CD90** *(Figure 3 B)*.

To determine absolute numbers of MSCs, the total yield of bone cells from preparation of two mice was counted. Flowcytometric analysis was performed and absolute numbers of MSCs were calculated. Analysis of five independent experiments revealed **a significant absolute reduction of MSCs in Itch$^{-/-}$ mice**

(1303 ± 257 vs. 555 ± 106 per 1 x 10^6 total bone cells, P = 0.0273) *(Figure 3 C, app. Table 11)*.

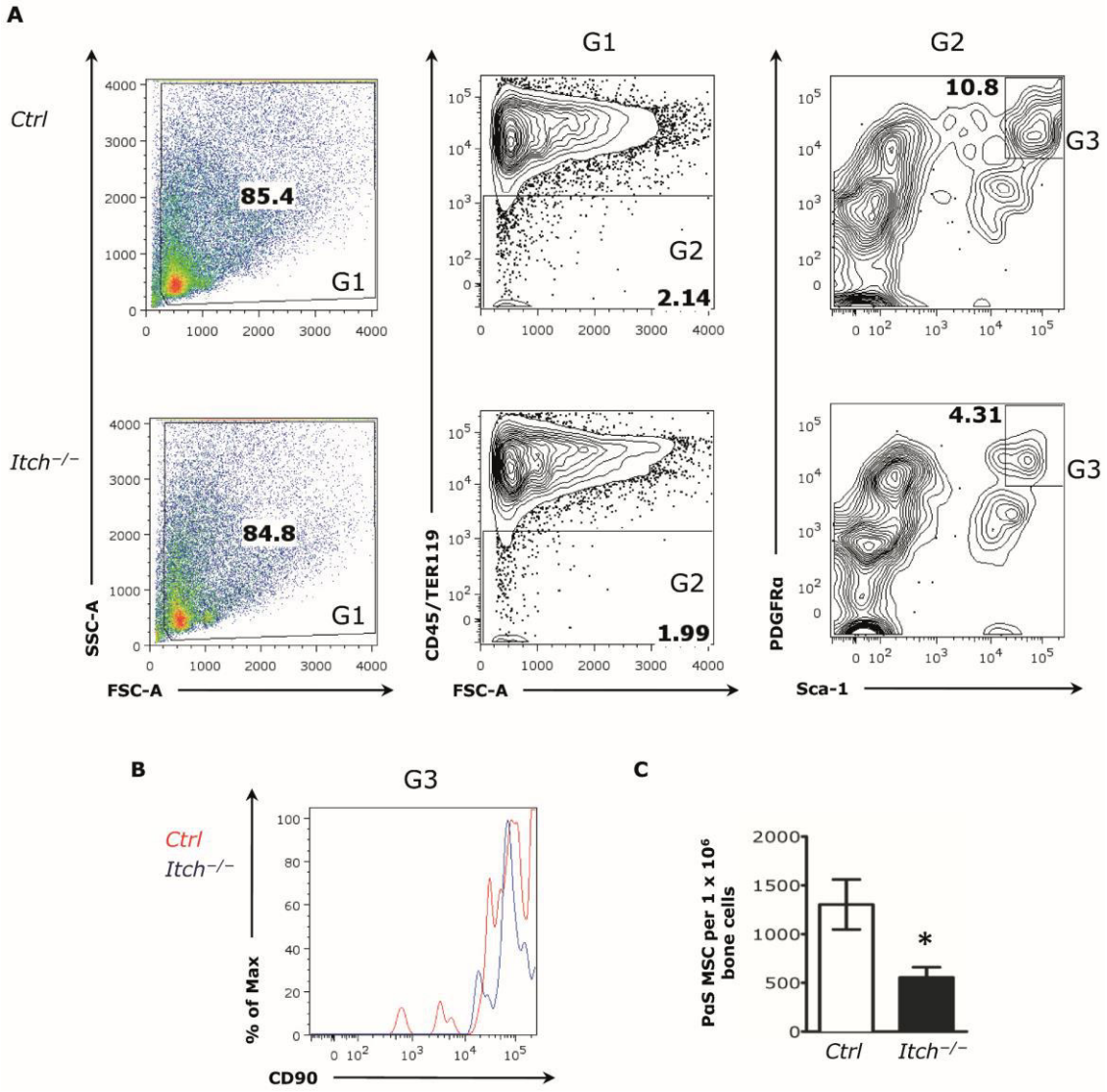

Figure 3. Reduction of PαS MSCs in Itch$^{-/-}$ mice. (A) Flow cytometry was performed on freshly isolated total bone cells (pool of two mice per genotype). The first gate (G1) comprised potentially viable cells. Then, non-hematopoietic cells (CD45-TER1119-) were gated (G2). Among the nonhematopoietic compartment the PαS fraction (PDGFRα+Sca-1+) was identified (G3). The relative frequencies (%) of the gated fractions are indicated. Data are representative of five independent experiments (N = 5). (B) Representative overlay histogram on PαS fraction. X axis indicates level of CD90 expression. Y axis indicates events. Maximum height on Y axis is scaled to 100 % for individual curves. Data is representative of two independent experiments (N = 2). (C) Total bone cells (four femora and four tibiae) were counted and frequency of PαS MSCs was determined by flow cytometry. Absolute numbers of MSCs were normalized to 1 x 10^6 total bone cells in five independent experiments (N = 5) (pool of two mice per genotype). Data represent mean ± SEM. Two-tailed Student's t tests were used to assess statistical significance.

3.1.3 PαS MSCs are Reduced in Itch$^{-/-}$ Mice at Different Ages.

Itch-deficient mice develop signs of autoinflammation at 3 - 4 months of age. On C57BL/6 background they develop severe systemic inflammatory disease involving their skin. Most of the mice die at the age of 4 - 6 months (Hustad et al., 1995).

MSCs have been demonstrated to possess unique immunoregulatory functions and regenerative capacities (Bianco, 2014). Furthermore, it has been shown that MSCs can migrate to sites of infection or wound healing (Mackenzie and Flake, 2001; Wu et al., 2003). Pathogens and proinflammatory cytokines, on the other hand, regulate MSC function (Huang et al., 2006; Pevsner-Fischer et al., 2007).

In the experiments 3.1.1 and 3.1.2 mice at the age of 6 - 8 weeks had been investigated. To examine whether MSC reduction in Itch$^{-/-}$ mice was primarily driven by the systemic autoinflammation, MSC numbers in mice at different ages were analyzed. To this end 2 to 4-week-old mice (“young mice”) as well as one-year-old mice (“old mice”) were studied. Importantly, the young animals showed no obvious signs of inflammation. Mice that survive until one year of age do regularly develop severe signs of illness.

PαS MSCs were detected by flow cytometry as it had been established in experiment 3.1.2. Two to four young mice were pooled per experiment to isolate total bone cells (N = 3 independent experiments). One old mouse was examined per genotype (N = 2 independent experiments). **Frequencies of PαS MSCs were at least two-fold decreased in the young** *(Figure 4 A)* **as well as in the old** *(Figure 4 B)* **Itch$^{-/-}$ mice when compared with the age-matched controls**. These results indicated a robust and age-independent reduction of PαS MSCs in the absence of Itch. Overall, there was a tendency of higher PαS MSC frequencies in younger as compared with older animals of both genotypes.

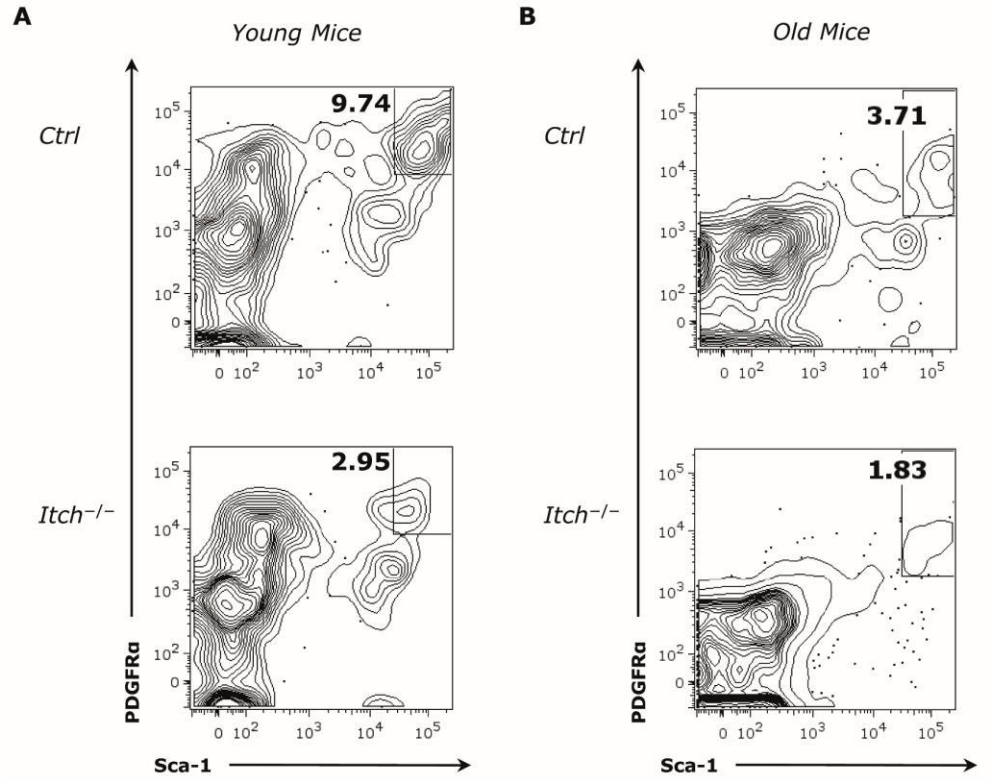

Figure 4. Reduction of PαS MSCs in Itch$^{-/-}$ mice at different ages. Flow cytometry was performed on freshly isolated total bone cells (young: pool of two to four mice per genotype, old: one mouse per genotype). Parent gate includes CD45−TER119− fraction. (A) Four-week-old mice. Data are representative of three independent experiments (N = 3). (B) One-year-old mice. Data are representative of two independent experiments (N = 2). The relative frequencies (%) of the gated fractions are indicated.

3.2 Characterization of Itch$^{-/-}$ MSCs in Vitro.

3.2.1 Itch$^{-/-}$ MSCs Exhibit No Morphological Abnormality.

To study the functional consequences of the loss of Itch in MSCs on a cellular level, primary Itch$^{-/-}$ and control MSC cultures were established. Total bone cells were isolated from a pool of femora and tibiae of two to four mice per genotype. Control cells were seeded at 1 x 10^5 cells per cm². Itch$^{-/-}$ cells were seeded at a higher density of 2 x 10^5 cells per cm² to achieve a similar clonal diversity among MSCs of both genotypes. Non-adherent cells were removed 24 hours after seeding. Subsequent medium changes were performed every 3 - 4 days. MSCs were passaged at 70 – 90 % confluency. First passage (P1) was typically accomplished three weeks after seeding (P0). Cells were detached from the dish by incubation with trypsin. MSCs were reseeded at 2000 cells per cm². At initial passages, bone cell cultures of both genotypes contained a varying proportion of contaminating hematopoietic cells. There was the tendency of a higher proportion of hematopoietic contaminants in the Itch$^{-/-}$ cultures that may be attributed to the hematopoietic phenotype of Itch$^{-/-}$ mice (Rathinam et al., 2011). Beside predominant MSCs, Itch$^{-/-}$ cultures contained a noteworthy fraction of compact and round cells that showed minimal growth. Contaminating cell types within the control culture were highly heterogenous, but compact and round cells were rarely seen.

To achieve efficient MSC expansion and a pure MSC culture at early passages, immunodepletion of hematopoietic cells was performed (Xu et al., 2010). CD45+ and TER119+ cells were separated from MSC cultures through a MACS separation at passage P2 - P3. Compact and round cells within Itch$^{-/-}$ cultures were efficiently depleted using this negative selection step.

Hereafter, MSC cultures of both genotypes contained spindle-shaped and highly translucent cells. No morphological differences in control and Itch$^{-/-}$ MSCs could be observed by light microscopy. Control and Itch$^{-/-}$ MSCs could be passaged for approximately 20 passages (more than 100 days) until growth capacity obviously decreased. The following experiments were performed using MSCs between passages P3 - P10.

3.2.2 Itch$^{-/-}$ MSCs Maintain Their Immunophenotype.

MSC identity can be assessed by immunophenotyping. It has been established, that in vitro culture affects not only functional properties but also surface marker expression of MSCs (Bara et al., 2014). Furthermore, MSC immunophenotypes differ between species and also between mouse strains (Peister et al., 2004). Among the proposed markers for in vitro cultured murine MSCs are Sca-1 and CD90 (Morikawa et al., 2009). **Sca-1 and CD90 expression was evaluated in culture at various timepoints by flow cytometry. There was no difference in the expression levels of these MSC markers in Itch$^{-/-}$ as compared with control MSCs** *(Figure 5 A & B)*. The higher the passage, the expression pattern of Sca-1 and CD90 became more homogenous within the control as well as in the Itch$^{-/-}$ culture *(Figure 5 B)*.

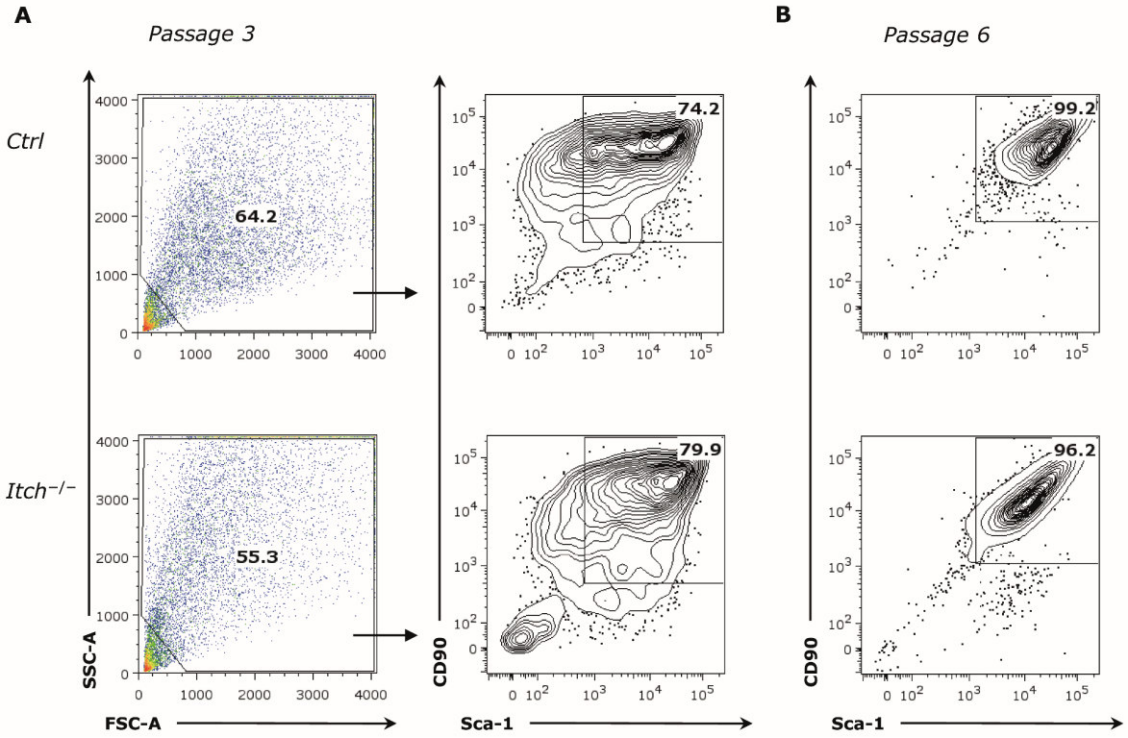

Figure 5. Itch$^{-/-}$ MSCs maintain their immunophenotype in vitro. Flowcytometric analysis of CD90 and Sca-1 expression at various passages. (A) P3 (Day 36 of culture). First gate comprises all potentially viable cells after trypsinization. Second gate marks Sca-1 and CD90 double positive MSCs. Representative experiment (N = 10). (B) P6 (Day 50 of culture). Same gating strategy. Parent gate includes potentially viable cells. Representative experiment (N = 10). In all experiments the relative frequencies (%) of the gated fractions are indicated.

3.2.3 No Alteration of MSC Viability in the Absence of Itch.

Next, the viability of Itch$^{-/-}$ MSCs was evaluated using propidium iodide (PI) staining. Cells that have lost their cellular membrane integrity, i.e. necrotic or apoptotic cells, become positive upon staining with the intercalator PI that can be detected by flow cytometry. MSCs were detached with trypsin prior to staining with PI.

Firstly, **MSCs under steady state culture conditions were investigated. Analysis of three independent experiments revealed no difference in the PI positive fractions of control and Itch$^{-/-}$ MSCs** (60.6 ± 5.3 vs. 64.8 ± 7.2, P = 0.6617) *(Figure 6 A & B, app. Table 12)*.

Secondly, **MSCs were investigated in serum starvation**. For this purpose, MSCs of both genotypes were washed twice with PBS and cultured in serum free medium for 24 hours. As expected, the PI negative fractions were considerably reduced. However, very **similar PI negative relative frequencies between control and Itch$^{-/-}$ MSCs were observed** (two independent experiments) *(Figure 6 C)*.

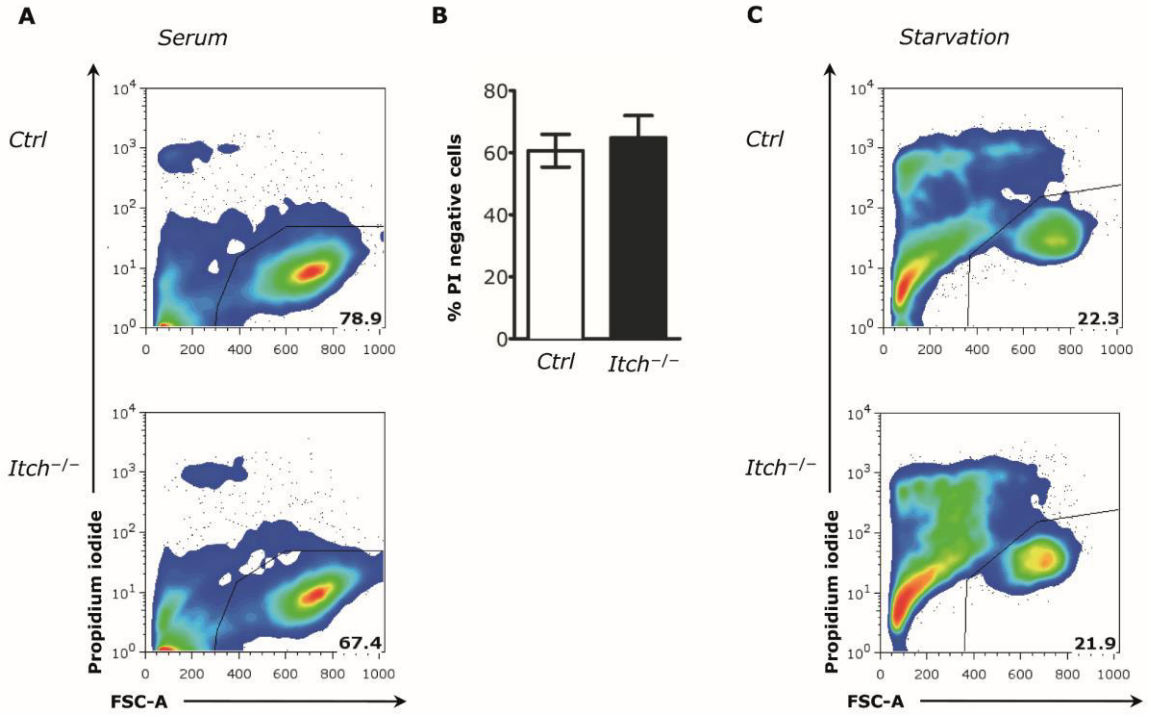

Figure 6. Viability of in vitro cultured Itch$^{-/-}$ MSCs. Flowcytometric analysis of in vitro cultured MSCs. Cells were trypsinized, washed and stained with propidium iodide. (A+B) Serum containing culture medium. (A) Representative analysis. (B) Relative proportion of PI negative MSCs (N = 3). Data represent mean ± SEM. Two-tailed Student's t tests were used to assess statistical significance. (C) Medium starvation. Cells were washed with PBS twice and cultured in serum-free medium for 24 hours. Representative analysis (N = 2). In all experiments the relative frequencies (%) of the gated fractions are indicated.

3.2.4 Hyperproliferation of Itch$^{-/-}$ MSCs.

Itch$^{-/-}$ and control MSCs were stained with CFSE to assess cell proliferation in vitro. Fluorescence intensity was measured by flow cytometry on the consecutive days. Equal fluorescence intensities in cells of both genotypes were confirmed by flow cytometry after the staining procedure (day 0). CFSE intensity was on background level on day 6.

The intracellular dye CFSE is divided between both daughter cells upon cell division. **At day 2 and 4 flowcytometric analysis revealed a reduced CFSE fluorescence intensity in Itch$^{-/-}$ MSCs** in three independent experiments *(Figure 7 A)*. **These results indicate a higher number of cell divisions in Itch$^{-/-}$ MSCs as compared with control MSCs**.

To exclude non-specific differences in the elimination of CFSE dye between MSCs of both genotypes, fluorescence intensity was measured after culture of MSCs in serum free medium. Analysis on day 4 revealed no significant proliferation in MSCs of both genotypes. There was no difference in fluorescence intensity between control and Itch$^{-/-}$ MSCs on day 4 *(Figure 7 B)* (N = 2).

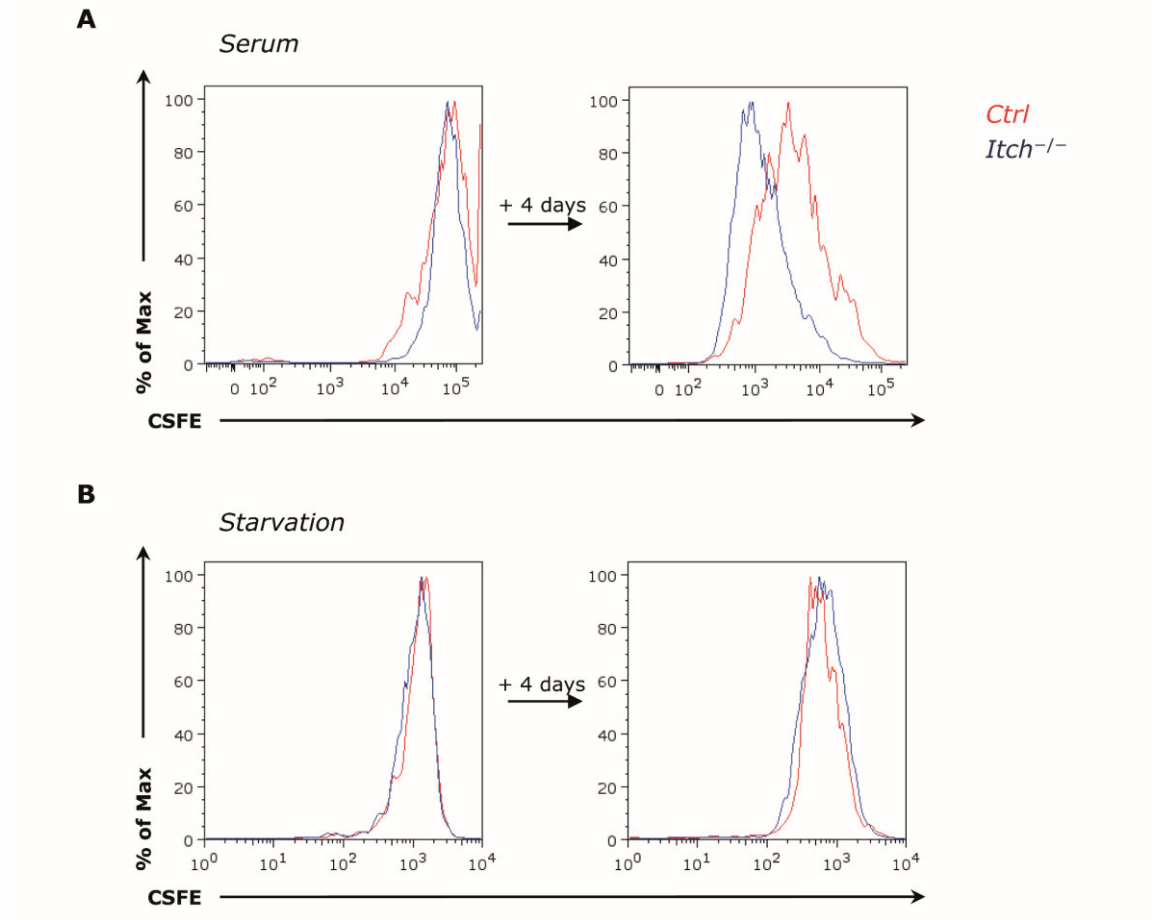

Figure 7. CFSE dilution reveals hyperproliferation of Itch$^{-/-}$ MSCs. In vitro cultured MSCs were labeled with CFSE (day 0). CFSE dilution was determined by flow cytometry on subsequent days. (A & B) Each representative histogram shows CFSE measurement on a particular day. Day 0 (left) and day 4 (right). Results are presented in overlay histograms (Ctrl MSCs = red, Itch$^{-/-}$ MSCs = blue). X axis indicates CFSE fluorescence intensity. Y axis indicates events. Maximum height on Y axis is scaled to 100% for individual curves. (A) Medium containing culture (N = 3). (B) Serum free control culture (N = 2).

3.3 MSC Differentiation Experiments.

3.3.1 Establishing Reproducible Differentiation Conditions.

Next, differentiation capacity of MSCs in the absence of Itch was investigated. Multipotent MSCs give rise to differentiated mesenchymal progeny within the bone, such as adipocytes and osteoblasts in vivo. In vitro differentiation experiments can model the differentiation capacities of MSCs partially. In preliminary experiments, the efficiency of MSC differentiation could be correlated with the number of divisions in culture: Differentiation capacity obviously decreased when a low number of MSC clones was seeded at a low density for maximum expansion. Likewise, differentiation capacity gradually dropped with the number of passages.

Itch$^{-/-}$ and control MSCs differed in frequency at P0 and in proliferation rate over the passages. Hence, the assessment of MSC differentiation capacities in direct comparison was hampered. To circumvent these issues, the following protocol was established to guarantee equal and reproducible baseline conditions that allow a head to head comparison of Itch$^{-/-}$ and control MSC differentiation:

1. Total bone cells were freshly isolated and MSC frequencies were determined by flow cytometry.
2. Equal absolute numbers of Itch$^{-/-}$ and control MSCs with bone cells were seeded in MSC culture medium.
3. After 24 hours non-adherent cells were removed and medium was changed to respective differentiation medium.

3.3.2 Osteoblast Differentiation is Impaired in the Absence of Itch.

Total bone cells were isolated from femora and tibiae of a pool of two to four mice per genotype. In an aliquot of the cell suspension, PαS counts were determined by flow cytometry. Total bone cells containing 500 PαS MSCs were seeded in a 10 cm dish. 24 hours after seeding, non-adherent cells were removed and osteoblast differentiation medium was added.

MSCs divide and differentiate through different progenitor states into functional osteoblasts (Karsenty et al., 2009). Upon culture in osteoblast differentiation

medium, MSCs of both genotypes showed colony-forming growths (CFU-Ob) before morphological changes with a loss of the typical spindle-shape became apparent. CFU-Ob were counted at day 10. **Analysis of three independent experiments revealed a significant reduction of CFU-Ob numbers in Itch$^{-/-}$ mice** (16.00 ± 2.65 vs. 5.33 ± 1.20 per 10 cm dish, P = 0.0214) *(Figure 8 A, app. Table 13)*.

Cultures were finally stained with Alizarin red after three weeks. Alizarin red staining indicates calcium phosphate deposits produced by functionally active osteoblasts. **Calcium phosphate deposits were rare in Itch$^{-/-}$ cultures. There was a significant higher portion of alizarin red positive areas in the control cultures** (367 ± 57 mm² vs. 105 ± 6 mm² per 10 cm dish, P = 0.0102) *(Figure 8 B & C, app. Table 14)*.

3.3.3 Itch-Deficient MSCs Show no Abnormality in Adipocyte Differentiation.

Total bone cells containing 500 PαS MSCs were seeded per 9 cm² dish. 24 hours after seeding, non-adherent cells were removed and adipocyte induction medium was added. After 3 days of culture in adipocyte induction medium, MSCs were cultured for 3 days in adipocyte maintenance medium. Three cycles of induction and maintenance culture were performed.

Upon adipocyte induction, there was poor expansion of MSCs. After 3 weeks of culture, cells were stained with Oil-red-O, a fat-soluble dye that marks adipocytes. **Two independent experiments revealed no significant difference in Oil-red-O positive adipocytes between Itch$^{-/-}$ and control cultures** (17 ± 12 vs. 20 ± 2 mm² per 9 cm², P = 0.8209) *(Figure 8 D & E, app. Table 15)*.

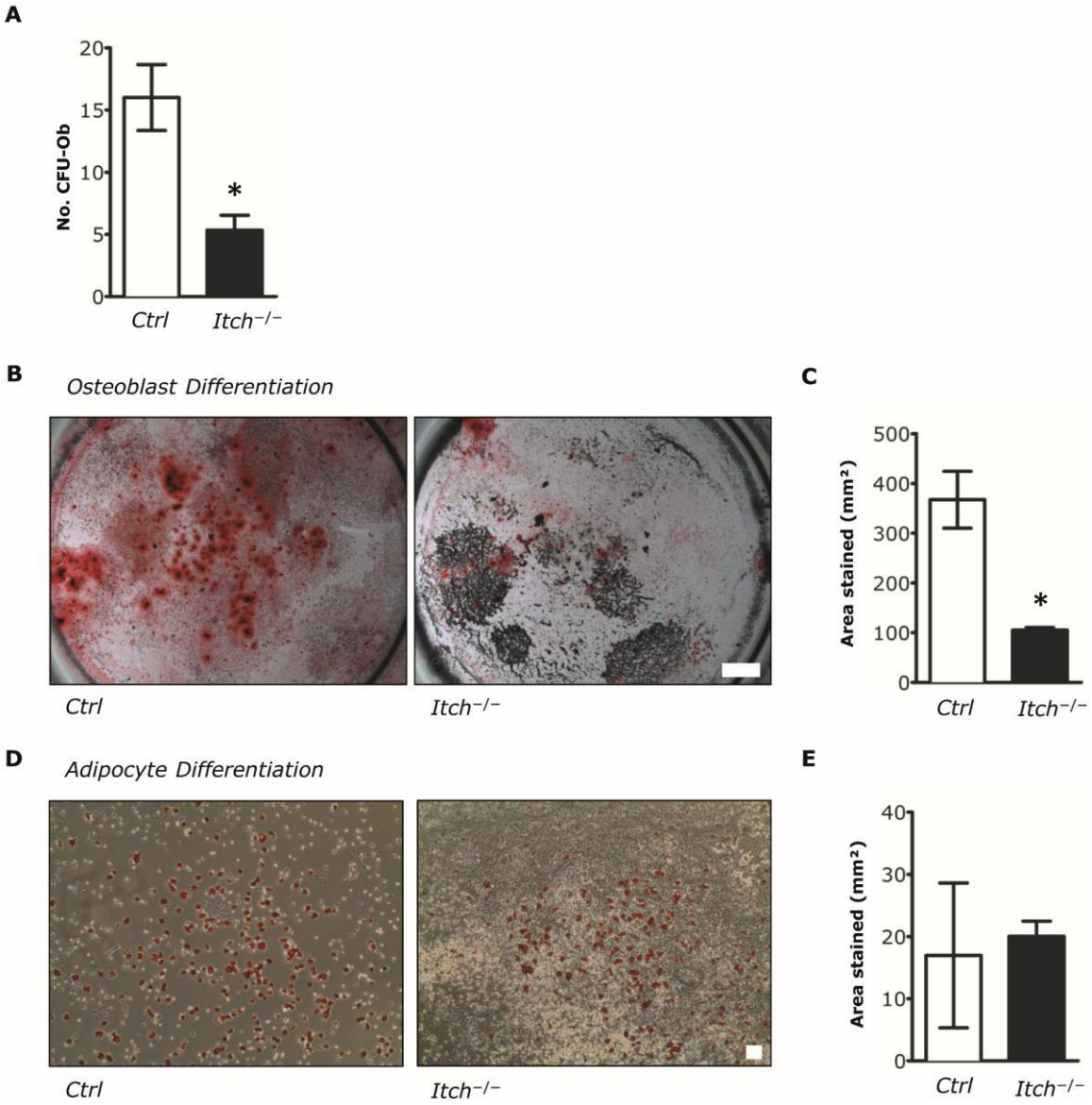

Figure 8. Impaired osteoblast differentiation of Itch$^{-/-}$ MSCs. 500 PαS cells in a freshly isolated total bone cell suspension (pool of 2 - 4 mice per genotype) were seeded. (A - C) Osteoblast differentiation was performed in a 10 cm dish: 24 hours after seeding, medium was changed to osteoblast differentiation medium. (A) CFU-Ob at day 10 (N = 3). (B) Alizarin red staining after 3 weeks. Left = Ctrl, right = Itch$^{-/-}$. Representative experiment. Bar indicates 10mm. (C) Alizarin red positive area in mm² per 10cm dish (N = 3). (D & E) Adipocyte differentiation was performed in 9 cm² wells: 24 hours after seeding, medium was changed to adipocyte induction medium. 3 alternating cycles of culture in adipocyte induction and maintenance medium were performed. (D) Oil-red-O staining after 3 weeks. Left = Ctrl, right = Itch$^{-/-}$. Bar indicates 100µm. Representative experiment. (E) Oil-red-O positive area in mm² per 9 cm² dish (N = 2). All data represent mean ± SEM. Two-tailed Student's t tests were used to assess statistical significance.

3.4 Characterization of Bone in Itch$^{-/-}$ Mice.

3.4.1 Osteoblasts are Reduced in Itch$^{-/-}$ Bone.

Following the demonstration of MSC reduction in Itch$^{-/-}$ mice as well as impaired bone formation in vitro, a reduction of osteoblast number in vivo was hypothesized. To investigate osteoblast counts, femora of Itch$^{-/-}$ and control mice were harvested, cleaned from soft tissue and fixed in 4% paraformaldehyde. Decalcification, preparation of sections and staining with H&E was performed by the central facility for musculoskeletal disorders, Yale University School of Medicine. H&E stained sections were received *(Figure 9 A)*. Region of interest was defined within the secondary spongiosa of the distal femur proximal to the growths plate that represents an area of postnatal bone remodeling. Subsequently, bone perimeter and osteoblasts were determined.

Analyses of two experiments revealed a significant reduction of osteoblasts in Itch$^{-/-}$ mice (27.92 ± 2.73 vs. 14.32 ± 1.55 osteoblasts per mm, P = 0.0493) *(Figure 9 B & C, app. Table 16)*.

3.4.2 Reduced Osteocalcin Serum Levels in Itch$^{-/-}$ Mice.

The protein osteocalcin is solely produced by osteoblasts and osteocalcin serum levels correlate with osteoblast activity, i.e. bone formation (Confavreux et al., 2009). Osteocalcin interacts with different endocrine systems and has been identified as a regulator of energy metabolism (Confavreux et al., 2009). Osteocalcin serum levels were determined by Elisa in Itch$^{-/-}$ and control mice[1]. **The osteocalcin level was significantly reduced in the serum of Itch$^{-/-}$ mice** (37.60 ± 2.06 vs. 20.40 ± 2.72, P < 0.001, n = 5 mice per group) *(Figure 9 D, app. Table 17)*.

[1] This experiment was conducted by Dr. Chozha V. Rathinam. Data were received and included here because they had major influence on the experimental direction.

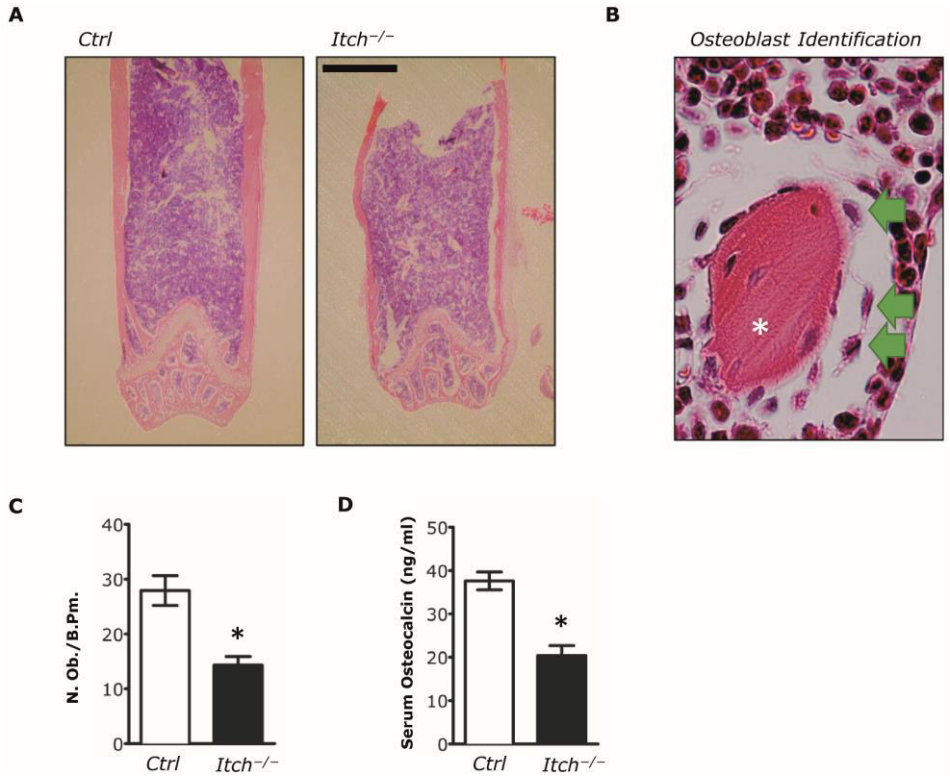

Figure 9. Osteoblast number in Itch$^{-/-}$ mice. (A) H&E staining of distal femur. Left: Ctrl, right: Itch$^{-/-}$. Bar indicates 1mm. (B) Osteoblasts (arrows) were counted within the secondary spongiosa of the distal femur. Osteoblasts were identified as bone lining cuboidal cells with perinuclear clear zone. Decalcification can lead to disruption from bone surface. * marks trabecular bone. (C) Number of osteoblasts per bone perimeter (mm), N = 2. (D) Serum osteocalcin levels were detected by Elisa, N = 5 (this experiment was conducted by Dr. Chozha V. Rathinam). All data represent mean ± SEM. Two-tailed Student's t tests were used to assess statistical significance.

3.4.3 Micro-CT Analysis Reveals Substantial Defects of Bone in Itch$^{-/-}$ Mice.

Bone morphometric studies were conducted to elucidate the functional consequences of MSC reduction, impaired osteoblastogenesis and reduced osteoblast numbers on Itch$^{-/-}$ bone. Femora of four mice were harvested, dissected from soft tissue and fixed in 70% ethanol at 4°C. Micro-CT analyses were performed by the Yale University School of Medicine Micro-CT Core Facility. Preprocessed 2D and 3D data were received. Analyses were finalized by the author in accordance with current recommendations (Bouxsein et al., 2010).

Investigation of Itch$^{-/-}$ trabecular bone within the distal metaphysis of the femur *(Figure 10 A & B, app. Table 18)* revealed a trend of decreased trabecular number (Tr.No, *Figure 10 C*; 2.58 ± 0.21 vs. 2.08 ± 0.11 per mm, P = 0.0866), increased trabecular separation (Tr.Sp, *Figure 10 D*; 0.40 ± 0.03 mm vs. 0.49 ± 0.03 mm, P = 0.0994) and significantly thinner trabeculae (Tr.Th, *Figure 10 E*; 39.60 ± 1.20 µm vs. 31.60 ± 0.70 µm, P = 0.0014) as compared with control mice. These findings cumulated in a significantly reduced trabecular bone volume in Itch$^{-/-}$ mice (Tr.BV, *Figure 10 F*; 0.12 ± 0.01 mm³ vs. 0.07 ± 0.01 mm³, P = 0.0230). Trabecular total volume (Tr.TV) was unaffected in the absence of Itch (*Figure 10 G*; 2.40 ± 0.13 mm³ vs. 2.28 ± 0.22 mm³, P = 0.6650). Therefore Itch$^{-/-}$ bone exhibited a significantly reduced trabecular bone volume fraction (Tr.BV/TV, *Figure 10 H*; 5.08 ± 0.71 % vs. 2.98 ± 0.24 %, P = 0.0312). **These results indicated a reduction of mineralized bone irrespective of mineralization density with unaffected total tissue volume in the trabecular region**.

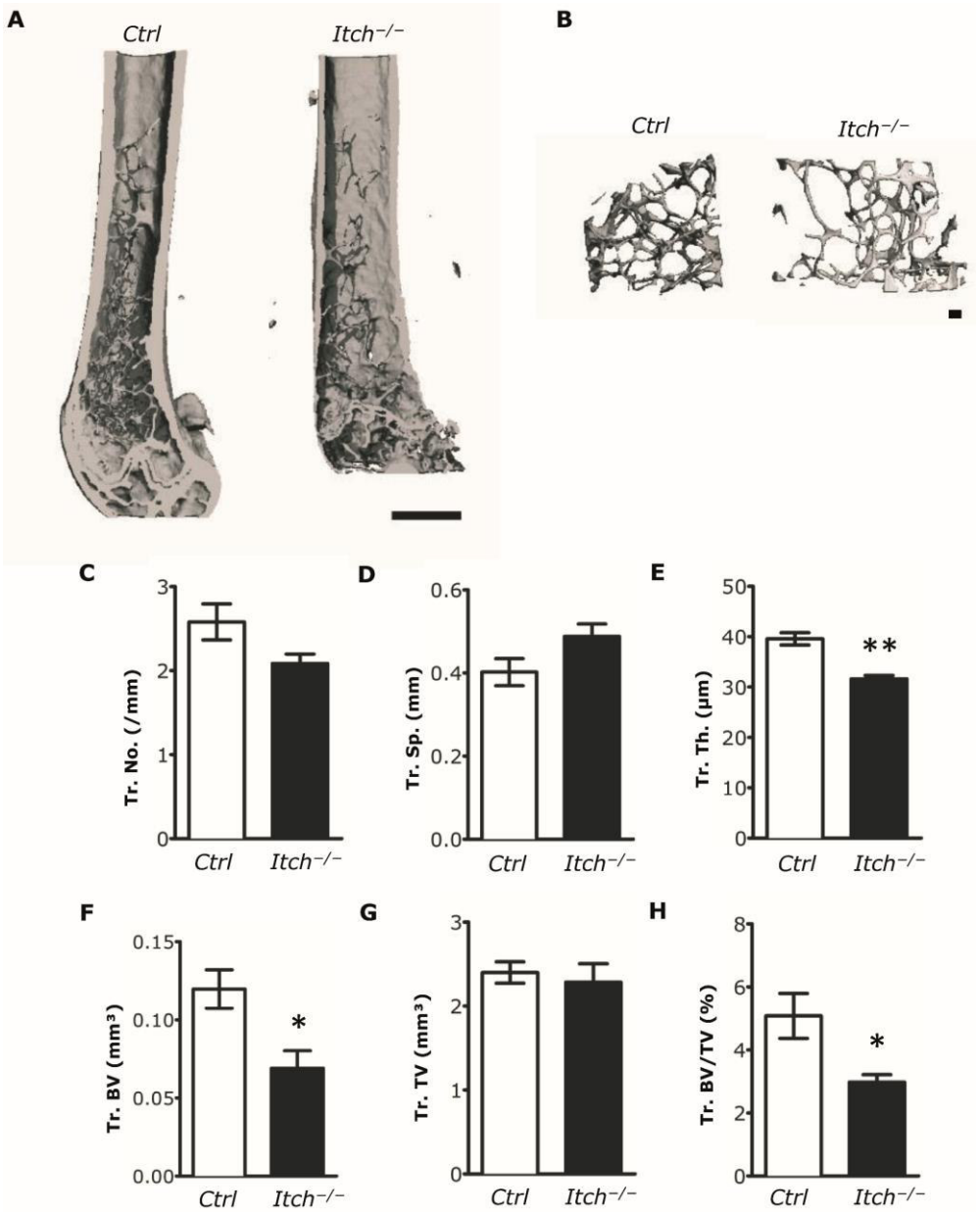

Figure 10. Micro-CT of distal femora: Trabecular bone microarchitecture. (A) Micro-CT scan of femoral diaphysis, distal metaphysis and epiphysis. Left: Ctrl. Right: Itch$^{-/-}$. Bar indicates 1mm. (B) Three-dimensional reconstruction of distal metaphyseal region Left: Ctrl. Right: Itch$^{-/-}$. Bar indicates 100µm. (C - H) Trabecular bone morphometry. N = 4 mice per group. (C) Tr.No. = Trabecular number. (D) Tr.Sp = Trabecular separation. (E) Tr.Th = Trabecular thickness. (F) Tr.BV = Trabecular bone volume. (G) Tr.TV = Trabecular total volume. (H) Tr.BV/TV = Trabecular bone volume fraction. All data represent mean ± SEM. Two-tailed Student's t tests were used to assess statistical significance.

Analyses of Itch$^{-/-}$ femoral diaphyses *(Figure 11 A, app. Table 19)* showed significant thinner cortical bone (Ct.Th, *Figure 11 B*; 183.30 ± 1.80 µm vs. 120.30 ± 8.00 µm, P < 0.001) as compared with control femora. This investigation further revealed a significantly reduced bone volume of Itch$^{-/-}$ femur cortical region (Ct.BV, *Figure 11 C*; 1.03 ± 0.03 mm³ vs. 0.67 ± 0.02 mm³, P < 0.001) with a reduction of total volume (Ct.TV *Figure 11 D*, 1.09 ± 0.03 mm³ vs. 0.73 mm³ ± 0.02 mm³, P < 0.001). **These results indicated a loss of bone mass and consecutive smaller bone tissue, i.e. reduced lengths and / or diameter of the diaphysis.** A significantly decreased cortical bone volume fraction in the absence of Itch (Ct.BV/TV, *Figure 11 E*, 0.95 ± 0.0010 mm³ vs. 0.92 mm³ ± 0.0056 mm³, P = 0.003) further demonstrated an excessive reduction of cortical bone volume over cortical total volume. Moreover, **bone tissue density was significantly reduced in Itch$^{-/-}$ cortical bone** (*Figure 11 F*,1094 ± 9 vs. 1055 ± 12 mg HA per cm³, P = 0.0404). This finding exhibits a characteristic feature of human osteoporosis.

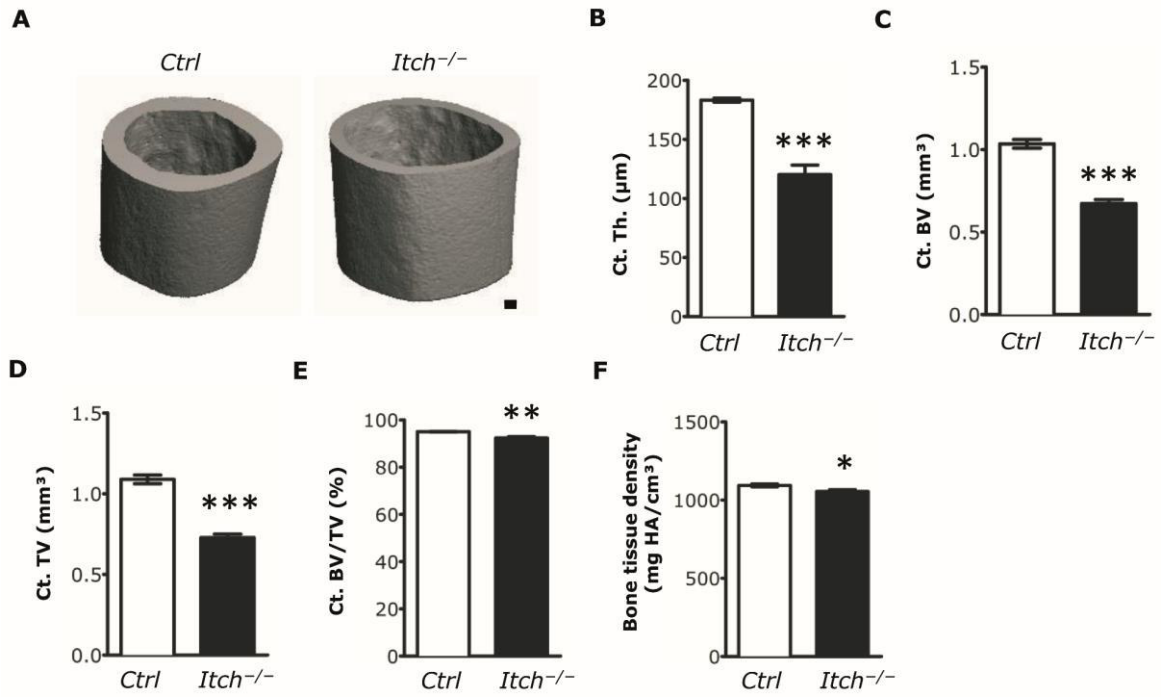

Figure 11. Micro-CT of distal femora: Cortical bone microarchitecture. (A) Three-dimensional reconstruction of diaphyseal region. Left: Ctrl. Right: Itch$^{-/-}$. Bar indicates 100µm. (B - E) Cortical bone morphometry. N = 4 per group. (B) Ct.Th = Cortical thickness. (C) Ct.BV = Cortical bone volume. (D) Ct.TV = Cortical total volume. (E) Ct.BV/TV = Cortical bone volume fraction. (F) Bone tissue density, mg HA/cm³ = Hydroxiapatite density. All data represent mean ± SEM. Two-tailed Student's t tests were used to assess statistical significance.

3.5 Elucidation of the Molecular Function of Itch in MSCs.

3.5.1 Itch$^{-/-}$ MSCs Show Increased Intracellular Notch 1 (Icn1) Protein Levels.

The E3 Ligase Itch exerts its function through protein-protein-interactions in a proteolysis-dependent or proteolysis-independent manner (Aki et al., 2015). To identify pathways that were directly or indirectly affected by the loss of Itch in MSCs, a screening experiment was performed on protein level by Western Blot. For this purpose, in vitro cultured MSCs were lysed and proteins were extracted.

Initially, the expression of Itch was validated through a Western Blot of Itch in control MSCs *(Figure 12 A)*.

Itch has been previously involved in a variety of intracellular signaling cascades in different cell types (Aki et al., 2015). In the previous experiments Itch$^{-/-}$ MSCs exhibited a marked increase in proliferation. To identify affected signaling pathways in the absence of Itch in MSCs, alterations of mitogenic signaling pathways and / or protein levels of previously established Itch targets were hypothesized. Investigation of potential candidates was performed in a non-systematic manner through individual Western Blot experiments.

Mitogen-activated protein kinases (Mapk) Erk 1/2 and p38 as well as their phosphorylated states were detected in equal amounts between Itch$^{-/-}$ and control MSCs *(Figure 12 B & C)* (N = 3 and N = 2 independent experiments). **The Map kinase Jnk was not detected in MSCs of both genotypes** (N = 2). **The Mapk kinases Mek 1/2 as well as phospho-Mek 1/2 protein levels did not differ in Itch$^{-/-}$ and control MSCs** *(Figure 12 D)* (N = 2).

Western Blot of Notch 1 revealed an increase of the 120 kDa cleavage fragment of Notch1 receptor in Itch$^{-/-}$ MSCs *(Figure 12 E)* (N = 3). The Notch receptor is cleaved upon receptor activation. The intracellular cleavage product Icn (Intracellular Notch) translocates to the nucleus and activates gene transcription with cooperating factors (Kopan and Ilagan, 2009). Thus, an increase in Icn-1 protein level in Itch$^{-/-}$ MSCs could depict a relative excess of Notch 1 signaling.

Further, the Phosphatidylinositol-4,5-bisphosphate 3-kinase (Pi3k) pathway was investigated. **Equal amounts of phospho-Pi3k as well phospho-Pdk1 proteins**

were detected in Itch$^{-/-}$ MSCs (N = 2). Additionaly, **there was no difference in Akt as well as in phospho-Akt protein (Thr308) levels** *(Figure 12 F)* (N = 5 and N = 2).

Moreover, **phosphorylated tyrosine kinase Src as well as phosphorylated transcription factor Nfkb protein levels were investigated. There was no difference in protein amounts between Itch$^{-/-}$ and control MSCs** *(Figure 12 G)* (N = 1).

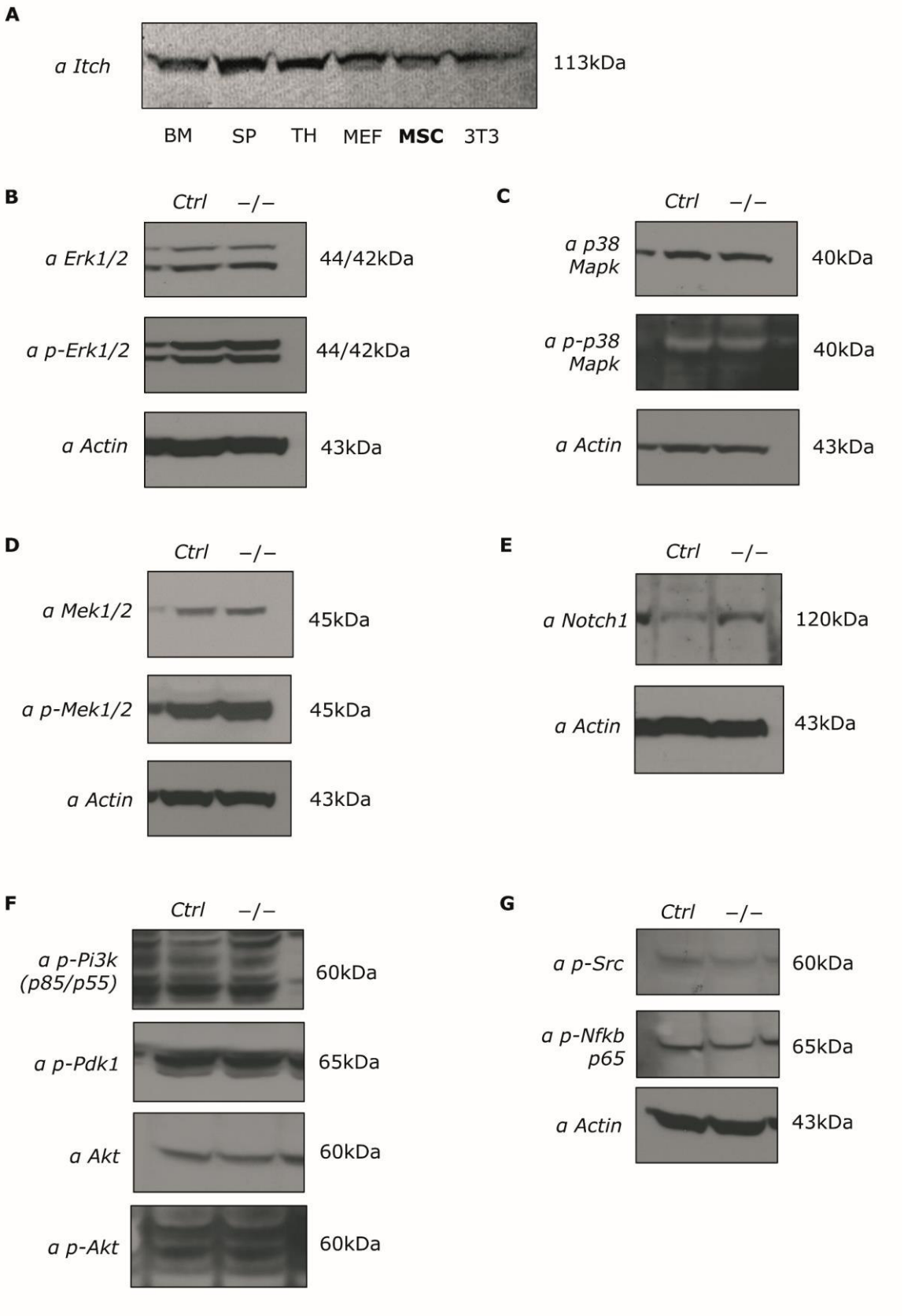
A
α Itch
113kDa
BM SP TH MEF MSC 3T3
B
Ctrl −/−
α Erk1/2
44/42kDa
α p-Erk1/2
44/42kDa
α Actin
43kDa
C
Ctrl −/−
α p38 Mapk
40kDa
α p-p38 Mapk
40kDa
α Actin
43kDa
D
Ctrl −/−
α Mek1/2
45kDa
α p-Mek1/2
45kDa
α Actin
43kDa
E
Ctrl −/−
α Notch1
120kDa
α Actin
43kDa
F
Ctrl −/−
α p-Pi3k (p85/p55)
60kDa
α p-Pdk1
65kDa
α Akt
60kDa
α p-Akt
60kDa
G
Ctrl −/−
α p-Src
60kDa
α p-Nfkb p65
65kDa
α Actin
43kDa

Figure 12. Western Blot experiments on MSCs. In vitro cultured MSCs were trypsinized, washed, lyzed and proteins were extracted. Antibody is annotated left, molecular weight was validated through a protein ladder and is annotated right. kDa = kilodaltons. (A) Western Blot of Itch in different mouse tissues. BM = bone marrow, SP = spleen, TH = thymus, MEF = mouse embryonic fibroblasts, MSC = mesenchymal stem cells, 3T3 cell line. (B - G) Representative data. Equal protein loading was validated with actin as a control in every experiment. (B) α Erk 1/2 = anti-Extracellular signal-regulated kinases 1/2, α p-Erk 1/2 = anti-phosphorylated Erk 1/2 (Thr202/Tyr204). N = 3. (C) α p38 Mapk = anti-p38 Mitogen-activated protein kinase, α p-p38 Mapk = anti-phosphorylated p38 Mapk (Thr180/Tyr182). N = 2. (D) α Mek 1/2 = anti-Mapk kinases 1/2, α p-Mek 1/2 = anti-phophorylated Mek 1/2 (Ser221). N = 2. (E) α Notch1, full lengths and transmembrane domain. N = 3. (F) α p-Pi3k = anti-phosphorylated Phosphatidylinositol-4,5-bisphosphate 3-kinase p85 (Tyr458) / p55 (Tyr199), N = 2. α p-Pdk 1 = anti-phosphorylated Phosphoinositide-dependent kinase-1 (Ser241), N = 2. α Akt = anti-pan Akt (Protein kinase B)(1-3), N = 5. α p-Akt = anti-phosphorylated Akt (Thr308), N = 2. (G) α p-Src = anti-phosphorylated proto-oncogene tyrosine-protein kinase Src, N = 2. α p-Nfkb p65 = anti-phosphorylated nuclear factor kappa B p65 (Rela), N = 2.

3.5.2 Upregulation of Notch Signaling Pathway Targets in the Absence of Itch.

The Notch signaling pathway in MSCs was explored on an mRNA level. Firstly, Notch receptor expression was evaluated. **Notch receptor 1, 2, 3 and 4 expression could be detected in in vitro cultured control MSCs** (*Figure 13 A*).

Secondly, increased Notch signaling in Itch$^{-/-}$ MSCs was hypothesized. Icn acts as a transcription factor of multiple genes of the Hes and Hey gene families (Kopan and Ilagan, 2009). To investigate the hypothesis, expression levels of the established Notch target genes Hes-1, Hes-5, Hey-1, and HeyL were investigated. Cultured MSCs were harvested and lysed for mRNA extraction and cDNA synthesis. Primers for Notch target genes were designed for detection by RT-PCR using the SYBR green method.

Three experiments were analyzed using the delta-delta CT method. **Analyses of Hes-1, Hey-1, and Heyl expression revealed a significant increase in Itch$^{-/-}$ MSCs as compared with control MSCs** *(Figure 13 B)*. There was no detection of Hes-5 in either genotype.

3.5.3 Demonstration of Itch and ICN1 Interaction in MSCs by Co-Immunoprecipitation.

It was hypothesized that Itch interacts and directly downregulates Icn1 on a protein level in MSCs. To investigate this hypothesis, interaction studies through co-immunoprecipitation were performed. In preliminary experiments, pull-down of Notch in MSC protein lysates was inefficient. Pull-down of endogenously expressed Itch in MSC protein lysate was not possible with the commercially available antibody.

To circumvent low pull-down efficiencies, MSCs were retrovirally transduced with either Itch or ICN1. For this purpose, Itch sequence was cloned into pGFP RV backbone. Sequence of Itch-pGFP-RV was validated by sequencing. Retroviruses were produced with the PhoenixGP cell line and Itch-pGFP-RV, pGFP-RV (control) as well as MSCV ICN1-IRES-GFP (Rathinam et al., 2006). MSCs were transduced and flow cytometry revealed transduction efficiencies of 5 – 15 %. GFP-high expressing MSCs were sorted and subcultered. Overexpression of proteins was evaluated by Western Blot *(Figure 13 C)*. Overexpression of Itch did not result in decreased Icn1 protein levels (N = 3).

Immunoprecipitation (IP) with anti-Notch1 antibody was performed on ICN1^{high} MSC protein lysates. Isotype was used for control IP (negative control). In a subsequent Western Blot of Itch on the yielded protein precipitate, the protein could be successfully detected *(Figure 13 D)* (N = 2).

Immunoprecipitation with anti-Itch antibody was performed on Itch^{high} MSC protein lysates. Isotype was used for control IP (negative control). In the subsequent Western Blots on the yielded protein extract, Notch1 was detected in two independent experiments. There was a faint band of Icn1 in the negative control (IP with isotype control). Thus, the result of this experiment cannot be assessed. The strong band of Icn1 in the Itch-IP fraction in contrast to the faint band in the negative control may suggest a specific co-immunoprecipitation, however *(Figure 13 E)*.

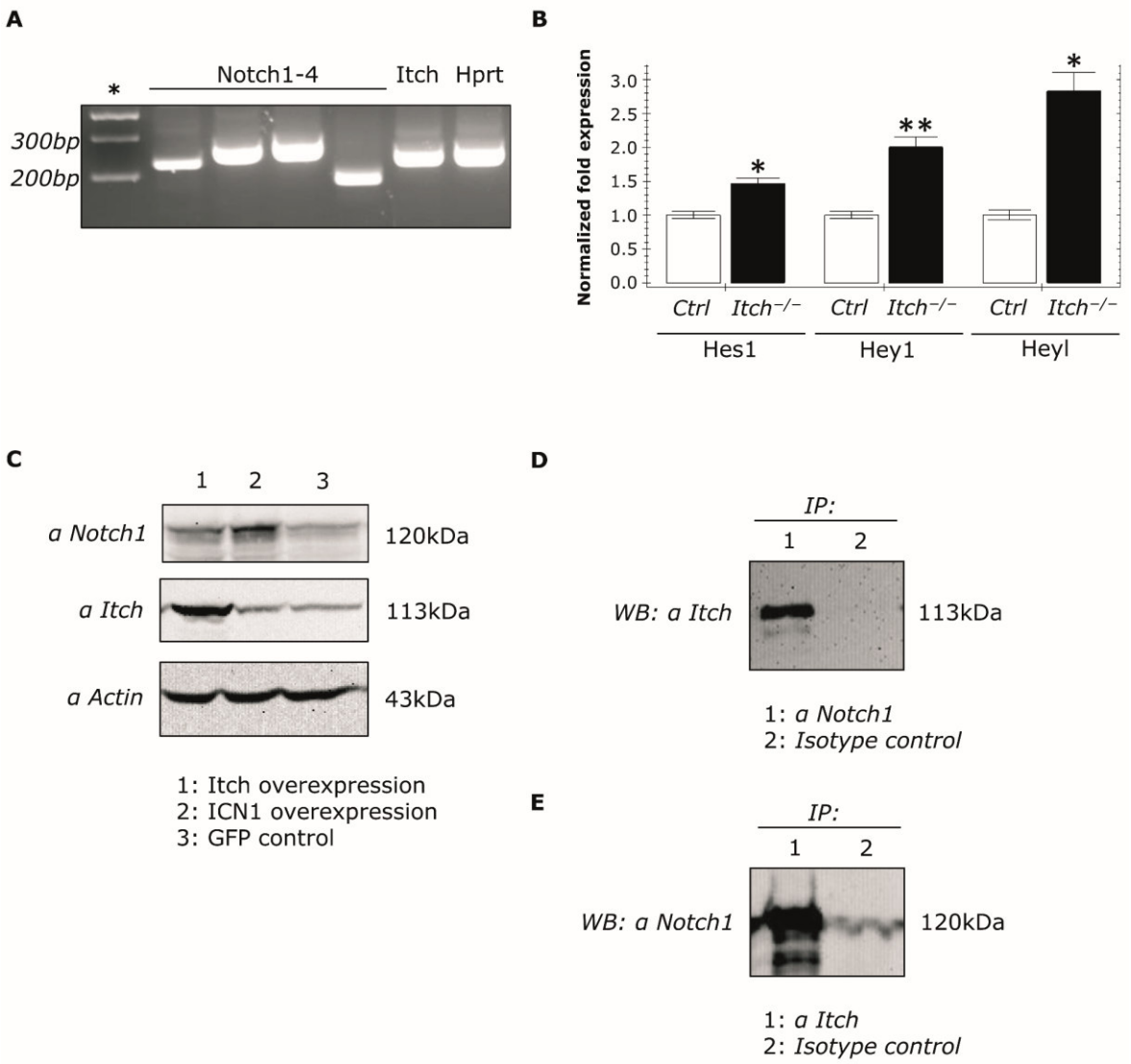

Figure 13. Investigation of Notch signaling in MSCs. (A) Qualitative assessment of Notch1-4 receptor expression in control MSCs. Agarose gel electrophoresis of RT-PCR products using specific primer pairs for individual genes. * DNA ladder. (B) Expression of Notch signaling target genes in cultured MSCs. Representative experiment. Expression fold changes were calculated using the ddCT method. Housekeeping gene: Hprt. Gene expression in control MSCs was normalized to 1. Data represent mean ± SEM. Two-tailed Student's t tests were used to assess statistical significance. N = 3. (C) Validation of protein expression by Western Blot. Control MSCs were transduced with 1: Itch-pGFP; 2: ICN1-pGFP; 3: pGFP empty vector control retroviruses. GFP^{high} MSCs were enriched by sorting, subcultured and lysed for protein extraction. Western Blot of Notch1 and Itch were performed to validate protein expression. Loading control: Actin. (D) Co-Immunoprecipitation. $ICN1^{high}$ MSCs were lyzed for protein extraction. IP was conducted using anti-Notch1 antibody and isotype as a negative control. Western Blot of Itch was performed using the immunoprecipitate. Representative experiment. N = 2. (E) Co-Immunoprecipitation. $Itch^{high}$ MSCs were lyzed for protein extraction. IP was conducted using anti-Itch antibody and isotype as a negative control. Western Blot of Notch1 was performed using the immunoprecpitate. Representative experiment. N = 2.

4. DISCUSSION

4.1 Major Findings.

The most important results of this study comprise: 1. The reduction of MSCs in the absence of Itch. 2. Maintenance of an MSC phenotype but hyperproliferation and decreased osteoblastic differentiation of Itch$^{-/-}$ MSCs in vitro. 3. Reduced osteoblasts and severe bone defects in Itch$^{-/-}$ mice. 4. Increased Notch 1 signaling in the absence of Itch as well as protein interaction of Itch and Notch 1 in MSCs.

4.2 Reduction of MSCs in Itch$^{-/-}$ Mice.

Results of two independent experimental approaches in this study suggested a reduction of mesenchymal stem cells in Itch$^{-/-}$ mice: CFU-F experiments as well as flowcytometric analyses revealed at least two-fold decreased MSC frequencies. Absolute quantification further documented a significant reduction of MSCs within long bones of Itch$^{-/-}$ mice. Methodological aspects need to be considered to interpret these data. Standardized in vivo and in vitro surface marker to define murine MSCs are lacking. Moreover, the technique of murine MSC isolation, preparation and culture can differ significantly between investigators. In contrast to human MSCs, the isolation of pure murine MSCs is challenged by low yield, growth capacity and purity of stem cells (Phinney et al., 1999). Hence, the original technique of MSC isolation that includes plating of total bone marrow and removal of non-adhering cells was refined. Isolation of MSCs in this study included collagenase digestion of solid bone fragments and immunodepletion of contaminating hematopoietic cells. These steps have been proven to enhance culture efficiency (Baddoo et al., 2003; Xu et al., 2010; Zhu et al., 2010).

Other investigators have improved MSC isolation and culture using hypoxic conditions (Lennon et al., 2001) or through the addition of growths factors, especially FGF-2 (Baddoo et al., 2003). Experiments with MSCs under hypoxic conditions or stimulation of Itch$^{-/-}$ MSCs with defined growth factors remained behind the scope of this study. The commercially available MSC culture medium that was used in this study consists of basal medium and a serum containing MSC stimulatory

supplement. A list of ingredients is not available. It cannot be ruled out that the composition of this medium affected Itch$^{-/-}$ and control MSCs differently and contributed to the described phenotype.

In the present study, MSCs derived from compact bone whereas most bone marrow cells were removed prior to collagenase digestion. Isolation of murine MSCs from compact bone has been implemented by various groups and systematic comparisons of compact bone-derived versus bone marrow-derived MSCs have been conducted. Compact bone-derived MSCs resemble bone marrow-derived MSCs and exhibit increased clonal proliferation as well as differentiation capacity in culture (Cai et al., 2015; Blashki et al., 2016). Compact bone-derived MSCs have been shown to exhibit multilineage differentiation potential upon transplantation in vivo and localize to the bone marrow sinusoids where they contribute to the HSC niche (Morikawa et al., 2009; Houlihan et al., 2012). A systematic analysis of MSCs derived from solid bone or bone marrow in Itch$^{-/-}$ mice was not included in this study. Of note, however, flowcytometric analyses of bone cells revealed that most cells (> 95 %) isolated from compact bone were CD45 and TER119 positive, i. e. were hematopoietic progeny. Additionally, CFU-F assays performed on bone marrow suggested a similar reduction of bone marrow-derived MSCs in Itch$^{-/-}$ mice. Fluorescence microscopy studies on bone and bone marrow could complement the investigation of the MSC pool in the absence of Itch. Microscopic investigations may not only clarify the distribution of MSCs to compact regions of the bone versus the bone marrow. Additionally, it can be investigated whether the spatial localization within the tissue will be altered in Itch$^{-/-}$ mice. At this point of time, the microscopic analysis of the MSC pool in Itch-deficient mice remains a future goal.

The concept of mesenchymal stem cells that possess multipotency in vivo and expand upon serial transplantation experiments has been demonstrated with the Nestin reporter mouse (Méndez-Ferrer et al., 2010). Currently, various surface marker combinations and transgene-based reporter strains are in use to investigate mesenchymal stem cells in genetic mouse models (Mohamed and Franceschi, 2017). Further, the concept of Skeletal Stem Cells (SSC) has been proposed to emphasize the skeletal origin of multipotent cells that can differentiate into all skeletal tissues and are capable of bone organogenesis (Bianco and Robey, 2015). Significant overlap between cells with different MSC or SSC signatures is

hypothesized. Experimental evidence to support this hypothesis is incomplete and conflicting data exist (Bianco, 2014; Chen et al., 2018). In the present study, direct identification of MSCs in vivo was accomplished through labeling with PDGFRα and Sca-1 (PαS MSCs). PαS MSCs have been demonstrated to differentiate into osteoblasts and adipocytes upon transplantation in vivo (Morikawa et al., 2009). Zhou et al. identified that expression of the Leptin receptor (LepR) highly enriches for MSCs in the bone marrow (Zhou et al., 2014). LepR+ MSCs are PDGFRα+ and Sca-1− (Zhou et al., 2014). Isern et al. have demonstrated by RNA sequencing that Nestin+ PDGFRα+ cells resemble LepR+ MSCs as well as CXCL12+ perivascular stromal cells (described by Ding and Morrison, 2013) (Isern et al., 2014). Nestin− PDGFRα+ cells, in contrast, exhibited a distinct gene expression profile (Isern et al., 2014). It has been further described that Mx1+ stromal cells exhibit transplantable osteoblastic precursors and fulfill in vitro MSC criteria. Mx1+ cells can be identified within the PαS subset (Park et al., 2012). Recently, Nusspaumer et al. performed systematic analyses on mesenchymal cells with different MSC signatures at different embryonic, fetal and postnatal stages (Nusspaumer et al., 2017): PDGFRα+ CD51+ MSCs that exhibit significant overlap with Nestin+ MSCs (Pinho et al., 2013) encompassed PαS cells at all developmental stages. Number of PαS cells increases throughout fetal development and peaks around birth (Nusspaumer et al., 2017). CD90− 6C3− CD105− CD51+ CD200+ Skeletal Stem Cells have been identified through lineage tracing experiments and demonstrated to form cartilage and bone as well as bone marrow stroma upon ectopic transplantation in vivo (Chan et al., 2015). Interestingly, CD51+ CD200+ SSCs and PαS MSCs exhibited mutually exclusive cellular subsets of similar frequency within postnatal long bones (Nusspaumer et al., 2017). Finally, Gremlin1+ SSCs that generate osteoblasts, chondrocytes and bone marrow reticular cells in vivo showed low levels of PDGFRα and Sca-1 expression (Worthley et al., 2015). The analysis of MSCs or SSCs in Itch$^{-/-}$ mice using different stem cell signatures remained behind the scope of the present study. Hence, caution is mandatory when the present data will be compared with studies that use other MSC models.

Lineage tracing experiments and thorough ontogenetic studies depend on conditional and inducible knockout mouse models and were not included in this study. Regarding the investigation of MSCs in a generic Itch$^{-/-}$ mouse model as performed throughout this study, further limitations need to be annotated. Itch$^{-/-}$

mice develop severe autoinflammation at three to four months that is at least partially caused by alteration of T cell subsets (Hustad et al., 1995). These mice further exhibit an excessive HSPC pool (Rathinam et al., 2011). To investigate whether the reduction of MSCs in Itch$^{-/-}$ mice depended on the autoinflammation, the MSC pool was investigated at different ages. Similar reductions of MSCs in two to four-week-old animals and in aged mice provided no evidence for a connection of both phenotypes. Certainly, this experiment is of limited validity. Alterations of the hematopoietic system are likely to develop early or even at developmental stages. Moreover, osteoclasts that regulate bone remodeling conversely to osteoblasts are hematopoietic progeny. Ideally, conditional deletion of Itch in mesenchymal lineage cells will be needed to demonstrate an intrinsic phenotype of MSCs, MSC progeny and skeletal tissue.

4.3 Hyperproliferation and Reduced Osteoblastogenesis of Itch$^{-/-}$ MSCs.

Stem cells require a tight regulation of cell intrinsic as well as extrinsic signals to maintain their stem cell identity or stemness (Orford and Scadden, 2008). Deregulations that result in increased lineage commitment and differentiation or reduced self-renewal may lead to depletion of the stem cell pool (He et al., 2009). To study different hypotheses regarding the cellular mechanism leading to a reduced number of MSCs in Itch$^{-/-}$ mice, in vitro cultured MSCs served as a model system.

Itch$^{-/-}$ MSCs showed no abnormalities in morphology or regarding their in vitro immunophenotype as well as in the maximum number of culture passages. Viability assessment throughout the culture revealed no differences between Itch$^{-/-}$ and control MSCs. Proliferation studies revealed increased growth of Itch$^{-/-}$ MSCs in culture. Of note, results of the CFSE labeling studies underscored the growth advantage of Itch$^{-/-}$ MSCs that was noticed upon their expansion in culture.

Deregulation of proliferation in stem cells and the loss of a quiescent state can lead to stem cell exhaustion (Orford and Scadden, 2008). Thus, hyperproliferation of Itch$^{-/-}$ MSCs presents a potential mechanism for the diminished MSC pool in Itch-deficient mice. In the future, the investigation of MSC cell cycle regulation may help

to understand whether quiescence was lost and self-renewal was compromised in the absence of Itch (Orford and Scadden, 2008). Furthermore, systematic investigations on Itch$^{-/-}$ MSC response to cytokines such as Fgf-2 or Bmp-2 may refine our understanding of self-renewal versus lineage commitment (Hanada et al., 1997).

At this point of time, however, data is insufficient to proof the mechanism of MSC depletion in vivo. MSC pool exhaustion will be the future experimental hypothesis. Of note, MSC properties are profoundly altered by the expansion in culture (Bianco, 2014). For this reason, it will be crucial to investigate proliferation, cell cycle and lineage commitment *in vivo*. As mentioned above, lineage tracing requires experimentation with an inducible knockout mouse. At this point of time, lineage commitment studies in vivo as well as BrdU pulse labeling or Ki67 labeling remain behind the scope of the study. Finally, the gold standard to address a loss of stemness in Itch-deficient MSCs will be (serial) transplantation experiments.

Technically, a reduced number of Itch$^{-/-}$ MSCs in vivo that exhibited a growth advantage in vitro challenged the comparability between Itch$^{-/-}$ and control MSCs upon expansion in culture. Increased total Itch$^{-/-}$ bone cells were plated for culture experiments (except for CFU-F assays) and solved this issue partially. During the experimental set-up it was considered that this technique comprised plating and culturing increased numbers of contaminating cells (non-MSCs) at P0 to P1. These cells might have secreted cytokines or provided cell-to-cell contact that affected MSC growths. However, these adjustments were necessary to obtain comparable MSC cultures at a low passage number.

Prospective isolation of MSCs by sorting may finally circumvent limitations that depend on the Itch$^{-/-}$ MSC phenotype. Prospective identification and single cell sorting as described previously (Morikawa et al., 2009; Méndez-Ferrer et al., 2010) allow the investigation of individual MSC clones. In the present study, differentiation experiments were performed on freshly isolated MSCs that were seeded in bulk cultures with bone cells. Culture in osteoblastogenic differentiation medium revealed a reduced number of clonally expanding progenitor cells in the absence of Itch. Furthermore, Itch$^{-/-}$ cultures generated fewer functional osteoblasts which were quantified by calcium deposition. The significance of this experiment regarding the

differentiation capacity of MSCs is limited in two different ways: Firstly, committed osteoblast progenitors could have expanded and differentiated in the culture as well. Secondly, contaminating cells of other mesenchymal lineages and hematopoietic cells might have affected osteoblastogenesis in the culture. Despite these limitations, the reduced osteoblast differentiation in the model system strongly suggested reduced osteoblastogenesis in the absence of Itch in vivo. Adipocyte and chondrocyte differentiation in culture depend on progenitor cell proximity. Because of sparse seeding density of MSCs, adipocyte differentiation was relatively inefficient overall. No difference in adipogenesis was observed in the absence of Itch. The investigation of chondrogenesis remains behind the scope of this study. For an ideal comparison of trilineage differentiation in vitro between Itch$^{-/-}$ and control MSCs, the technique of single cell sorting would be most suitable. Multiple MSC clones of both genotypes could be individually assessed for their differentiation capacity. To further substantiate any differences in the differentiation capacity of MSCs, gene expression studies regarding master transcription factors for a particular lineage can be of interest (Karsenty et al., 2009). The evaluation of osteoblastic transcription factors such as Runx2 in Itch$^{-/-}$ MSCs, however, remains beyond the scope of this study.

4.4 Reduced Osteoblast Numbers and Osteopenia in Itch$^{-/-}$ Mice.

Functional consequences of reduced MSC numbers and impaired osteoblastogenesis included a reduction of osteoblasts in Itch-deficient bone. Reduced serum osteocalcin further substantiated this finding. Osteocalcin levels may alternatively indicate a reduced osteoblast activity. Osteoblast function may be further assessed through quantification of the bone formation rate. Finally, functional capacity of the osteoprogenitor and osteoblast pool can be investigated in a fracture repair model. These investigations were not part of this study.

Micro-CT analyses revealed reduced and thinner trabeculae in Itch$^{-/-}$ mice that resulted in a decreased trabecular bone volume. Scans on cortical bone further suggested reduced bone mass within the diaphyseal region of Itch-deficient bone. The postnatal process of bone formation by osteoblasts and bone resorption by

osteoclasts is referred to as bone remodeling. Activity of osteoblasts and osteoclasts is regulated by each other, e. g. osteoblasts can inhibit osteoclast differentiation from hematopoietic progeny through the RANKL decoy receptor Osteoprotegerine (OPG) (Karsenty et al., 2009). The data on the osteoblast pool in the absence of Itch suggested, that osteoblast dysfunction contributed to the bone phenotype of the mouse. Increased osteoclast numbers and / or activity could equally well contribute to the described phenotype. The investigation of osteoclasts and their interaction will contribute to the understanding of bone remodeling in Itch$^{-/-}$ mice in the future. Of note, Itch is a regulator of the hematopoietic stem and progenitor pool (Rathinam et al., 2011). The investigation of a conditional Itch knockout mouse may provide substantial benefit regarding the role of mesenchymal-derived osteoblasts versus hematopoietic-derived osteoclasts on bone remodeling.

Though the present work did not include the investigation of osteoclasts, Zhang and Xing et al. have focused on osteoclastogenesis as well as on osteoblastogenesis in the absence of Itch (Zhang et al., 2013; Zhang and Xing, 2013). The authors describe increased osteoclast differentiation and osteoclast numbers in the same generic Itch knockout mouse model that is used in the present study (Zhang et al., 2013). They identify Itch as a negative regulator of osteoclastogenesis through negative regulation of Nfkb signaling via inhibition of Traf6 (Zhang et al., 2013). The group investigated femora of Itch$^{-/-}$ mice by micro-CT at the ages of 1, 3, 6 and 12 months. They found that 1 months old mice exhibited a high bone mass phenotype (Zhang and Xing, 2013), 3 and 6 months old mice showed no abnormalities in bone morphometry (Zhang et al., 2013) whereas 12 months old mice developed an osteoporotic phenotype (Zhang and Xing, 2013) (data of 6 and 12 months old mice not shown). The authors hypothesized that the aging process affected bone remodeling in Itch-deficient mice and favored catabolic effects that explained osteoporosis at one year of age (Zhang and Xing, 2013). In four-week-old animals, in contrast, they demonstrated increased osteoblastogenesis and bone formation in vitro as well as in vivo (Zhang and Xing, 2013). The latter findings explained the high bone mass observed in young mice. The authors identified negative regulation of JunB as a mechanism through which Itch acted as a negative regulator of osteoblastogenesis. Finally, Zhang and Xing showed an increase in CFU-F and similar frequencies of Sca-1+ CD105+ mesenchymal stem and progenitor cells in 4-week-old Itch$^{-/-}$ mice (Zhang and Xing, 2013).

In the present study, Itch-deficient mice exhibited osteopenia at the age of 8 weeks already. The increase in osteoclasts described by Zhang et al. may contribute to osteopenia (Zhang et al., 2013). Whether the bone phenotype of Itch$^{-/-}$ mice was dynamic remains behind the scope of my work as well as the aging process in the absence of Itch. The discrepancies regarding the experimental findings on osteoblast differentiation in the absence of Itch between my work and the aforementioned group may be partially explained by the different ages of investigated mice (4 weeks by Zhang and Xing (Zhang and Xing, 2013) vs. 6 - 8 weeks in the present study). Zhang and Xing stated, that MSCs were isolated from bone marrow and cultured in α-MEM (Zhang and Xing, 2013). In my experiments, MSCs were isolated from compact bone and cultured in commercially available MSC culture medium, what may also explain certain differences. Controversy regarding the experimental discrepancies remains, however. CFU-F assay as well as osteoblast differentiation and quantification resulted in opposing findings (Zhang and Xing, 2013). It must be noted, that the presented experimental thoroughness regarding the MSC pool in the absence of Itch exceeded the previously published approach. Zhang and Xing presented no difference of CD105+ Sca-1+ mesenchymal stem and progenitor cells (Zhang and Xing, 2013). There is good evidence, that CD105+ Sca-1+ cells encompass PαS MSCs which display a more primitive progenitor subset (Morikawa et al., 2009; Chen et al., 2017). PαS MSCs were reduced in young as well as in old Itch$^{-/-}$ mice. Because PαS MSCs exhibit osteoblastic progeny in vivo (Morikawa et al., 2009), my findings will inevitably complement studies on osteoblastogenesis in the Itch$^{-/-}$ mouse model.

4.5 Elevated Notch Signaling in Itch-Deficient MSCs.

Biochemical studies demonstrated an increase in intracellular Notch 1 (Icn1) as well as interaction of Itch and ICN1 in MSCs. Gene expression studies further suggested excessive Notch signaling in Itch-deficient MSCs. Of note, non-systematic screening on mitogenic pathways and previously described Itch targets revealed no other alteration of signaling intermediates on a protein level in Itch$^{-/-}$ MSCs.

Methodologically, a comprehensive understanding of the E3 ligase function in MSCs is behind the scope of this approach. A comprehensive experimental strategy could involve immunoprecipitation of Itch and consecutive mass spectrometry. Furthermore, kinetic studies of mitogenic pathways including Notch signaling will complement the function of the E3 ligase in MSCs. At this point of time, it cannot be ruled out that Itch regulates MSC functions via alternative pathways.

The Notch signaling pathway is evolutionary conserved and regulates a broad range of cellular functions within several different cell types (Kopan and Ilagan, 2009). Notch signaling is involved in the control of several stem and progenitor cell subsets. Thus, Notch signals contribute to development and homeostasis of multiple specialized tissues including the skeleton and the hematopoietic system (Kushwah et al., 2014; Zanotti and Canalis, 2016). Upon ligand binding, Notch receptor undergoes sequential proteolytic cleavages through ADAM metalloproteases and the γ-Secretase complex. Icn (intracellular Notch) or Nicd (Notch intracellular domain) translocates to the nucleus and associates with Rbpjk and other factors to activate gene transcription. Posttranslational modifications and cellular trafficking play a major role in the regulation of Notch signaling (Kopan and Ilagan, 2009). The E3 ligase Itch has been demonstrated to interact with Notch N-terminal intracellular domain through its WW domain and promotes Notch ubiquitination via its HECT ligase domain. Ubiquitination increases upon proteasome inhibition, suggesting a downregulation of Notch via proteasomal degradation (Qiu et al., 2000). The E3 ligase Itch has been identified as a negative regulator of HSC development and function. Itch ubiquitinates Notch1 in HSCs and downregulation of Notch signaling in the absence of Itch partially reverses the phenotype of $Itch^{-/-}$ HSCs (Rathinam et al., 2011).

The present study identified Itch as a positive regulator of the MSC pool in vivo. Whether augmented Notch signaling plays a causal role in this setting still needs to be proven. In contrast to HSCs, my current model regards Notch signaling as a negative regulator of the MSC pool. Functional studies on the Notch pathway will be required to further elucidate the impact of the Itch-Notch-axis in MSCs. Preferentially, the interaction of Itch and Notch will be demonstrated in MSCs that express endogenous levels of each protein. Overexpression of ICN1 or Itch may alter protein interactions as for example through protein aggregation. Fluorescent

labeling techniques and intracellular visualization of Itch and Notch protein may be attempted in the future. Intracellular staining may further reveal any changes of Notch subcellular localization in the absence of Itch.

The study of genetic mouse models revealed pleiotropic effects of Notch signaling in osteoblast differentiation (Zanotti and Canalis, 2016). Stage specific studies demonstrated Notch-mediated inhibition of early osteoblast differentiation but accumulation of dysfunctional osteoblasts at later stages. Possible mechanisms include the inhibition of the master transcription factor Runx2. It has been further demonstrated that Notch signaling may stimulate the function of terminally differentiated osteocytes (Zanotti and Canalis, 2016). The function of Notch signaling in mesenchymal stem cells in vivo remains hardly investigated. Hilton et al. investigated the conditional deletion of Presenilin 1 and 2 in cells derived from the limb bud mesenchyme using Prx1-Cre (Hilton et al., 2008). Deletion of Presenilin 1 and 2 led to the loss of function of the γ-Secretase complex and thus the abrogation of Notch signaling. The authors described excessive osteoblast differentiation and almost total depletion of mesenchymal progenitor cells. They inferred that Notch signaling inhibits osteoblastogenesis through the maintenance of mesenchymal progenitors. The investigation of MSCs in vivo, however, was not part of the study (Hilton et al., 2008). The same group has further studied Notch signaling through conditional deletion of other Notch signaling pathway core components such as Rbpjk or through ICN knockin at different stages of bone development. Experiments on the MSC subset in vivo were not examined in these studies, either (Dong et al., 2010). Sato et al. demonstrated on an mRNA level that Notch 2 receptor was at least 10-fold higher expressed than Notch 1, 3 and 4 in freshly isolated PαS MSCs (Sato et al., 2016). Notch 2 signaling was upregulated under hypoxic conditions in vitro. Inhibition or knockdown of Notch 2 significantly impaired the proliferation capacity of MSCs (Sato et al., 2016).

At this point of time, conclusive data to decipher the role of Notch signaling in MSCs is lacking. Different loss-of-function and gain-of-function studies on the Notch signaling pathway in different cell types have generated partially conflicting results. It has been established, though, that the cell's exposure to Notch signaling will directly impact the experimental outcome (Zanotti and Canalis, 2016). In this regard, the Itch knockout mouse exhibits a unique model to study Notch signaling in MSCs.

In contrast to constitutive activation through ICN knockin, Notch signaling still depends on physiological ligand-dependent receptor activation in the absence of Itch. Furthermore, four Notch receptors exist and all of them were expressed in MSCs. Redundancy between Notch receptors may influence certain experimental models. The role of each Notch receptor in MSCs and the association with Itch awaits further experimentation at this point of time.

4.6 Relevance of the Study and Clinical Perspective.

This study represents the first investigation of the role of Itch in MSCs. The E3 ligase Itch was identified as an essential positive regulator of the mesenchymal stem cell pool in vivo. This finding is of interest in the field, as the molecular circuitry that controls MSC stemness remains incompletely understood. Especially the role of posttranslational modifiers such as E3 ligases has been examined sparsely.

In the last 20 years, many preclinical and clinical MSC transplantation studies have been conducted. Generally, these studies pursued two major concepts: Firstly, MSC transplantation was investigated for reconstruction, e. g. for regenerative purposes in degenerative diseases or upon tissue damage. Secondly, the immunomodulatory and anti-inflammatory effects of MSC transplantation was utilized to treat autoinflammatory conditions. Though tissue repair and immunomodulation cannot be separated from each other in vivo, MSC transplantation for autoimmune diseases is a more advanced clinical application to date. For example MSC infusion is approved to treat steroid-refractory GvHD in different countries and third-party MSC products are commercially available (Galipeau and Sensébé, 2018). It must be noted that MSC transplantation in this sense refers to the concept of “mesenchymal stromal cells” as suggested by the ISCT in 2006. Immunosuppressive capacities are no unique feature of mesenchymal stem cells, as they have been proven for other cultured tissues as well (Bianco, 2014). If intravenous infusion of in vitro cultured mesenchymal stromal cells resulted in long-term engraftment, this event was very rare. Instead, there is increasing data that transplanted stromal cells lose their cellular integrity quickly and that practically no living donor cell can be identified in the host organism after one week (Parekkadan and Milwid, 2010). The major benefit

of stromal cell transplantation may not depend on a functional mesenchymal stromal cell at all, as similarly beneficial immunomodulatory effects can be achieved through the transfer of MSC lysate, MSC membrane particles or MSC-derived conditioned medium and exosomes (Giebel et al., 2017; Galipeau and Sensébé, 2018).

Tissue regeneration, in contrast, depends on the engraftment of proliferating progenitor cells with differentiation potential into specialized cell types in vivo. For successful treatment of degenerative diseases, long-term engraftment through self-renewing MSCs would be the goal. Gene therapeutic approaches to treat inherited monogenic diseases of the skeleton, such as osteogenesis imperfecta, depend on ex vivo manipulation of MSCs that maintain their stemness. All these approaches require cells with genuine stem cell capacities.

Bona fide mesenchymal stem cells have been identified and these fundamentally differ from the mesenchymal stromal cell concept. However, successful translational research in the field will further depend on two objectives: Stem cell-based disease modeling and the identification of disease mechanisms that operate predominantly in MSCs. Additionally, MSC manipulation and delivery to the recipient will require a thorough understanding of the MSC physiology (Bianco et al., 2013). The presented findings of this study contribute to both objectives.

The depicted bone phenotype of Itch-deficient mice resembles human osteoporosis. The reduction of MSCs and impaired osteoblastogenesis is likely to contribute to this finding. The cellular and molecular mechanisms how MSCs and progeny contribute to the phenotype in Itch knockout mice will be valuable from a clinical perspective. The mouse presents a model system to study cellular therapies in osteopenia. Furthermore, the identification of the Itch-Notch axis in the control of MSCs and osteoblastogenesis reveals potential drug targets.

Itch-deficient mice have been previously described to develop osteopenia when they age. This phenotype was explained through increased osteoclast activity in the absence of Itch (Zhang et al., 2013). Concomitantly, Itch was described as a negative regulator of osteoblastogenesis (Zhang and Xing, 2013). The present findings complement the understanding of the role of Itch in osteoblastogenesis as such as already the MSC compartment depends on the E3 ligase's regulation. Furthermore, my data suggest that osteopenia develops at an earlier age of the

mouse already. Impaired osteoblastogenesis in vitro as well as reduced osteoblast number and osteocalcin activity in vivo in the absence of Itch challenge its negative regulatory role in osteoblast differentiation. These data are important as they demonstrate that osteopenia in Itch-deficient mice is a result of diverse mechanisms and more complex than initially stated. The role of Itch in osteoblastogenesis needs further clarification through methodologically refined studies.

Molecular studies identified elevated Notch signaling and Itch-Notch-interaction in MSCs. These data suggested that Itch negatively regulated Notch signaling in MSCs. Notch signaling has been described as an important regulator of bone development as well as of bone remodeling postnatally (Zanotti and Canalis, 2016). Mutations within the Notch signaling pathway have been identified in human skeletal diseases (Chen et al., 2014; Zanotti and Canalis, 2016): Allagile syndrome is a complex disorder that includes multiple fractures (loss-of-function mutation in JAG1 or NOTCH2). Patients with the autosomal-dominant Adams-Oliver-Syndrome suffer from distal limb defects (RBPJk missense mutation). Spondylocostal dysostosis comprises vertebral segmentation defects (mutations in DLL3, HES7 and others). Hajdu-cheney syndrome is an autosomal-dominant disease that includes craniofacial anomalies with intrasutural bones, osteoporosis and acroosteolysis (mutation in NOTCH2 leading to sustained receptor activation). Importantly, Notch signaling upregulation has been established in human osteosarcoma (Chen et al., 2014). These clinical examples support the importance of Notch signaling pathway in human bone development and bone homeostasis.

Notch inhibitors are highly investigated in oncology. Targeting the Notch signaling pathway comprises challenges such as the pathway's abundance and complexity. Modulation of Notch signaling via Itch depicts a unique mechanism of downregulation as the pathway activation still depends on physiological ligand binding and signaling is not completely abrogated. This mechanism may comprise novel strategies to target Notch signaling.

The described bone phenotype of Itch-deficient mice may open a new avenue to treat osteopetrotic diseases through the inhibition of Itch. Furthermore, Itch activation may exert beneficial effects in osteopenic conditions such as osteoporosis. Studies to elucidate the regulation of Itch in MSCs will be necessary

to develop therapeutic strategies. In this regard it is interesting to note that deletion of the HECT domain or pharmacological inhibition of the HECT domain active site result in downregulation of the E3 ligase function. Disruption of an autoinhibitory intramolecular interaction within the WW domains of Itch activates the E3 ligases catalytic activity instead (Aki et al., 2015).

ITCH deficiency in humans leads to a complex syndrome including multisystem autoinflammation and dysmorphic features. This rare disorder results from a mutation that leads to truncation of ITCH with the loss of WW domains and HECT domain (Lohr et al., 2010). The human phenotype resembles the mouse phenotype. This investigation of Itch in MSCs contributes to our understanding of the mechanism of the disease. On the other hand, this human phenotype reflects an important role of ITCH in human skeletal tissue.

5. SUMMARY

Mesenchymal stem cells are multipotent stem cells that differentiate into osteoblasts, chondrocytes, bone marrow adipocytes and stromal cells to maintain the skeleton's integrity throughout the lifespan. The intracellular signaling network that controls MSC functions remains poorly understood. The E3 ligase Itch has been implicated in the regulation of stem cells. Previously, Itch had not been studied in MSCs.

The present study aimed to investigate the role of Itch on MSC functions. The Itch knockout mouse model was employed to study Itch in MSCs through a loss of function approach. The E3 ligase Itch was identified as a positive regulator of the MSC pool. Itch-deficient mice exhibited markedly decreased PDGFRα+ Sca-1+ (PαS) MSCs in vivo. Notably, the reduction of MSCs seemed to be independent of the prominent autoinflammation though limitations apply due to the global knockout of Itch. Itch-deficient MSCs hyperproliferated in vitro but showed an unaffected viability and immunophenotype. These findings will be hypothesis-generating for further in vivo studies.

Itch-deficient MSCs had reduced capacity to differentiate into osteoblasts in vitro. Accordingly, osteoblasts and osteocalcin serum levels were reduced in vivo. Analyses of Itch-deficient bone revealed severe osteopenia and decreased bone mineral density that resembles human osteoporosis. A depletion of the MSC pool and impaired osteoblast differentiation are likely to contribute to the bone defects in Itch-deficient mice. In summary, Itch was identified as a positive regulator of osteoblast differentiation and bone mass but further regulatory roles on bone homeostasis cannot be excluded.

Increased Notch signaling was documented in Itch-deficient MSCs. Coimmunoprecipitation further revealed and interaction of Itch and intracellular Notch1 in MSCs. Itch has been previously established as a negative regulator of Notch signaling in other cell types. The functional impact of elevated Notch signaling in the absence of Itch needs to be finally proven. Of note, Notch signaling has been ascribed pleiotropic functions in bone formation. The importance of Notch signaling

within the skeleton is further reflected by inherited diseases with mutations in the Notch pathway that harbor significant skeletal defects.

Loss of ITCH in humans has been described as a rare disease and results in a complex phenotype including autoimmune disease and craniofacial dysmorphia. The function of Itch has been poorly investigated beyond the hematopoietic system so far. This study presents the first description of Itch as an essential positive regulator of MSCs. This finding will contribute to understand the pathology of human ITCH-deficiency. Moreover, the human phenotype suggests a major regulatory role of ITCH within the skeletal tissue. Translational strategies using MSC-based technologies will require a comprehensive understanding of MSC biology. In this regard, the identification of Itch as a regulator of MSC functions opens new avenues.

6. REFERENCES

Aki, D., Zhang, W., and Liu, Y.-C. (2015). The E3 ligase Itch in immune regulation and beyond. Immunological reviews *266*, 6-26.

Baddoo, M., Hill, K., Wilkinson, R., Gaupp, D., Hughes, C., Kopen, G.C., and Phinney, D.G. (2003). Characterization of mesenchymal stem cells isolated from murine bone marrow by negative selection. Journal of cellular biochemistry *89*, 1235-1249.

Bara, J.J., Richards, R.G., Alini, M., and Stoddart, M.J. (2014). Concise review: Bone marrow-derived mesenchymal stem cells change phenotype following in vitro culture: implications for basic research and the clinic. Stem cells (Dayton, Ohio) *32*, 1713-1723.

Bianco, P. (2014). "Mesenchymal" stem cells. Annual review of cell and developmental biology *30*, 677-704.

Bianco, P., Cao, X., Frenette, P.S., Mao, J.J., Robey, P.G., Simmons, P.J., and Wang, C.-Y. (2013). The meaning, the sense and the significance: translating the science of mesenchymal stem cells into medicine. Nature medicine *19*, 35-42.

Bianco, P., and Robey, P.G. (2015). Skeletal stem cells. Development (Cambridge, England) *142*, 1023-1027.

Bianco, P., Robey, P.G., and Simmons, P.J. (2008). Mesenchymal stem cells: revisiting history, concepts, and assays. Cell stem cell *2*, 313-319.

Blashki, D., Murphy, M.B., Ferrari, M., Simmons, P.J., and Tasciotti, E. (2016). Mesenchymal stem cells from cortical bone demonstrate increased clonal incidence, potency, and developmental capacity compared to their bone marrow–derived counterparts. Journal of Tissue Engineering *7*.

Bouxsein, M.L., Boyd, S.K., Christiansen, B.A., Guldberg, R.E., Jepsen, K.J., and Müller, R. (2010). Guidelines for assessment of bone microstructure in rodents using micro-computed tomography. Journal of bone and mineral research : the official journal of the American Society for Bone and Mineral Research *25*, 1468-1486.

Cai, Y., Liu, T., Fang, F., Xiong, C., and Shen, S. (2015). Comparisons of mouse mesenchymal stem cells in primary adherent culture of compact bone fragments and whole bone marrow. Stem cells international *2015*, 708906.

Caplan, A.I. (1991). Mesenchymal stem cells. Journal of orthopaedic research : official publication of the Orthopaedic Research Society *9*, 641-650.

Caplan, A.I. (1994). The mesengenic process. Clinics in plastic surgery *21*, 429-435.

Castro-Malaspina, H., Gay, R.E., Resnick, G., Kapoor, N., Meyers, P., Chiarieri, D., McKenzie, S., Broxmeyer, H.E., and Moore, M.A. (1980). Characterization of human bone marrow fibroblast colony-forming cells (CFU-F) and their progeny. Blood *56*, 289-301.

Chan, C.K.F., Seo, E.Y., Chen, J.Y., Lo, D., McArdle, A., Sinha, R., Tevlin, R., Seita, J., Vincent-Tompkins, J., and Wearda, T., et al. (2015). Identification and Specification of the Mouse Skeletal Stem Cell. Cell *160*, 285-298.

Chen, K.G., Johnson, K.R., McKay, R.D.G., and Robey, P.G. (2018). Concise Review: Conceptualizing Paralogous Stem-Cell Niches and Unfolding Bone Marrow Progenitor Cell Identities. Stem cells (Dayton, Ohio) *36*, 11-21.

Chen, K.G., Johnson, K.R., and Robey, P.G. (2017). Mouse Genetic Analysis of Bone Marrow Stem Cell Niches: Technological Pitfalls, Challenges, and Translational Considerations. Stem cell reports *9*, 1343-1358.

Chen, S., Lee, B.H., and Bae, Y. (2014). Notch signaling in skeletal stem cells. Calcified tissue international *94*, 68-77.

Ciechanover, A. (2015). The unravelling of the ubiquitin system. Nature Reviews Molecular Cell Biology *16*, 322.

Clague, M.J., Heride, C., and Urbé, S. (2015). The demographics of the ubiquitin system. Trends in cell biology *25*, 417-426.

Confavreux, C.B., Levine, R.L., and Karsenty, G. (2009). A paradigm of integrative physiology, the crosstalk between bone and energy metabolisms. Molecular and cellular endocrinology *310*, 21-29.

da Silva Meirelles, L., Chagastelles, P.C., and Nardi, N.B. (2006). Mesenchymal stem cells reside in virtually all post-natal organs and tissues. Journal of cell science *119*, 2204-2213.

Ding, L., and Morrison, S.J. (2013). Haematopoietic stem cells and early lymphoid progenitors occupy distinct bone marrow niches. Nature *495*, 231-235.

Dominici, M., Le Blanc, K., Mueller, I., Slaper-Cortenbach, I., Marini, F., Krause, D., Deans, R., Keating, A., Prockop, D., and Horwitz, E. (2006). Minimal criteria for defining multipotent mesenchymal stromal cells. The International Society for Cellular Therapy position statement. Cytotherapy *8*, 315-317.

Dong, Y., Jesse, A.M., Kohn, A., Gunnell, L.M., Honjo, T., Zuscik, M.J., O'Keefe, R.J., and Hilton, M.J. (2010). RBPjκ-dependent Notch signaling regulates mesenchymal progenitor cell proliferation and differentiation during skeletal development. Development (Cambridge, England) *137*, 1461-1471.

Fang, D., Elly, C., Gao, B., Fang, N., Altman, Y., Joazeiro, C., Hunter, T., Copeland, N., Jenkins, N., and Liu, Y.-C. (2002). Dysregulation of T lymphocyte function in itchy mice: a role for Itch in TH2 differentiation. Nature immunology *3*, 281-287.

Friedenstein, A.J., Chailakhjan, R.K., and Lalykina, K.S. (1970). The development of fibroblast colonies in monolayer cultures of guinea-pig bone marrow and spleen cells. Cell and tissue kinetics *3*, 393-403.

Friedenstein, A.J., Piatetzky-Shapiro, I.I., and Petrakova, K.V. (1966). Osteogenesis in transplants of bone marrow cells. Journal of embryology and experimental morphology *16*, 381-390.

Galipeau, J., and Sensébé, L. (2018). Mesenchymal Stromal Cells: Clinical Challenges and Therapeutic Opportunities. Cell stem cell *22*, 824-833.

Giamboi-Miraglia, A., Cianfarani, F., Cattani, C., Lena, A.M., Serra, V., Campione, E., Terrinoni, A., Zambruno, G., Odorisio, T., and Di Daniele, N., et al. (2015). The E3 ligase Itch knockout mice show hyperproliferation and wound healing alteration. The FEBS journal *282*, 4435-4449.

Giebel, B., Kordelas, L., and Börger, V. (2017). Clinical potential of mesenchymal stem/stromal cell-derived extracellular vesicles. Stem cell investigation *4*, 84.

Glickman, M.H., and Ciechanover, A. (2002). The ubiquitin-proteasome proteolytic pathway: destruction for the sake of construction. Physiological reviews *82*, 373-428.

Greenbaum, A., Hsu, Y.-M.S., Day, R.B., Schuettpelz, L.G., Christopher, M.J., Borgerding, J.N., Nagasawa, T., and Link, D.C. (2013). CXCL12 in early mesenchymal progenitors is required for haematopoietic stem-cell maintenance. Nature *495*, 227-230.

Hanada, K., Dennis, J.E., and Caplan, A.I. (1997). Stimulatory effects of basic fibroblast growth factor and bone morphogenetic protein-2 on osteogenic differentiation of rat bone marrow-derived mesenchymal stem cells. Journal of bone and mineral research : the official journal of the American Society for Bone and Mineral Research *12*, 1606-1614.

He, S., Nakada, D., and Morrison, S.J. (2009). Mechanisms of stem cell self-renewal. Annual review of cell and developmental biology *25*, 377-406.

Hilton, M.J., Tu, X., Wu, X., Bai, S., Zhao, H., Kobayashi, T., Kronenberg, H.M., Teitelbaum, S.L., Ross, F.P., and Kopan, R., et al. (2008). Notch signaling maintains bone marrow mesenchymal progenitors by suppressing osteoblast differentiation. Nature medicine *14*, 306-314.

Horwitz, E.M., Le Blanc, K., Dominici, M., Mueller, I., Slaper-Cortenbach, I., Marini, F.C., Deans, R.J., Krause, D.S., and Keating, A. (2005). Clarification of the nomenclature for MSC: The International Society for Cellular Therapy position statement. Cytotherapy *7*, 393-395.

Houlihan, D.D., Mabuchi, Y., Morikawa, S., Niibe, K., Araki, D., Suzuki, S., Okano, H., and Matsuzaki, Y. (2012). Isolation of mouse mesenchymal stem cells on the basis of expression of Sca-1 and PDGFR-α. Nature protocols *7*, 2103-2111.

Huang, W., La Russa, V., Alzoubi, A., and Schwarzenberger, P. (2006). Interleukin-17A: a T-cell-derived growth factor for murine and human mesenchymal stem cells. Stem cells (Dayton, Ohio) *24*, 1512-1518.

Hussain, I., Magd, S.A., Eremin, O., and El-Sheemy, M. (2012). New approach to isolate mesenchymal stem cell (MSC) from human umbilical cord blood. Cell biology international *36*, 595-600.

Hustad, C.M., Perry, W.L., Siracusa, L.D., Rasberry, C., Cobb, L., Cattanach, B.M., Kovatch, R., Copeland, N.G., and Jenkins, N.A. (1995). Molecular genetic characterization of six recessive viable alleles of the mouse agouti locus. Genetics *140*, 255-265.

Isern, J., García-García, A., Martín, A.M., Arranz, L., Martín-Pérez, D., Torroja, C., Sánchez-Cabo, F., and Méndez-Ferrer, S. (2014). The neural crest is a source of mesenchymal stem cells with specialized hematopoietic stem cell niche function. eLife *3*, e03696.

Jaenisch, R., and Young, R. (2008). Stem cells, the molecular circuitry of pluripotency and nuclear reprogramming. Cell *132*, 567-582.

Jilka, R.L., Weinstein, R.S., Bellido, T., Roberson, P., Parfitt, A.M., and Manolagas, S.C. (1999). Increased bone formation by prevention of osteoblast apoptosis with parathyroid hormone. The Journal of clinical investigation *104*, 439-446.

Karsenty, G., Kronenberg, H.M., and Settembre, C. (2009). Genetic control of bone formation. Annual review of cell and developmental biology *25*, 629-648.

Kopan, R., and Ilagan, M.X.G. (2009). The Canonical Notch Signaling Pathway: Unfolding the Activation Mechanism. Cell *137*, 216-233.

Kriegel, M.A., Rathinam, C., and Flavell, R.A. (2009). E3 ubiquitin ligase GRAIL controls primary T cell activation and oral tolerance. Proceedings of the National Academy of Sciences of the United States of America *106*, 16770-16775.

Kushwah, R., Guezguez, B., Lee, J.B., Hopkins, C.I., and Bhatia, M. (2014). Pleiotropic roles of Notch signaling in normal, malignant, and developmental hematopoiesis in the human. EMBO reports *15*, 1128-1138.

Lennon, D.P., Edmison, J.M., and Caplan, A.I. (2001). Cultivation of rat marrow-derived mesenchymal stem cells in reduced oxygen tension: effects on in vitro and in vivo osteochondrogenesis. Journal of cellular physiology *187*, 345-355.

Liao, B., Zhong, X., Xu, H., Xiao, F., Fang, Z., Gu, J., Chen, Y., Zhao, Y., and Jin, Y. (2013). Itch, an E3 ligase of Oct4, is required for embryonic stem cell self-renewal and pluripotency induction. Journal of cellular physiology *228*, 1443-1451.

Livak, K.J., and Schmittgen, T.D. (2001). Analysis of relative gene expression data using real-time quantitative PCR and the 2(-Delta Delta C(T)) Method. Methods (San Diego, Calif.) *25*, 402-408.

Lohr, N.J., Molleston, J.P., Strauss, K.A., Torres-Martinez, W., Sherman, E.A., Squires, R.H., Rider, N.L., Chikwava, K.R., Cummings, O.W., and Morton, D.H., et al. (2010). Human ITCH E3 ubiquitin ligase deficiency causes syndromic multisystem autoimmune disease. American journal of human genetics *86*, 447-453.

Mackenzie, T.C., and Flake, A.W. (2001). Human mesenchymal stem cells persist, demonstrate site-specific multipotential differentiation, and are present in sites of wound healing and tissue regeneration after transplantation into fetal sheep. Blood cells, molecules & diseases *27*, 601-604.

Mangiavini, L., Merceron, C., Araldi, E., Khatri, R., Gerard-O'Riley, R., Wilson, T.L., Rankin, E.B., Giaccia, A.J., and Schipani, E. (2014). Loss of VHL in mesenchymal progenitors of the limb bud alters multiple steps of endochondral bone development. Developmental biology *393*, 124-136.

Mangiavini, L., Merceron, C., Araldi, E., Khatri, R., Gerard-O'Riley, R., Wilson, T.L., Sandusky, G., Abadie, J., Lyons, K.M., and Giaccia, A.J., et al. (2015). Fibrosis and hypoxia-inducible factor-1α-dependent tumors of the soft tissue on loss of von Hippel-Lindau in mesenchymal progenitors. The American journal of pathology *185*, 3090-3101.

Marshall, O.J. (2004). PerlPrimer: cross-platform, graphical primer design for standard, bisulphite and real-time PCR. Bioinformatics (Oxford, England) *20*, 2471-2472.

Maruyama, T., Jeong, J., Sheu, T.-J., and Hsu, W. (2016). Stem cells of the suture mesenchyme in craniofacial bone development, repair and regeneration. Nature communications *7*, 10526.

MCCULLOCH, E.A., and TILL, J.E. (1960). The radiation sensitivity of normal mouse bone marrow cells, determined by quantitative marrow transplantation into irradiated mice. Radiation research *13*, 115-125.

Méndez-Ferrer, S., Michurina, T.V., Ferraro, F., Mazloom, A.R., Macarthur, B.D., Lira, S.A., Scadden, D.T., Ma'ayan, A., Enikolopov, G.N., and Frenette, P.S. (2010). Mesenchymal and haematopoietic stem cells form a unique bone marrow niche. Nature *466*, 829-834.

Mizoguchi, T., Pinho, S., Ahmed, J., Kunisaki, Y., Hanoun, M., Mendelson, A., Ono, N., Kronenberg, H.M., and Frenette, P.S. (2014). Osterix marks distinct waves of primitive and definitive stromal progenitors during bone marrow development. Developmental cell *29*, 340-349.

Mohamed, F.F., and Franceschi, R.T. (2017). Skeletal Stem Cells: Origins, Functions and Uncertainties. Current molecular biology reports *3*, 236-246.

Morikawa, S., Mabuchi, Y., Kubota, Y., Nagai, Y., Niibe, K., Hiratsu, E., Suzuki, S., Miyauchi-Hara, C., Nagoshi, N., and Sunabori, T., et al. (2009). Prospective identification, isolation, and systemic transplantation of multipotent mesenchymal stem cells in murine bone marrow. The Journal of experimental medicine *206*, 2483-2496.

Noyes, N.C., Hampton, B., Migliorini, M., and Strickland, D.K. (2016). Regulation of Itch and Nedd4 E3 Ligase Activity and Degradation by LRAD3. Biochemistry *55*, 1204-1213.

Nusspaumer, G., Jaiswal, S., Barbero, A., Reinhardt, R., Ishay Ronen, D., Haumer, A., Lufkin, T., Martin, I., and Zeller, R. (2017). Ontogenic Identification and Analysis of Mesenchymal Stromal Cell Populations during Mouse Limb and Long Bone Development. Stem cell reports *9*, 1124-1138.

Ono, N., Ono, W., Nagasawa, T., and Kronenberg, H.M. (2014). A subset of chondrogenic cells provides early mesenchymal progenitors in growing bones. Nature cell biology *16*, 1157-1167.

Orford, K.W., and Scadden, D.T. (2008). Deconstructing stem cell self-renewal: genetic insights into cell-cycle regulation. Nature reviews. Genetics *9*, 115-128.

Owen, M., and Friedenstein, A.J. (1988). Stromal stem cells: marrow-derived osteogenic precursors. Ciba Foundation symposium *136*, 42-60.

Parekkadan, B., and Milwid, J.M. (2010). Mesenchymal stem cells as therapeutics. Annual review of biomedical engineering *12*, 87-117.

Parfitt, A.M., Drezner, M.K., Glorieux, F.H., Kanis, J.A., Malluche, H., Meunier, P.J., Ott, S.M., and Recker, R.R. (1987). Bone histomorphometry: standardization of nomenclature, symbols, and units. Report of the ASBMR Histomorphometry Nomenclature Committee. Journal of bone and mineral research : the official journal of the American Society for Bone and Mineral Research *2*, 595-610.

Park, D., Spencer, J.A., Koh, B.I., Kobayashi, T., Fujisaki, J., Clemens, T.L., Lin, C.P., Kronenberg, H.M., and Scadden, D.T. (2012). Endogenous bone marrow MSCs are dynamic, fate-restricted participants in bone maintenance and regeneration. Cell stem cell *10*, 259-272.

Peister, A., Mellad, J.A., Larson, B.L., Hall, B.M., Gibson, L.F., and Prockop, D.J. (2004). Adult stem cells from bone marrow (MSCs) isolated from different strains of inbred mice vary in surface epitopes, rates of proliferation, and differentiation potential. Blood *103*, 1662-1668.

Perry, W.L., Hustad, C.M., Swing, D.A., O'Sullivan, T.N., Jenkins, N.A., and Copeland, N.G. (1998). The itchy locus encodes a novel ubiquitin protein ligase that is disrupted in a18H mice. Nature genetics *18*, 143-146.

Pevsner-Fischer, M., Morad, V., Cohen-Sfady, M., Rousso-Noori, L., Zanin-Zhorov, A., Cohen, S., Cohen, I.R., and Zipori, D. (2007). Toll-like receptors and their ligands control mesenchymal stem cell functions. Blood *109*, 1422-1432.

Phinney, D.G., Kopen, G., Isaacson, R.L., and Prockop, D.J. (1999). Plastic adherent stromal cells from the bone marrow of commonly used strains of inbred mice: variations in yield, growth, and differentiation. Journal of cellular biochemistry *72*, 570-585.

Pinho, S., Lacombe, J., Hanoun, M., Mizoguchi, T., Bruns, I., Kunisaki, Y., and Frenette, P.S. (2013). PDGFRα and CD51 mark human nestin+ sphere-forming mesenchymal stem cells capable of hematopoietic progenitor cell expansion. The Journal of experimental medicine *210*, 1351-1367.

Qiu, L., Joazeiro, C., Fang, N., Wang, H.Y., Elly, C., Altman, Y., Fang, D., Hunter, T., and Liu, Y.C. (2000). Recognition and ubiquitination of Notch by Itch, a hect-type E3 ubiquitin ligase. The Journal of biological chemistry *275*, 35734-35737.

Rathinam, C., Matesic, L.E., and Flavell, R.A. (2011). The E3 ligase Itch is a negative regulator of the homeostasis and function of hematopoietic stem cells. Nature immunology *12*, 399-407.

Rathinam, C., Sauer, M., Ghosh, A., Rudolph, C., Hegazy, A., Schlegelberger, B., Welte, K., and Klein, C. (2006). Generation and characterization of a novel hematopoietic progenitor cell line with DC differentiation potential. Leukemia *20*, 870-876.

Rossi, M., Aqeilan, R.I., Neale, M., Candi, E., Salomoni, P., Knight, R.A., Croce, C.M., and Melino, G. (2006). The E3 ubiquitin ligase Itch controls the protein stability of p63. Proceedings of the National Academy of Sciences of the United States of America *103*, 12753-12758.

Rux, D.R., Song, J.Y., Swinehart, I.T., Pineault, K.M., Schlientz, A.J., Trulik, K.G., Goldstein, S.A., Kozloff, K.M., Lucas, D., and Wellik, D.M. (2016). Regionally Restricted Hox Function in Adult Bone Marrow Multipotent Mesenchymal Stem/Stromal Cells. Developmental cell *39*, 653-666.

Sato, Y., Mabuchi, Y., Miyamoto, K., Araki, D., Niibe, K., Houlihan, D.D., Morikawa, S., Nakagawa, T., Nakajima, T., and Akazawa, C., et al. (2016). Notch2 Signaling Regulates the Proliferation of Murine Bone Marrow-Derived Mesenchymal Stem/Stromal Cells via c-Myc Expression. PloS one *11*, e0165946.

Scanlon, V., Walia, B., Yu, J., Hansen, M., Drissi, H., Maye, P., and Sanjay, A. (2017). Loss of Cbl-PI3K interaction modulates the periosteal response to fracture by enhancing osteogenic commitment and differentiation. Bone *95*, 124-135.

Schneider, C.A., Rasband, W.S., and Eliceiri, K.W. (2012). NIH Image to ImageJ: 25 years of image analysis. Nat Methods *9*, 671-675.

Strikoudis, A., Guillamot, M., and Aifantis, I. (2014). Regulation of stem cell function by protein ubiquitylation. EMBO reports *15*, 365-382.

Swift, S., Lorens, J., Achacoso, P., and Nolan, G.P. (2001). Rapid production of retroviruses for efficient gene delivery to mammalian cells using 293T cell-based systems. Current protocols in immunology *Chapter 10*, Unit 10.17C.

Tavassoli, M., and Crosby, W.H. (1968). Transplantation of marrow to extramedullary sites. Science (New York, N.Y.) *161*, 54-56.

Weissman, A.M. (2001). Themes and variations on ubiquitylation. Nature reviews. Molecular cell biology *2*, 169-178.

Weng, T., Xie, Y., Huang, J., Luo, F., Yi, L., He, Q., Di Chen, and Chen, L. (2014). Inactivation of Vhl in osteochondral progenitor cells causes high bone mass phenotype and protects against age-related bone loss in adult mice. Journal of bone and mineral research : the official journal of the American Society for Bone and Mineral Research *29*, 820-829.

Werner, A., Manford, A.G., and Rape, M. (2017). Ubiquitin-Dependent Regulation of Stem Cell Biology. Trends in cell biology *27*, 568-579.

Woodbury, D., Schwarz, E.J., Prockop, D.J., and Black, I.B. (2000). Adult rat and human bone marrow stromal cells differentiate into neurons. J. Neurosci. Res. *61*, 364-370.

Worthley, D.L., Churchill, M., Compton, J.T., Tailor, Y., Rao, M., Si, Y., Levin, D., Schwartz, M.G., Uygur, A., and Hayakawa, Y., et al. (2015). Gremlin 1 identifies a skeletal stem cell with bone, cartilage, and reticular stromal potential. Cell *160*, 269-284.

Wu, G.D., Nolta, J.A., Jin, Y.-S., Barr, M.L., Yu, H., Starnes, V.A., and Cramer, D.V. (2003). Migration of mesenchymal stem cells to heart allografts during chronic rejection. Transplantation *75*, 679-685.

Wu, Y., Tworkoski, K., Michaud, M., and Madri, J.A. (2009). Bone marrow monocyte PECAM-1 deficiency elicits increased osteoclastogenesis resulting in

trabecular bone loss. Journal of immunology (Baltimore, Md. : 1950) *182*, 2672-2679.

Xu, S., Becker, A. de, van Camp, B., Vanderkerken, K., and van Riet, I. (2010). An improved harvest and in vitro expansion protocol for murine bone marrow-derived mesenchymal stem cells. Journal of biomedicine & biotechnology *2010*, 105940.

Yao, G.-Q., Troiano, N., Simpson, C.A., and Insogna, K.L. (2017). Selective deletion of the soluble Colony-Stimulating Factor 1 isoform in vivo prevents estrogen-deficiency bone loss in mice. Bone research *5*, 17022.

Zanotti, S., and Canalis, E. (2016). Notch Signaling and the Skeleton. Endocrine reviews *37*, 223-253.

Zhang, H., Wu, C., Matesic, L.E., Li, X., Wang, Z., Boyce, B.F., and Xing, L. (2013). Ubiquitin E3 ligase Itch negatively regulates osteoclast formation by promoting deubiquitination of tumor necrosis factor (TNF) receptor-associated factor 6. The Journal of biological chemistry *288*, 22359-22368.

Zhang, H., and Xing, L. (2013). Ubiquitin e3 ligase itch negatively regulates osteoblast differentiation from mesenchymal progenitor cells. Stem cells (Dayton, Ohio) *31*, 1574-1583.

Zhao, H., Feng, J., Ho, T.-V., Grimes, W., Urata, M., and Chai, Y. (2015). The suture provides a niche for mesenchymal stem cells of craniofacial bones. Nature cell biology *17*, 386-396.

Zhou, B.O., Yue, R., Murphy, M.M., Peyer, J.G., and Morrison, S.J. (2014). Leptin-receptor-expressing mesenchymal stromal cells represent the main source of bone formed by adult bone marrow. Cell stem cell *15*, 154-168.

Zhu, H., Guo, Z.-K., Jiang, X.-X., Li, H., Wang, X.-Y., Yao, H.-Y., Zhang, Y., and Mao, N. (2010). A protocol for isolation and culture of mesenchymal stem cells from mouse compact bone. Nature protocols *5*, 550-560.

7. LIST OF ABBREVIATIONS

Table 7. List of abbreviations.

µCT and micro-CT	Computed tomography
aa	Amino acid
Acan	Aggrecan
ACK	Ammonium-chloride-potassium
AIP4	Atrophin-interacting-protein 4
APS	Ammonium persulfate
B6	C57BL/6 strain
BD	Becton, Dickinson and Company, Franklin Lakes, New Jersey, USA
bp	Base pairs
BSA	Bovine serum albumin
Cbl	Casitas b-lineage lymphoma
CD	Cluster of differentiation
cDNA	Complementary DNA
Cell Signaling	Cell Signaling Technology, Danvers, Massachusetts, USA
CFU-F	Colony forming unit fibroblast
CFU-Ob	Colony forming unit osteoblast
cJun	Jun proto-oncogene
cMyc	Myc proto-oncogene, bHLH transcription factor
Col	Collagen
Cre	Cre recombinase
CreER	Cre recombinase estrogen receptor ligang binding domain fusion protein
CSFE	Carboxyfluorescein succinimidyl ester
Ct.BV	Cortical bone volume
Ct.BV/TV	Cortical bone volume fraction
Ct.Th	Cortical thickness
Ct.TV	Cortical total volume
Ctgf	Connective tissue growth factor
Ctrl	Control
CXCL12	C-X-C motif chemokine ligand 12
DLL	Drosophila distal-less
DMEM	Dulbecco's Modified Eagle Medium

DMSO	Dimethyl sulfoxide
DNA	Deoxyribonucleic acid
DUB	Deubiquitinating enzyme
E. coli	Escherichia coli
E1	Ubiquitin activating enzyme
E2	Ubiquitin conjugating enzyme
E3	Ubiquitin ligase
EDTA	Ethylenediaminetetraacetic acid
ES cells	Embryonic stem cells
Exp.	Experiment
FCS	Fetal calf serum
FGF-2	Fibroblast growth factor 2
GFP	Green fluorescent protein
Gli1	GLI-Kruppel family member GLI1
Grem1	Gremlin 1
GvHD	Graft-versus-Host-Disease
H&E	Hematoxylin and eosin
HECT	Homologous to the E6-AP COOH terminus
Hes	Hes family bHLH transcription factor
Hey1	Hairy/enhancer-of-split related with YRPW motif 1
Heyl	Hairy/enhancer-of-split related with YRPW motif-like
Hif	Hypoxia inducible factor
Hoxa11	Homeobox A11
Hprt	Hypoxanthine-guanine phosphoribosyltransferase
HRP	Horseradish peroxidase
HSC	Hematopoietic stem cell
HSPC	Hematopoietic stem and progenitor cell
IBMX	3-isobuty-l-methyl-xanthine
Icn	Intracellular Notch
IL	Interleukine
IP	Immunoprecipitation
iPS cell	Induced pluripotent stem cell
ISCT	International Society for Cellular Therapy
Itch	Itchy, E3 ubiquitin protein ligase
JAG1	JAGGED1

Jnk	Jnk Mitogen-activated protein kinase
JunB	Jun B proto-oncogene
Klf4	Kruppel-like factor 4
LB	Lysogeny broth
LepR	Leptin receptor
Lys	Lysine
MACS	Magnetic-activated cell sorting
Mapk	Mitogen-activated protein kinase
mRNA	Messenger RNA
MSC	Mesenchymal stem cell
Mx-1	MX dynamin like GTPase 1
Nes	Nestin
Nfkb	Nuclear factor kappa B
NICD	Notch intracellular domain
Ocn	Osteocalcin
Oct4	POU domain, class 5, transcription factor 1
OPG	Osteoprotegerine
Osx	Osterix
p38	P38 Mitogen-activated protein kinase
p63	Tumor protein 63
PBS	Phosphate-buffered saline
PCR	Polymerase chain reaction
PDGFRα	Platelet-derived growth factor receptor alpha
Pdk1	Phosphoinositide-dependent kinase-1
PI	Propidium iodide
Pi3k	Phosphoinositide-3-kinase
Pi3k	Phosphatidylinositol-4,5-bisphosphate
Prx1	Paired related homeobox 1
PVDF	Polyvinylidene difluoride
PX	Passage X
PαS MSCs	CD45−TER119−PDGFRα+Sca-1+ MSCs
RANKL	Receptor activator of nuclear factor kappa-B ligand
Rbpjk	Recombination signal binding protein for immunoglobulin kappa J region
RFP	Red fluorescent protein
RING	Really new interesting gene

RNA	Ribonucleic acid
Runx2	Runt-related transcription factor 2
S100	S100 calcium binding protein
Santa Cruz	Santa Cruz Biotechnology, Dallas, Texas, USA
Sca-1	Stem cell antigen-1
SDS-PAGE	Sodium dodecyl sulfate–polyacrylamide gel electrophoresis
SEM	Standard error of measurement
sh-RNA	Small hairpin RNA
Sox	SRY (sex determining region Y)-box
Src	Proto-oncogene tyrosine-protein kinase Src
SSC	Skeletal stem cell
Tb.	Trabecular
TEMED	N,N,N',N'-tetramethylethylenediamine
Th2	Type 2 helper T cell
Tr.BV	Trabecular bone volume
Tr.BV/TV	Trabecular bone volume fraction
Tr.No.	Trabecular number
Tr.Sp	Trabecular separation
Tr.Th	Trabecular thickness
Tr.TV	Trabecular total volume
Traf6	TNF receptor associated factor
Ub	Ubiquitin
USA	United States of America
Vhl	Von Hippel-Lindau tumor suppressor
vs.	Versus
VSV-G	Vesicular stomatits virus envelope glycoprotein

8. APPENDIX

Table 8. List of reagents and equipment.

2-Mercaptoethanol	Sigma-Aldrich Corporation, St. Louis, Missouri, USA
ACK (ammonium-chloride-potassium) red cell lysis buffer	Thermo Fisher Scientific, Waltham, Massachusetts, USA
Adipogenic induction medium	Lonza Group, Basel, Switzerland
Adipogenic maintenance medium	Lonza Group, Basel, Switzerland
Alizarin red salt	Sigma-Aldrich Corporation, St. Louis, Missouri, USA
Ampicillin	Sigma-Aldrich Corporation, St. Louis, Missouri, USA
APS (ammonium persulfate)	Bio-Rad Laboratories, Inc., Hercules, California, USA
AxioCam MRm Rev 3	Carl Zeiss AG, Oberkochen, Germany
Biotin-conjugated anti-mouse CD45 antibody	BioLegend, San Diego, California, USA
Biotin-conjugated anti-mouse TER119 antibody	BioLegend, San Diego, California, USA
Bovine serum albumin (BSA)	Thermo Fisher Scientific, Waltham, Massachusetts, USA
Cell Lysis Buffer	Cell Signaling Technology, Danvers, Massachusetts, USA
CellQuest	Becton, Dickinson and Company (BD), Franklin Lakes, New Jersey, USA
CFSE Cell Proliferation Kit	Thermo Fisher Scientific, Waltham, Massachusetts, USA
CFX Connect Real-Time PCR Detection System	Bio-Rad Laboratories, Inc., Hercules, California, USA
CFX manager Version 3.1	Bio-Rad Laboratories, Inc., Hercules, California, USA
Collagenase P	Hoffmann-La Roche, Basel, Switzerland
Dimethyl sulfoxide (DMSO)	Sigma-Aldrich Corporation, St. Louis, Missouri, USA
Dulbecco's Modified Eagle Medium (DMEM)	Thermo Fisher Scientific, Waltham, Massachusetts, USA
Electrophoresis chambers	Bio-Rad Laboratories, Inc., Hercules, California, USA
FACSAria II	Becton, Dickinson and Company (BD), Franklin Lakes, New Jersey, USA
FACScan	Becton, Dickinson and Company (BD), Franklin Lakes, New Jersey, USA
FACSDIVA software	Becton, Dickinson and Company (BD), Franklin Lakes, New Jersey, USA
FlowJo software Version 9	TreeStar Inc., Ashland, Oregon, USA

Gibco Opti-MEM	Thermo Fisher Scientific, Waltham, Massachusetts, USA
GraphPad Prism Version 5	GraphPad Software Inc., La Jolla, California, USA
ImageJ 1.52a	Wayne Rasband, National Institute of Health, USA
Image station 440	Kodak, Rochester, New York, USA
Invitrogen Lipofectamine 2000	Thermo Fisher Scientific, Waltham, Massachusetts, USA
Invitrogen Platinum Taq DNA Polymerase High Fidelity	Thermo Fisher Scientific, Waltham, Massachusetts, USA
Invitrogen SuperScript II Reverse Transcriptase	Thermo Fisher Scientific, Waltham, Massachusetts, USA
Kanamycin	Sigma-Aldrich Corporation, St. Louis, Missouri, USA
Kapa SYBR Fast mastermix	Hoffmann-La Roche, Basel, Switzerland
L-Glutamine	Thermo Fisher Scientific, Waltham, Massachusetts, USA
LSRII	Becton, Dickinson and Company (BD), Franklin Lakes, New Jersey, USA
MACS midi columns	Miltenyi Biotec, Bergisch Gladbach, Germany
Mesencult Basal Medium	Stemcell Technologies, Vancouver, British Columbia, Canada
Mesencult Stimulatory Supplement	Stemcell Technologies, Vancouver, British Columbia, Canada
NuPAGE LDS sample buffer	Thermo Fisher Scientific, Waltham, Massachusetts, USA
Oil Red O powder	Sigma-Aldrich Corporation, St. Louis, Missouri, USA
Oligo(dT)12-18	Thermo Fisher Scientific, Waltham, Massachusetts, USA
One shot TOP10 chemically competent E. coli	Thermo Fisher Scientific, Waltham, Massachusetts, USA
Osteogenic differentiation medium	Lonza Group, Basel, Switzerland
Penicillin-Streptomycin	Thermo Fisher Scientific, Waltham, Massachusetts, USA
Pierce Co-Immunoprecipitation Kit	Thermo Fisher Scientific, Waltham, Massachusetts, USA
Plasmid maxiprep kit	Bioland Scientific LLC, Paramount, Clifornia, USA
Polybrene	Sigma-Aldrich Corporation, St. Louis, Missouri, USA
Propidium iodide	Sigma-Aldrich Corporation, St. Louis, Missouri, USA
Protease Inhibitor Cocktail complete, EDTA-free	Hoffmann-La Roche, Basel, Switzerland
PVDF (polyvinylidene difluoride) membrane	Bio-Rad Laboratories, Inc., Hercules, California, USA
QIAprep Spin Miniprep Kit	Qiagen, Hilden, Germany

QIAquick Gel Extraction Kit	Qiagen, Hilden, Germany
Quick CIP, Quick Dephosphorylation Kit	New England Biolabs, Ipswich, Massachusetts, USA
Restriction enzymes	New England Biolabs, Ipswich, Massachusetts, USA
RNeasy Mini Kit	Qiagen, Hilden, Germany
Scanco µCT-35	Scanco Medical, Brüttisellen, Switzerland
SDS (sodium dodecyl sulfate) solution, acrylamide	Bio-Rad Laboratories, Inc., Hercules, California, USA
Streptavidin Micro Beads	Miltenyi Biotec, Bergisch Gladbach, Germany
SuperSignal West Pico Chemiluminescent Substrate Kit	Thermo Fisher Scientific, Waltham, Massachusetts, USA
T100 Thermal Cycler	Bio-Rad Laboratories, Inc., Hercules, California, USA
T4 DNA Ligase	New England Biolabs, Ipswich, Massachusetts, USA
Tanks for wet electroblotting	Bio-Rad Laboratories, Inc., Hercules, California, USA
TEMED (N,N,N',N'-tetramethylethylenediamine)	Bio-Rad Laboratories, Inc., Hercules, California, USA
TOPO XL PCR CloningKit	Thermo Fisher Scientific, Waltham, Massachusetts, USA
Tris buffer	Sigma-Aldrich Corporation, St. Louis, Missouri, USA
Trypsin-EDTA	Thermo Fisher Scientific, Waltham, Massachusetts, USA
Tween 20	Sigma-Aldrich Corporation, St. Louis, Missouri, USA

Table 9. Colony Forming Unit assay. Bone cells.

	Control	**Itch$^{-/-}$**
Exp.1	8	0
Exp.2	12	6
Exp.3	5	1
Exp.4	14	3
Mean ± SEM	**9.750 ± 2.016**	**2.500 ± 1.323**
P value	0.0238	
P value summary	*	

Table 10. Colony Forming Unit assay. Bone marrow.

	Control	Itch$^{-/-}$
Exp.1	13	1
Exp.2	8	2
Mean ± SEM	**10.500 ± 2.500**	**1.500 ± 0.5000**
P value	0.0717	
P value summary	No significant difference	

Table 11. Absolute numbers of MSCs ex vivo.

	Control	Itch$^{-/-}$
Exp.1	2116.80	801.66
Exp.2	869.12	294.40
Exp.3	704.90	333.06
Exp.4	1619.90	772.80
Exp.5	1204.74	570.40
Mean ± SEM	**1303.00 ± 256.7**	**554.50 ± 106.2**
P value	0.0273	
P value summary	*	

Table 12. Viability of in vitro cultured MSCs. Percentage PI-negative fraction (in %).

	Control	Itch$^{-/-}$
Exp.1	50.20	60.00
Exp.2	67.40	78.90
Exp.3	64.20	55.50
Mean ± SEM	**60.60 ± 5.281**	**64.80 ± 7.169**
P value	0.6617	
P value summary	No significant difference	

Table 13. Colony Forming Unit Osteoblasts. Number of colonies (per 1 x 10^6 cells seeded).

	Control	Itch$^{-/-}$
Exp.1	21	3
Exp.2	12	6
Exp.3	15	7
Mean ± SEM	**16.00 ± 2.646**	**5.333 ± 1.202**
P value	0.0214	
P value summary	*	

Table 14. Differentiation of bone cells into osteoblasts ex vivo. Alizarin red positive area (in mm² per dish (10 cm)).

	Control	Itch$^{-/-}$
Exp.1	432.332	110.920
Exp.2	415.524	110.236
Exp.3	253.592	93.484
Mean ± SEM	**367.100 ± 56.990**	**104.900 ± 5.701**
P value	0.0102	
P value summary	*	

Table 15. Differentiation of bone cells into adipocytes ex vivo. Oil-red-O positive area (in mm² per well (9 cm²)).

	Control	Itch$^{-/-}$
Exp.1	28.60	17.57
Exp.2	5.31	22.47
Mean ± SEM	**16.95 ± 11.64**	**20.02 ± 2.451**
P value	0.8209	
P value summary	No significant difference	

Table 16. Number of osteoblasts per bone perimeter. N.Ob (per mm).

	Control	Itch$^{-/-}$
Exp.1	30.65	15.87
Exp.2	25.20	12.78
Mean ± SEM	**27.92 ± 2.726**	**14.32 ± 1.549**
P value	0.0493	
P value summary	*	

Table 17. Serum osteocalcin level (ng/ml).

	Control	Itch$^{-/-}$
Exp.1	37	23
Exp.2	42	21
Exp.3	39	27
Exp.4	30	14
Exp.5	40	17
Mean ± SEM	**37.60 ± 2.064**	**20.40 ± 2.272**
P value	<0.001	
P value summary	***	

Table 18. Micro-CT analysis of trabecular bone morphometry.

	TV (mm^3)	BV (mm^3)	BV/TV	Conn-Dens. ($1/mm^3$)	SMI	Tb.N (/mm)	Tb.Th (mm)	Tb.Sp (mm)	App-Dens.*	B.T.-Dens.*	BS (mm^2)	BS/BV (1/mm)	DA
WT1	2.5942	0.1075	0.0415	113.1389	2.23	2.4110	0.0427	0.4210	19.83	866.85	7.1750	68.3008	1.23
WT2	2.4959	0.0912	0.0365	127.0102	1.81	2.1208	0.0373	0.4800	19.03	852.46	6.5136	73.0656	1.30
WT3	2.4777	0.1441	0.0581	110.7898	1.84	2.6523	0.0403	0.3818	44.67	871.51	9.3999	66.2317	1.27
WT4	2.0264	0.1360	0.0671	257.3536	2.08	3.1306	0.0379	0.3247	55.52	848.47	9.8784	74.2640	1.39
KO1	1.8587	0.0491	0.0264	109.2142	1.76	1.7771	0.0304	0.5652	4.85	864.38	4.1736	87.6935	1.26
KO2	1.9561	0.0572	0.0292	149.0224	1.91	2.0418	0.0331	0.5033	9.91	865.65	4.4562	80.4632	1.26
KO3	2.5672	0.0692	0.0269	64.8566	2.50	2.2329	0.0303	0.4388	3.65	882.43	6.1125	92.4873	1.22
KO4	2.7489	0.1005	0.0366	122.9567	1.98	2.2792	0.0325	0.4440	8.51	849.07	8.2035	83.5671	1.16
Mean WT	2.3986	0.1197	0.0508	152.0731	1.99	2.5787	0.0396	0.4019	34.77	859.82	8.2417	70.4655	1.30
Mean KO	2.2827	0.0690	0.0298	111.5125	2.04	2.0828	0.0316	0.4878	6.73	865.38	5.7365	86.0528	1.22
SEM WT	0.1267	0.0123	0.0071	35.2755	0.10	0.2137	0.0012	0.0327	9.13	5.55	0.8238	1.9105	0.03
SEM KO	0.2207	0.0113	0.0024	17.6069	0.16	0.1141	0.0007	0.0297	1.48	6.82	0.9269	2.6064	0.02
P value	0.6650	0.0230	0.0312	0.3433	0.8083	0.0866	0.0014	0.0994	0.0230	0.5503	0.0899	0.0029	0.1206
P value summary	n.s.	*	*	n.s.	n.s.	n.s.	**	n.s.	*	n.s.	n.s.	**	n.s.

TV=Total volume, BV=Bone volume, Conn.-Dens.=Connectivity density, SMI=Structure model index, Tr.N.=Trabecular number, Tb.Th=Trabecular thickness, Tr.Sp=Trabecular separation, App.-Dens.=Apparent density, B.T.-Dens.=Bone tissue density, BS=Bone surface, DA=Degree of anisotropy.

*unit: mg HA/cm^3 (Hydroxiapatite density)

Table 19. Micro-CT analysis of cortical bone morphometry.

	TV (mm^3)	BV (mm^3)	BV/TV	App-Dens.*	B.T.-Dens.*	BS (mm^2)	BS/BV (1/mm)	Ct.Th (mm)	DA	pMOI
WT1	1.1181	1.0642	0.9518	1051.36	1120.22	11.48	10.78	0.185	8.27	0.33
WT2	1.0464	0.991	0.9471	1016.94	1085.59	11.1	11.189	0.178	8.59	0.28
WT3	1.1494	1.0932	0.9511	1022.27	1087.26	11.8	10.786	0.185	7.78	0.35
WT4	1.0418	0.9901	0.9503	1018.47	1083.19	10.687	10.788	0.185	7.82	0.26
KO1	0.7838	0.7334	0.9357	1000.29	1084.19	10.579	14.389	0.139	8.46	0.19
KO2	0.7362	0.6843	0.9295	967.80	1052.36	10.668	15.547	0.128	7.72	0.18
KO3	0.6791	0.6224	0.9164	957.01	1058.62	11.629	18.604	0.107	9.10	0.19
KO4	0.7147	0.6516	0.9118	927.58	1025.06	12.242	18.7	0.107	9.35	0.22
Mean WT	1.0889	1.0346	0.9501	1027.2591	1094.0647	11.27	10.8858	0.1833	8.11	0.30
Mean KO	0.7285	0.6729	0.9234	963.1671	1055.0602	11.28	16.8100	0.1203	8.66	0.19
SEM WT	0.0267	0.0261	0.0010	8.1127	8.7574	0.24	0.1011	0.0018	0.19	0.02
SEM KO	0.0219	0.0238	0.0056	15.0119	12.1401	0.40	1.0896	0.0080	0.36	0.01
P value	<0.001	<0.001	0.0033	0.0094	0.0404	0.9791	0.0016	<0.001	0.2340	0.0032
P value summary	***	***	**	**	*	n.s.	**	***	n.s.	**

TV=Total volume, BV=Bone volume, App.-Dens.=Apparent density, B.T.-Dens.=Bone tissue density, BS=Bone surface, Ct.Th=Cortical thickness, DA=Degree of anisotropy, pMOI=polar Moment of inertia.

*unit: mg HA/cm^3 (Hydroxiapatite density)

9. ACKNOWLEDGEMENT

My special thanks go to Professor Chozha V. Rathinam for his outstanding mentorship.

Special thanks also go to Professor Michael Heuser for his phenomenal support.

I further thank Professor Arnold Ganser, Professor Richard Flavell and Professor Christoph Klein. I thank the late International Academy of Life Sciences (IALS) president and BMEP director Professor Hilmar Stolte.

Thanks go to all my colleagues, especially Dr. Victoria Panagiota, Dr. Masahiro Marshall Nakagawa and Dr. Anthony Rongvaux. I thank the central facility for Musculoskeletal Disorders and Micro-CT core facility at Yale University School of Medicine. Further thanks go to the Flow Cytometry core facility, Department of Microbiology and Immunology at Columbia University.

I thank my family and friends for their support and their patience. I am especially grateful to my parents for their never-ending love and trust in me.

Vorträge und Poster:

Schünemann CR, Heuser M, Ganser A and Rathinam CV; **The E3 Ligase Itch Is a Regulator of Bone Marrow Mesenchymal Stem Cells and the Hematopoietic Stem Cell Niche**; 59th Annual Meeting and Exhibition of the American Society of Hematology (ASH) in Atlanta, USA, 9 – 23 December 2017; Blood 130:1158 (2017). **Auszeichnung „Abstract Achievement Award".**

Schünemann C, Schmidt JJ, Ganser A, David S, Hoeper MM; Successful treatment of ecstasy induced TTP by therapeutic plasma exchange; Jahrestagung der Deutschen, Österreichischen und Schweizerischen Gesellschaften für Hämatologie und Medizinische Onkologie in Stuttgart, 29. September – 3. Oktober 2017; Oncol Res Treat 40(suppl 3):154 (2017).

Eder M, Dammann E, Beutel G, Stamer K, Hambach L, Schwarzer A, Hamwi I, Lueck C, Ehrlich S, Ritter U, **Schuenemann C**, Schultze-Florey C, Thol F, Heuser M, Koenecke C, Stadler M, Ganser A; Comparison of three reduced intensity conditioning (RIC) regimens for allogeneic stem cell transplantation of adult patients with high-risk acute myeloid leukemia (AML) or myelodysplastic syndromes (MDS); 42st Annual Meeting of the European Society for Blood and Marrow Transplantation (EBMT) in Valencia, Spain, 3 - 6 April 2016; Bone Marrow Transplantation 51:241 (2016).

Fiedler W, Chromik J, Kebenko M, Thol F, Trummer A, **Schünemann C**, Brandts CH, Köhler A, Schlipfenbacher V, Bokemeyer C, Theile S, Kranich AL and Heuser M; Selinexor, ARA-C and Idarubicin: An Effective and Tolerable Combination in Patients with Relapsed/Refractory AML: A Multicenter Phase II Study; 57th Annual Meeting and Exhibition of the American Society of Hematology (ASH) in Orlando, USA, 5 – 8 December 2015; Blood 126:3789 (2015).

Eder M, Dammann E, Beutel G, Ehrlich S, Ritter U, Stamer K, Lueck C, Gehoff P, Schwarzer A, **Schuenemann C**, Diedrich H, Schultze-Florey C, Koenecke C, Stadler M, Ganser A; Comparison of three TBI-based myeloablative conditioning regimens for allogeneic stem cell transplantation of adult patients with acute lymphoblastic leukemia (ALL); 41st Annual Meeting of the European Society for

Blood and Marrow Transplantation (EBMT) in Istanbul, Turkey, 22 - 25 March 2015; Bone Marrow Transplantation 50:438 (2015).

_____ _____

Ort, Datum Christoph Schünemann

11. Erklärung nach §2 Abs. 2 Nr. 7 + 8 der Promotionsordnung

Ich erkläre, dass ich die der Medizinischen Hochschule Hannover zur Promotion eingereichte Dissertation mit dem Titel „The E3 Ligase Itch is a Novel Positive Regulator of Mesenchymal Stem Cells“ in der Klinik für Hämatologie, Hämostaseologie, Onkologie und Stammzelltransplantation der Medizinischen Hochschule Hannover unter Betreuung von Prof. Dr. med. Michael Heuser in Zusammenarbeit mit Prof. Dr. rer. nat. Chozha V. Rathinam am Department of Genetics and Development, Columbia University, USA, ohne sonstige Hilfe durchgeführt und bei der Abfassung der Dissertation keine anderen als die dort aufgeführten Hilfsmittel benutzt habe.

Die Gelegenheit zum vorliegenden Promotionsverfahren ist mir nicht kommerziell vermittelt worden. Insbesondere habe ich keine Organisation eingeschaltet, die gegen Entgelt Betreuerinnen und Betreuer für die Anfertigung von Dissertationen sucht oder die mir obliegenden Pflichten hinsichtlich der Prüfungsleistungen für mich ganz oder teilweise erledigt.

Ich habe diese Dissertation bisher an keiner in- oder ausländischen Hochschule zur Promotion eingereicht. Weiterhin versichere ich, dass ich den beantragten Titel bisher noch nicht erworben habe.

Ergebnisse der Dissertation wurden als Poster auf der 59. Jahrestagung der American Society of Hematology (ASH) veröffentlicht; Abstract veröffentlicht in Blood 2017 130:1158; Auszeichnung „Abstract Achievement Award“.

_____ _____

Ort, Datum Christoph Schünemann